Synthesis of Three-dimensional Polymer Nanostructures via Chemical Vapor Deposition

by

Kenneth Cheng

A dissertation submitted in partial fulfillment
of the requirements for the degree of
Doctor of Philosophy
(Materials Science and Engineering)
in the University of Michigan
2017

Doctoral Committee:

Professor Joerg Lahann, Chair
Professor Zhan Chen
Professor Jinsang Kim
Professor Michael J. Solomon

Kenneth Cheng

kencheg@umich.edu

ORCID iD: 0000-0002-4478-5757

Acknowledgement

My PhD journey have been both joyful and rewarding, and this would not have been possible without support from many individuals. I would like to thank my research advisor, Professor Joerg Lahann, for being an incredible mentor and for all his guidance, support and encouragement throughout these years. I truly admire and have learned a lot from his brilliant and creative mindset. I would like to also thank my committee members, Professor Zhan Chen, Professor Jinsang Kim and Professor Michael Solomon for the insightful discussions that helped shaped my dissertation. Furthermore, I would like to thank all my collaborators, specifically Professor Zhan Chen, Professor William Giannobile, Professor Nicholas Abbott, Professor Stefan Braese, Professor Jinsang Kim, Professor Henry Hess, Professor Neil Marsh and Professor Charles Brooks III's group, for the fruitful collaborations over the past years. I have learned a great deal of knowledge from them that has broadened my horizon.

In addition, I would also like to thank all the wonderful Lahann Lab members for their supports and encouragement throughout my PhD. Specifically, I would like to thank Xiaopei Deng for being a great mentor and friend. I'd also like to thank Sahar Rahmani, Asish Misra, Jaewon Yoon, Aftin Ross and Thomas Eyster for being my big brothers and sisters and for their

support and guidance. I am grateful to have built valuable friendships with Jake Jordahl, Stacy Ramcharan, Ramya Kumar, Nahal Habibi, Kai Liu, Jason Gregory, Nathan Jones, Daniel Quevedo, Dylan Neale, Ayse Muniz and Jonathan Gerszberg, and would like to thank them for all the supports they gave me. I'd also like to thank our post-doctoral researchers, Drs. Sangyeul Hwang, Tae-Hong Park, Kyung-Jin Lee, Hakan Durmaz, Kathleen McEnnis, Bradley Plummer, Luis Solorio, and Stephanie Christau, for their generous help and mentorship. I would like to thank the Lahann Lab at Karlsruhe Institute of Technology, especially Dr. Domenic Kratzer, Christoph Hussal and Dr. Artak Shahnas for synthetic chemistry. Further, I would like to thank my undergraduate students, Alexander de France, Diego Vargas, Greg Monroe and Alec Georgoff, for providing me the much-needed help.

On a personal note, I would like to express my sincere gratitude to my parent, Wallace and Doris Cheng, for their unconditional love and care. I am also grateful to have my brother, Vincent Cheng and sister, Kathleen Cheng, for their support. I would also like to thank Yan Dong for everything she has done for me and for making my PhD journey both brightened and colorful. Last but not least, I would like to thank all my friends who have provided invaluable support over the past years.

Table of Contents

List of Tables

List of Figures

List of Schemes

List of Acronyms

CVD	Chemical Vapor Deposition
FTIR	Fourier transform infrared spectroscopy
XPS	X-ray photoelectron spectroscopy
CD	Circular dichroism spectroscopy
Abs	Absorption spectroscopy
PPX	Poly-para-xylylene
PCP	[2.2]paracyclophane
PPV	Poly-para-phenylenevinylene
LC	Liquid crystal
PFP	Pentafluorophenyl
TRITC	Tetramethylrhodamine
DPN	Dip-pen nanolithography
ELISA	Enzyme-linked immunosorbent assay
HUVEC	Human umbilical vein endothelial cell
BAECs	Bovine aortic endothelial cells
PCL	Polycaprolactone
PLGA	Poly(lactic-co-glycolic-acid)
μCP	Microcontact printing
AFM	Atomic force microscopy
hPDL	periodontal ligament fibroblasts
GFP	Green Fluorescence protein
HGF	Human gingival fibroblasts
BMSC	Human bone marrow-derived stem cells
HOK	Human oral keratinocytes
PDGF-BB	Platelet-derived growth factor

Ad-PDGFB	PDGFB-encoded adenoviral vector
Ad-BMP-7	BMP-7 encoded adenoviral vector
MTT	3-(4,5-Dimethylthiazol-2-Yl)-2,5-Diphenyltetrazolium Bromide
PCR	Polymerase chain reaction
OTS	Trichloro(octadecyl)silane
SS	Stainless steel
5CB	4-Cyano-4'-pentylbiphenyl
E7	Cyanobiphenyl-based liquid crystal mixture
TL205	Halogentated liquid crystal mixture
MDA-98-1602	Florinated liquid crystal mixture (by EMD Functional Materials)
S-811	(S)-octan-2-yl 4-((4-(hexyloxy)benzoyl)oxy)benzoate
R-811	(R)-octan-2-yl 4-((4-(hexyloxy)benzoyl)oxy)benzoate
PAN	Polyacrylonitrile
EDC	1-Ethyl-3-(3-dimethylaminopropyl)carbodiimide
PEG	Poly(ethylene glycol)

Abstract

Chemical vapor deposition (CVD) is a widely practiced methodology for preparing thin film polymer coatings, and the coatings can be applied to a broad range of materials, including three-dimensional solid structures and low-vapor pressure liquids. Reactive poly(p-xylylene) (PPX) coatings prepared by CVD can be used as a powerful tool for surface functionalization and bio-conjugation. The first portion of this dissertation serves to extend the use of CVD-based reactive PPX coatings as a surface functionalization strategy for the conjugation of biomolecules. Micro-structured PPX coatings having multiple surface reactive groups were fabricated. Multiple orthogonal click reactions were then employed to selectively immobilize galactose and mannobiose to the micro-structured polymer coatings. The presence of different types of carbohydrate enables lectins binding for examining ligands/cell receptor interactions. This dissertation also demonstrates the use of CVD-based reactive PPX coatings as intermediate layers to immobilize adenoviral vectors onto tissue scaffolds. The ability to tether adenoviral vectors on tissue scaffolds localizes the transduction near the scaffold surface and reduces acute toxicity and hepatic pathology cause by direct administration of the viral vector, providing a safe and efficient gene therapy delivery strategy. In the second portion of this dissertation, we

explore the CVD of PPX onto surfaces coated with a thin layer of liquid crystal (LC). Instead of forming a conformal PPX coating encapsulating the LC layer, PPX assembled into an array of high-aspect ratio nanofibers inside the LC layer. The LC layer was demonstrated to act as a template where the anisotropic internal ordering of the LC facilitated the formation of nanofibers. The diameter of the nanofibers was in the range of 100 nm and could be tuned by type of LC template used, and the length of the nanofibers could be precisely controlled by varying the thickness of the LC film. The overall shape of the nanofibers could be controlled by the internal ordering of the LC template, as exemplified by the assembly of helical nanofibers using cholesteric LC as the template. PPX nanofibers could be applied to a broad range of materials, such as curved surface, metal meshes and microparticles. We successfully created nanofibers with different surface functionalities and utilized them to capture molecules of interest. We also demonstrated the synthesis of twisted nanofibers using chiral-substituted precursors. The direction and the degree of twisting of nanofibers could be controlled by the handedness and the enantiomeric excess of the chiral precursor. Finally, we showed that the LC-templated CVD method could be extended to fabricating nanofibers made of other CVD-based polymer systems, such as poly(lutidine) and poly(p-phenylene vinylene). Our work opens a new platform for designing functional polymer nanostructures with programmable geometry, alignment and chemistry. The polymer nanostructures can be attractive for applications ranging from sensors, affinity filtration, and catalytic supports.

CHAPTER 1 Introduction

The materials in this chapter were adapted from the following book chapter with permission:

- Deng, X., Cheng K.C.K. and Lahann, J., Multifunctional Reactive Polymer Coatings, CVD Polymers: Fabrication of Organic Surfaces and Devices, Wiley-VCH, Ch. 9, pp. 199-218, 2015

1.1 Background

Recent developments in the area of biotechnology have sparked multidisciplinary research efforts in biology, chemistry, and materials science. Developing bioactive surfaces with accurate spatial arrangements at the sub-micrometer scale is required for numerous biomedical applications ranging from immunoassays and biosensors to drug delivery and development of novel medical implants. To date, many methods and surface chemistries have been used for controlled surface modification [1]–[4]. Most immobilization methods fall into two categories: physical adsorption or covalent immobilization [1], [4]. Physical adsorption is typically straightforward to carry out and can be applied to most biomedical material surfaces

and even complex devices. However, physically adsorbed surface layers have limited stability and lack the same control over molecular composition when compared to covalent immobilization [1]. Covalent binding of biomolecules to a surface is generally considered superior for long-term biomedical applications. However, covalent binding requires adequate reactive sites on the substrate surface, which are not available on most standard materials surfaces. Therefore, the choices of available conjugation chemistries for covalent immobilization are typically very limited and are highly substrate-dependent. Promising examples include silane chemistry for glass/silica/silicone substrates or organosulfur compounds for gold and coinage metal surfaces [5]. Surface functionalization techniques that are compatible with polymers include plasma or corona treatments, but similarly limit the choice of available functional groups.

Like other chemical vapor deposition polymerization techniques, CVD polymer coatings based on reactive poly(p-xylylene) (PPX) are solvent-free, substrate-independent, based on low-temperature deposition, and allow for easy integration into micro-/nanofabrication schemes [6]–[8] (Figure 1-1). The basic precursor used for CVD polymerization is [2.2]paracyclophane (PCP), which forms two di-radicals at high temperature under vacuum driven by the spontaneous release of ring strain in the paracyclophane molecule [9].The radicals polymerize on solid substrates at or below room temperature and form conformal and pinhole-free polymer films [10]. The Lahann group has established an entire

library of reactive coatings with a range of different functional groups (Scheme 1-1). Reactive PPX coatings constitute a versatile and substrate-independent surface functionalization platform [11]. Functional groups compatible with the above-described paracyclophane polymerization include ethynyl, vinyl, amine, hydroxyl, aldehyde, ketone, benzophenone, maleimide, anhydride, pentafluorophenyl (PFP) ester, and 2-bromoisobutyryl groups. Paracyclophane molecules carrying one of these functional groups have been successfully synthesized and polymerized via the CVD process. We note that some unlisted functional groups, such as carboxylic acid, underwent partial elimination under the conditions of pyrolysis, that is, temperatures above 500 ∘C. The polymer coatings carrying functional groups listed in the library have been used in a range of different biomedical studies such as immobilizing proteins, peptides, sugar, DNA, and polyethylene glycol (PEG) [12]–[17].

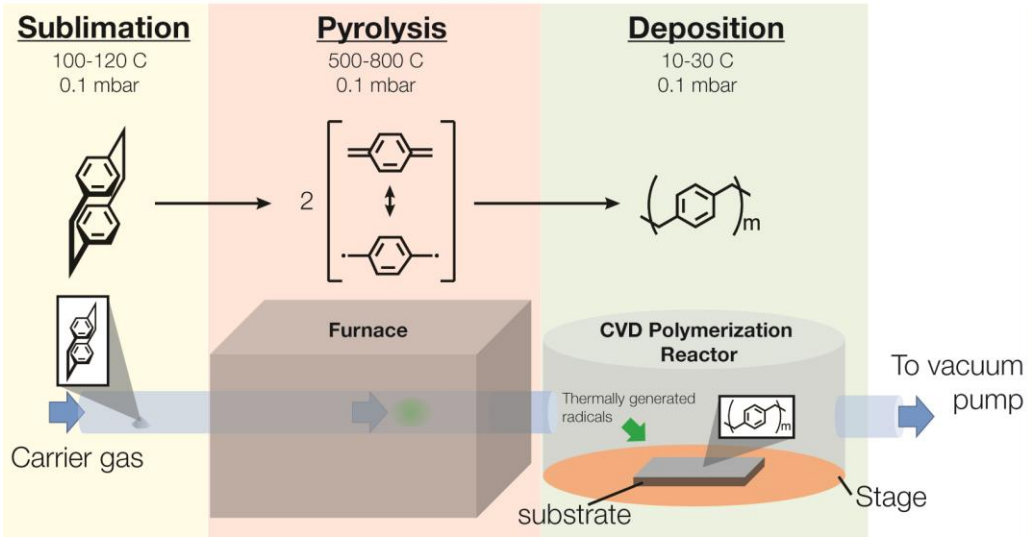

Figure 1-1: Schematic of the CVD polymerization of [2.2]paracyclophane into poly-p-xylylene thin film coating.

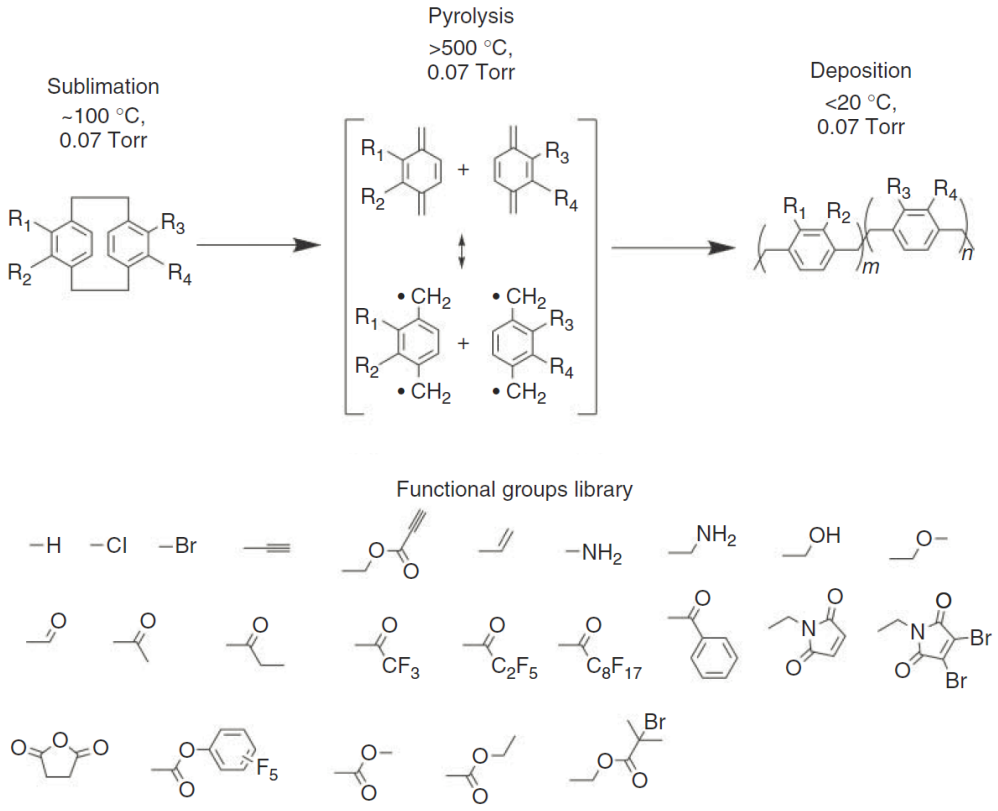

Scheme 1-1: Scheme of polymerizing different substituted [2.2]paracyclophanes via the CVD polymerization process and the functional groups library for functional PPX coatings. The functionalized [2.2]paracyclophanes sublimate around 100 ∘C under vacuum, flow with the argon carrier gas to the pyrolysis zone (>500 ◦C) and break into radicals. The radicals adsorb on the substrates placed on the cooled deposition stage (typically <20 ◦C) and polymerize to form functionalized polymer coatings [11].

To accommodate the requirements of high-precision biomedical surface engineering, the reactive polymer coatings provide many options for efficient conjugation of biomolecules and orthogonal immobilization strategies [11]. Moreover, the spatial distributions of the functional groups could be accurately controlled in many cases. Three different possible spatial arrangements for multiple functional groups are shown in Figure 1-2: gradients, random

distribution, and a micro-pattern. The three different spatial arrangements can enable different biomedical applications. The random distribution of functional groups (Figure 1-2a) is suitable for applications in need of multiple immobilized molecules evenly distributed on the substrate. Moreover, more than two reactive groups can be presented with adjustable and predefined surface ratios. This feature is ideal for preparing complex biomimetic surfaces. Gradient surfaces (Figure 1-2b) can provide continuous and gradual changes to the surface density of two orthogonal functional groups, which can in turn create a biological gradient of immobilized molecules. The gradient surfaces present interesting possibilities for cell migration or surface-directed molecular transport. A patterned surface (Figure 1-2c) can provide features for miniaturized high-throughput biomedical devices. This chapter reviews the recent progress made in using multifunctional PPX CVD coatings for high-precision bio-functionalization, with accurate control over chemical functionality as well as spatial arrangements.

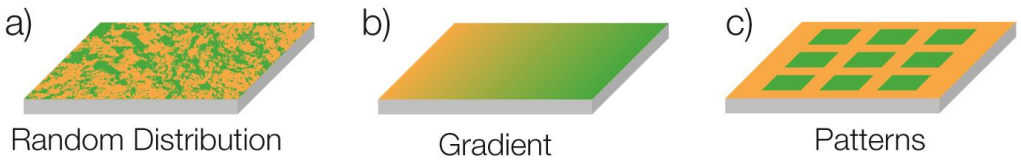

Figure 1-2: (a–c) Different functional group spatial arrangements for multifunctional polymer coatings with orthogonal functional groups. Red and green pixels each represents a different type of functional group. (Reproduced from [11])

1.2 CVD Copolymer Coatings with Randomly Distributed Functional Groups for Conjugation of Biomolecules

As summarized above, CVD copolymer coatings with randomly distributed functional groups are ideal for preparing biomimetic surface, which typically requires simultaneous presentation and manipulation of more than one biomolecule on the surface. Two or more functional groups for orthogonal surface reactions are required for avoiding chemical cross-reactions. Ideally, the surface density and ratio of each of the different functional groups can be changed. The adjustment of the surface density of the immobilized molecules can lead to different applications. Most functionalized [2.2]paracyclophane molecules carry only one single functional group. Hence, preparing multifunctional PPX CVD coatings usually involves feeding multiple types of functional [2.2]paracyclophane molecules through the CVD copolymerization process.

Figure 1-3 presents a typical example of the process underlying the deposition of multifunctional coatings via CVD copolymerization [18]. In this study, two different substituted [2.2]paracyclophanes (4-trifluoroacetyl [2.2]paracyclophane and 4-aminomethyl-[2.2]paracyclophane) were introduced into the CVD system for copolymerization. Copolymer coatings with different functional group ratios were prepared by changing the ratios of the two different precursors. Fourier transform infrared spectroscopy (FTIR), X-ray photoelectron spectroscopy (XPS), and X-ray Diffraction (XRD) were used to characterize the chemical

composition of the copolymers for different functional group ratios [18]. As shown in Figure 1-3b, the presence of amine groups was confirmed by reacting with Atto 655 NHS ester. Biotin hydrazide was used to react with the ketone group (trifluoroacetyl) followed by specific binding of tetramethylrhodamine-labeled streptavidin (TRITC-streptavidin) to the immobilized biotin. We found no cross-reaction for the two surface reactions for detecting different functional groups. The graph showing the change of normalized fluorescence intensity versus the precursor feed ratio demonstrates that the relative ratio of immobilized ligands can be changed by varying the feed ratio of different substituted [2.2]paracyclophanes. More recently, we reported the preparation a copolymer carrying PFP ester and ethynyl groups to orthogonally immobilize the growth factor and adhesion peptide on the surface (Scheme 1-2) [16]. The PFP ester is an active ester commonly used for peptide synthesis [19]. It can readily react with amine under physiological conditions and is yet more hydrolytically stable than the more widely used N-hydroxysuccinimide (NHS) ester [11]. In the specific study shown in Scheme 1-1, epidermal growth factor was immobilized by the highly efficient reaction of PFPester and amine groups. An orthogonal and highly efficient reaction, azide-ethynyl click reaction, was used to immobilize a cyclic arginyl-glycyl-aspartic acid (RGD) peptide with an azide end group. The orthogonally co-immobilized growth factor and adhesion peptide remained bioactive as shown in the study [16]. Similarly, a trifunctional PPX multifunctional CVD coating has been developed and reported by Chen et al. [20]. The trifunctional coating has an ethynyl, a

maleimide, and ketone groups, which were reacted with biomolecules functionalized with azide, thiol, and hydrazide, respectively. Simultaneous presentation of multiple ligands was demonstrated on the trifunctional coating deposited on a flat substrate as well as a stent surface with complex geometry.

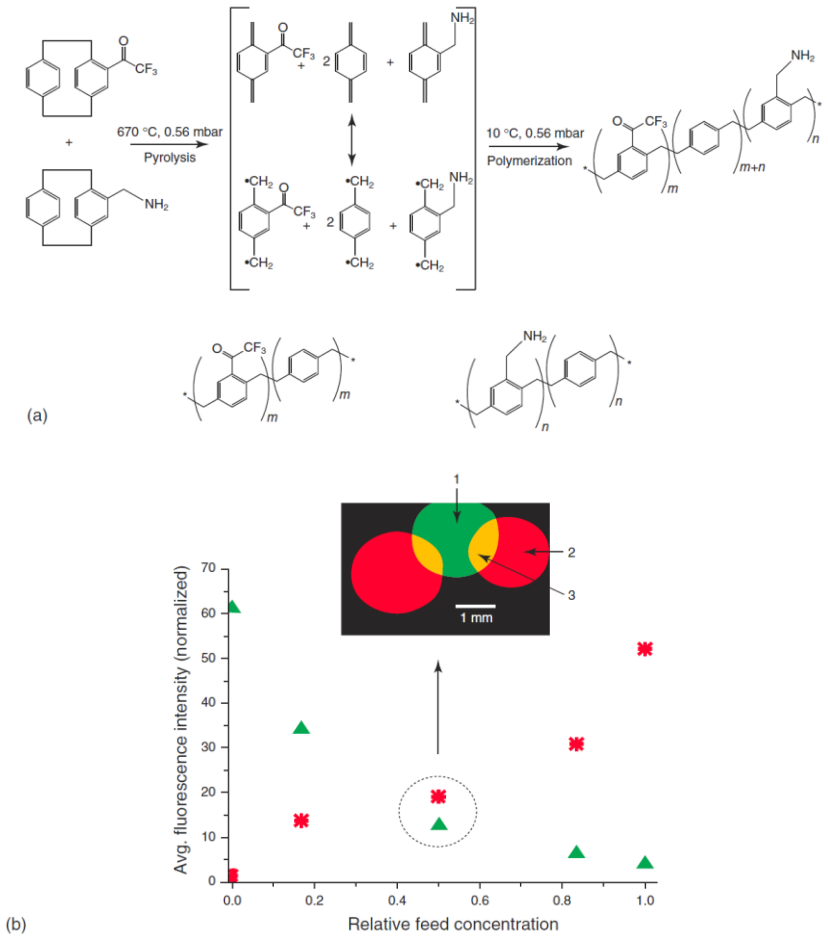

Figure 1-3: (a) Scheme of synthesizing a multifunctional copolymer via the CVD copolymerization of different functionalized [2.2]paracyclophanes. (b) Characterization of the chemical composition change of copolymers with different precursor ratios by fluorescent ligand binding. Biotin hydrazide followed by TRITC-streptavidin (green area, No. 1) and Atto 655 NHS ester (red area, No. 2) were applied to specifically target the ketone groups and amine groups, respectively. No cross reaction was observed in the overlapped areas (yellow area, No. 3) [18].

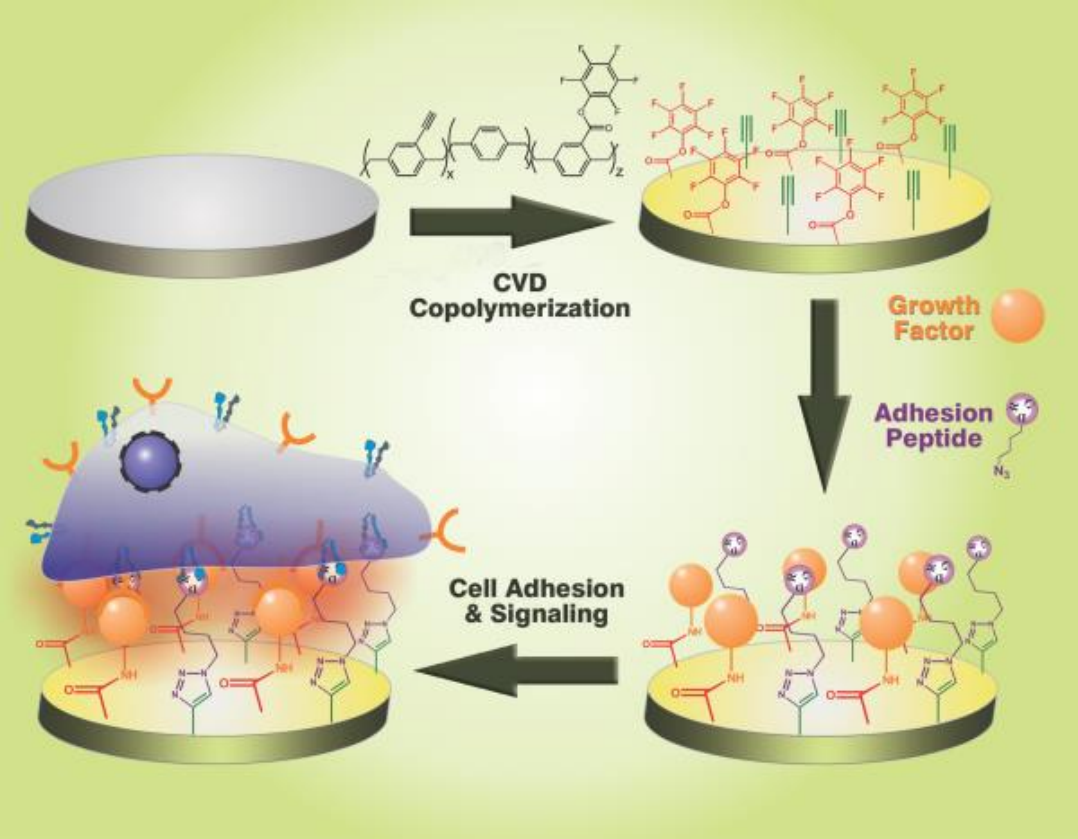

Scheme 1-2: Scheme of orthogonal co-immobilization of growth factor and adhesion peptide on a CVD copolymer by PFP ester-amine reaction and ethynyl-azide click reaction [16].

1.3 Multifunctional Gradient Coatings via CVD polymerization

Surface gradients with a gradual change in chemical composition play an important role in many applications as well as in the study of living cell migration and of combinatorial materials discovery [21]–[23]. In light of this, many gradient fabrication methods have been developed including those using microfluidics, photochemical methods, electron/X-ray irradiation, gel diffusion, and so on [23]–[26]. Nevertheless, many of these methods require relatively complicated procedures and are only applicable to certain substrates. In addition, they

are not all biocompatible. In this following section, we will discuss the use of chemical vapor deposition polymerization of substituted [2.2]paracyclophanes for generating biocompatible, continuous, and substrate-independent chemical composition gradients.

Elkasabi et al. [27] have demonstrated the use of a modified CVD system to generate polymer films bearing continuous chemical composition gradients. This CVD system for gradient fabrication consists of two separate sources that are connected, in a counter-flow setup, to the deposition chamber, as shown in Figure 1-4. With this counter-flow setup, radicals generated from two differently substituted precursors deposited anisotropically onto the substrates. The radicals copolymerized in the form of two composition gradients. In this proof-of-concept study, trifluoroacetyl-[2.2]paracyclophane and aminomethyl- [2.2]paracyclophane were used as the two precursors for the counter-flow CVD process. Both Fourier-transformed infrared spectroscopy (FTIR) and XPS con- firmed a gradual change in chemical composition along the longitude direction of the gradient (Figure 1-4). The composition gradients were found to be in the centimeter scale. Fluorescence-labeled ligands were also immobilized on the composition gradient to visualize and quantify the orthogonal reactivity of the two composition gradients [27]. These characterizations all confirmed that continuous composition gradients are successfully prepared using this counter- flow CVD system. Because CVD polymerization is a substrate-independent process, the composition gradients can be applied onto a wide range of materials. In addition, the materials to be coated do not require any pretreatments, making this

counter-flow CVD process a simple yet universal method for generating continuous composition gradients. In a more recent study, Elkasabi et al. [28] prepared a wider range of composition gradients and demonstrated the preparation of biomimetic gradients. Specifically, composition gradients bearing amino and aldehyde groups were prepared. The virus-biotin-avidin-biotin-method (VBABM) was used to chemically immobilize cell-signaling adenovirus onto gradients surfaces, resulting in a gradient of adenovirus. When cultured on these adenovirus gradients, human gingival fibroblasts exhibited asymmetric transduction with full confluency, showing that a controlled gradient of cellular activity can be achieved with these biomimetic gradients. These bioactive gradients have potential use for mimicking biological gradients to study cell migration and differentiations, as well as in other advanced delivery studies that involve gradients of therapeutic genes.

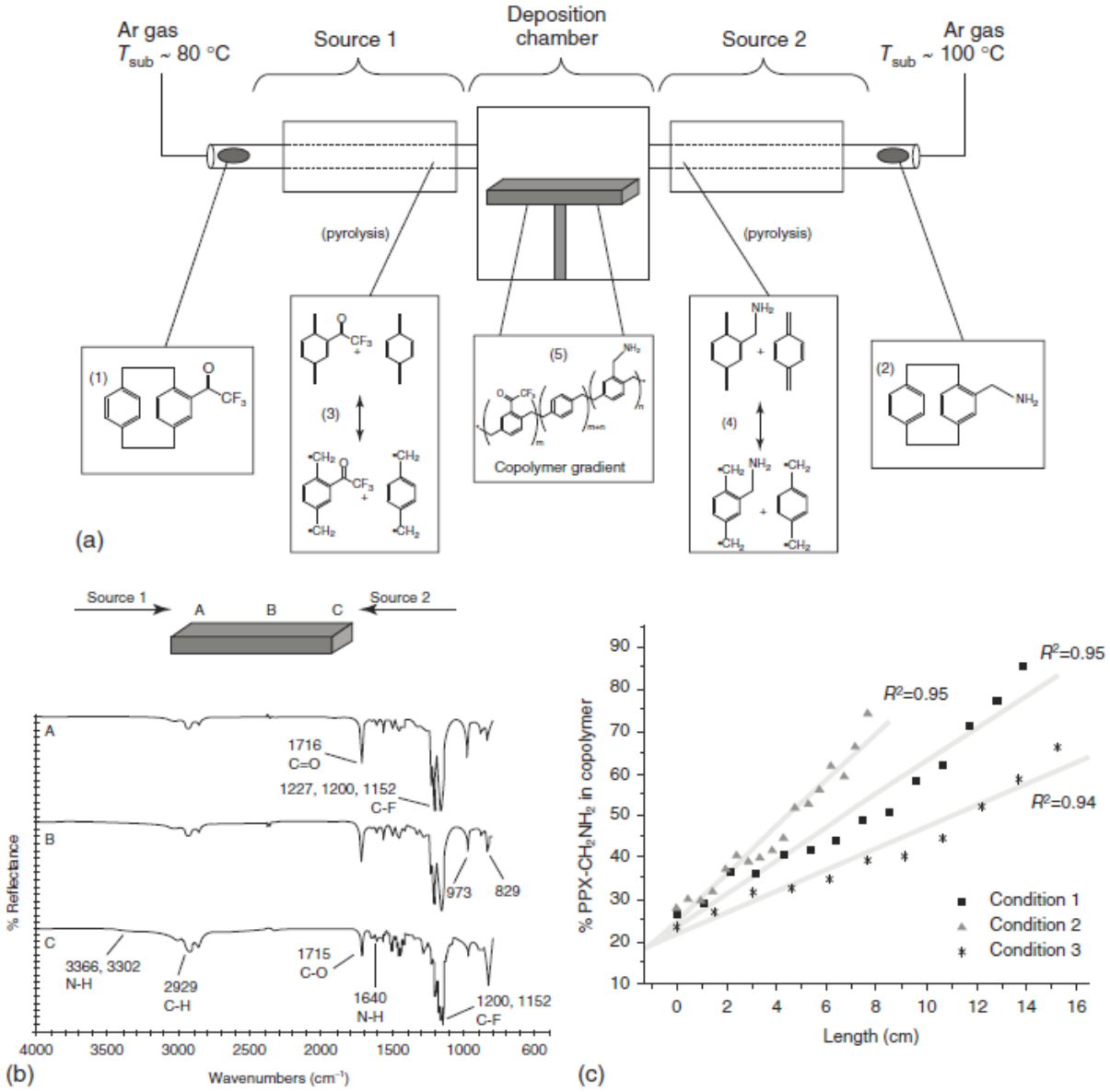

Figure 1-4: (a) Scheme of the custom-built two-source CVD system. Each source has a quartz tube passing through a three-zone furnace and connecting with the deposition chamber. The whole system is under vacuum during the CVD process. For gradient generation, the sample holder does not rotate. In this specific study, the trifluoroacetyl and the aminomethyl groups form a chemical composition gradient [27]. (b) FTIR spectra of the CVD polymer gradient. (c) Copolymer compositions along the surface gradient based upon XPS survey spectra. Changing sublimation rates and argon flow rates can be used to control the slope of the compositional change within a certain distance [27].

1.4 Functional Coatings with Micro- and Nano-patterns

Micro- and Nano-patterning techniques are widely used in electronics and a lot of the patterning techniques are also applicable for biomedical devices [29]–[31]. They are of vital importance to the development of high-throughput bioassays, miniaturized biomedical devices, and precise surface design and engineering for cell culture scaffolds/substrates. These techniques include soft lithography, photolithography, stencil-assisted patterning, jet patterning, laser-guided writing, and so on [30]. We have applied several different micro-/nano-patterning techniques to the functional PPX CVD coatings. As shown in Figure 1-5, the micro-patterns can be generated post CVD (e.g., micro-contact printing, photo patterning) or during CVD (e.g., applying micro-stencils during CVD) [32]. Nano-patterning technique such as dip-pen nanolithography (DPN) were also applied in our recent work [33]. Details of each patterning techniques are described in

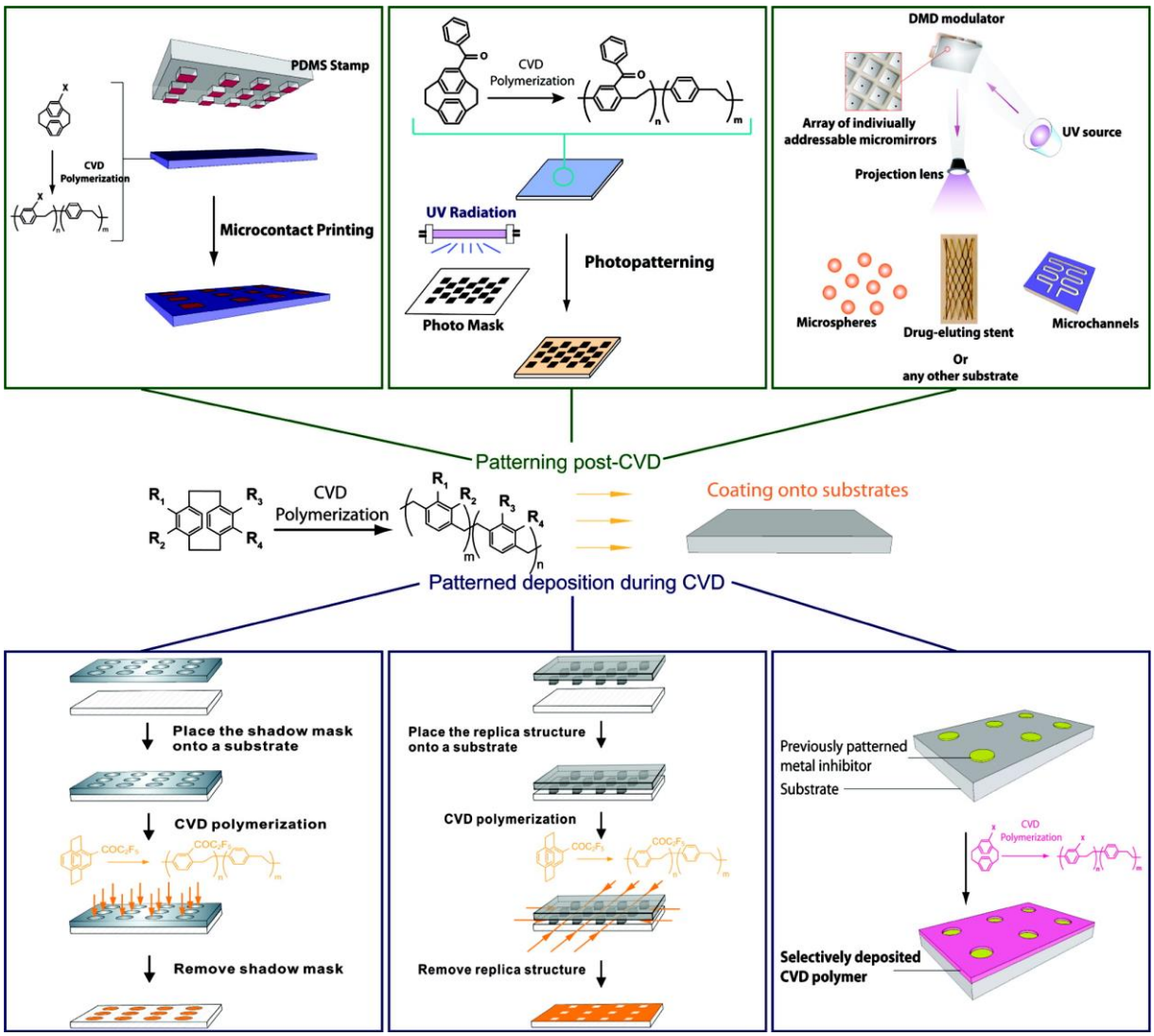

Figure 1-5: Scheme of surface patterning techniques using reactive CVD coatings. Methods can be categorized into two groups: patterning post-CVD (e.g., μCP and photopatterning processes), and patterning deposition during CVD with the assistance of masking molds/microstencils or metal inhibitors applied before the CVD process [32].

1.5 CVD polymerization onto liquid substrates

Polymer coatings prepared by CVD polymerization have traditionally been applied onto solid materials. Recently, a number of research groups has demonstrated that these CVD polymers can also be applied on liquids. In particular, Keppener et. al. demonstrated that when CVD polymerization of dichloro-[2.2]paracyclophanes is performed on liquid droplets with low vapor pressure, such as silicon oil and glycerol, polymerization occurs at the liquid-vapor interface [34]–[36] (Figure 1-6 & Figure 1-7). During CVD polymerization on liquid droplets, initiation first begin at the liquid-vapor interface, forming countless solid polymer aggregates, at the interface. As the polymer chains propagate further, the aggregates expand up to a point where they coalesce and form into an complete polymer film encapsulating the liquid droplet [37]. The ability to encapsulate liquid droplets via CVD polymerization enables the development of microlenses [38], sensors [39]and micro prisms [40]. CVD polymerization onto liquids is not limited to PPX polymer system. Gupta et. al. demonstrated using iCVD to encapsulated liquids with low vapor pressures, such as ionic liquids and silicone oils [41], [42].

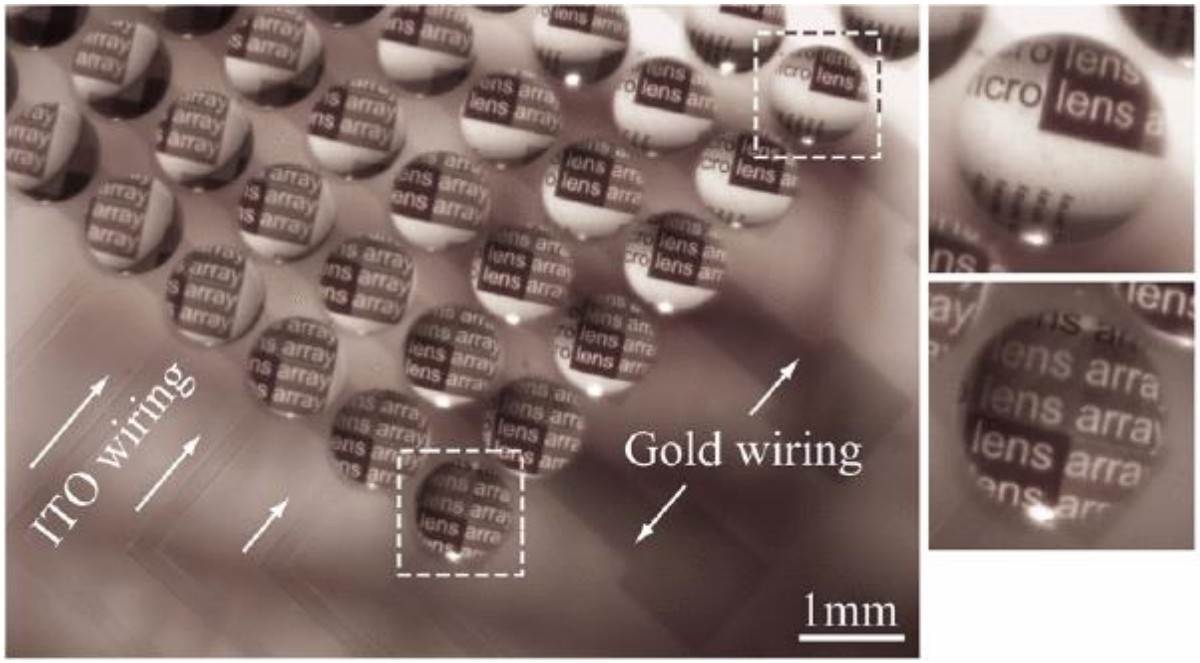

Figure 1-6: Lens array with lens diameter of 1mm. Each lens contains silicone oil encapsulated with a layer of parylene coating [35].

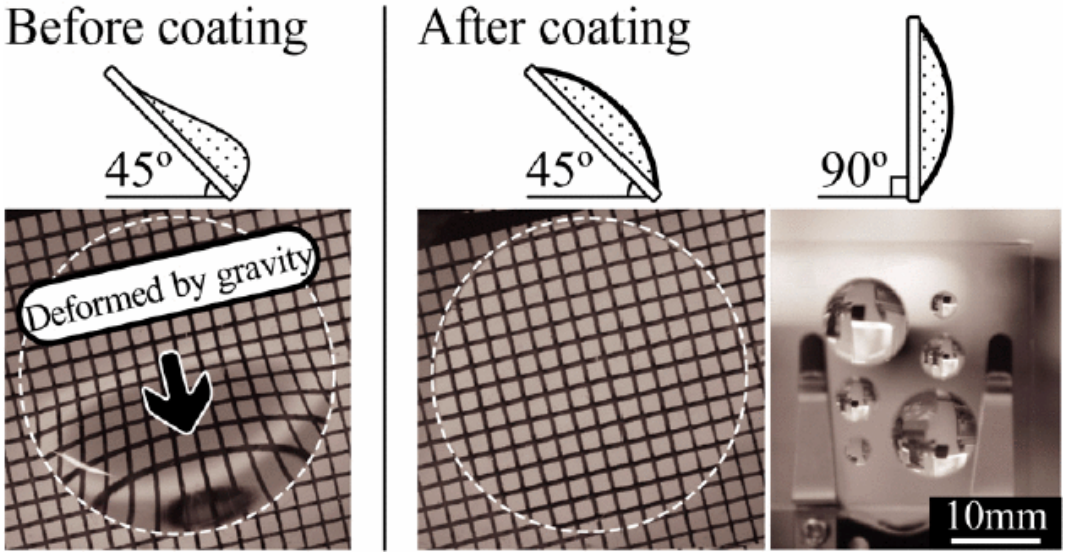

Figure 1-7: After coated with 1000nm parylene film, a liquid lens of 10mm diameter (liquid mass 43mg) can be used even in a vertical position without any deformation caused by gravity [35].

1.6 Thesis Outline

The work described in this dissertation can be divided into two parts: The first part of the dissertation (Chapter 2) builds upon previous works on using reactive polymer coatings prepared by CVD polymerization for bioconjugation and demonstrates how we can spatio-selectively conjugate carbohydrates and peptides. Chapter 2 also addresses the use of CVD polymer coatings as an intermediate layer to conjugate adenoviral vectors onto tissue scaffolds and demonstrates that the virus-conjugated tissue scaffolds allow for a safe and efficient gene therapy applications.

The second part of the dissertation (Chapter 3-5) explores the CVD of PPX onto liquid crystals (LC), a class of structured fluid. Chapter 3 shows that instead of forming thin films, the polymer assembles into an array of nanofibers inside the LC layer. The mechanism of the nanofiber formation is examined. The versatility of the nanofiber synthesis method is also evaluated. Chapter 4 addresses the discovery of the formation of twisted nanofibers via CVD polymerization of chiral-substituted [2.2]paracyclophane in nematic LC. The mechanism of the formation of twisted nanofibers is investigated. Chapter 5 describes the ability to extend this nanofiber synthesis method to other types of CVD-based polymer systems. Two classes of CVD-based polymer system, poly(lutidine) and poly(phenylene vinylene), are examined. Chapter 6 provides summary of key findings and outlines potential future directions.

CHAPTER 2 Engineering the Binding of Biomolecules on CVD-based Reactive Polymer Coatings

The materials shown in this section were adapted from the following peer-reviewed journal article with permission:

(1) Bally, F., **Cheng, K. C. K.**, Nandivada, H., Deng, X., Ross, A. M., Panades, A., Lahann, J., "Co-immobilization of biomolecules on ultrathin reactive chemical vapor deposition coatings using multiple click chemistry strategies," ACS Applied Materials and Interfaces, 2013, 5(19), 9262-9268.

(2) Hao, J., **Cheng, K. C. K.**, Kruger, L., Larsson, L., Sugai, J., Lahann, J., Giannobile, W. V., "Multi-Growth Factor Delivery via Immobilization of Gene Therapy Vectors". *Advanced Materials*, 2016, 28(16), 3145-3151.

2.1 Introduction

In this chapter, reactive polymer coatings prepared by CVD polymerization of substituted [2.2]paracyclophanes were used to engineer the binding of biomolecules onto the polymer coated-materials.

- In Section 2.2, we discuss the use of multiple orthogonal click chemistry reactions to selectively immobilize multiple biomolecules of interest.
- In Section 2.3, we demonstrate the ability to utilize the CVD-based reactive polymer coatings as an intermediate layer to immobilize viral vectors onto tissue scaffolds for use in gene-therapy for bone regeneration application.

2.2. Co-immobilization of Biomolecules on Ultrathin CVD-based Reactive Polymer Coatings using Multiple Click Chemistry Strategies

2.2.1 Background and Objective

Over the last decades, advanced biomaterials have been widely developed for medical applications.[43] The surface functionalities of the materials determine interactions between an abiotic material and a biological organism. Ubiquitous in nature, peptides, sugars, and other recognition ligands play a significant role in numerous biological events. For example, they may trigger some signaling cascades within the cell and modulate cell receptor activities that influence cell adhesion or proliferation. [44] As a result, mimicking this rich biomolecular environment is needed for improved understanding of cellular behavior and mechanisms. The spatially controlled distribution of biomolecules and the development of cell culture substrates require stable, yet designable surfaces.[1] Versatile surface engineering techniques have thus

become a major focus of material scientists. Tailoring surface properties, while preserving the inherent physical and mechanical properties of a bulk material, represents an elegant approach for the development of biomaterials. In this context, chemical vapor deposition (CVD) polymerization is a robust solvent-free process that enables surface modification.[45], [46] Stable, homogeneous coatings can be produced on a multitude of substrates including three-dimensional scaffolds and thermosensitive materials. Several adaptations of the CVD polymerization process have been reported in the literature,[6], [47] which contributes to the versatility of the technique. For instance, Gleason and co-workers have suggested plasma polymerization[48] or initiated chemical vapor deposition.[49] CVD polymerization of substituted [2.2]paracyclophanes has also been widely studied for the design of biointerfaces.[32] Originally developed by Gorham[50] and commercialized under the parylene brand, coatings made by vapor-based polymerization of [2.2]paracyclophanes have been approved by the FDA for biomedical use.[51] However, because of the lack of functional groups in these original parylene coatings, direct immobilization of biomolecules is not possible without subsequent surface modification. In contrast, the Lahann Lab has focused on CVD polymerization of substituted [2.2]paracyclophanes using a custom-designed CVD system in order to synthesize chemically active surfaces for controlled immobilization of biomolecules.[52] The synthesis of a wide range of [2.2]paracyclophanes with appropriate functional groups is now well-established[53] and substituted poly(*p*-xylylenes) were prepared

that contained amines,[54] esters,[12], [55] ketones with fluorinated groups,[56] or aldehydes.[57] In addition, CVD polymerization has also been extended to the production of multifunctional coatings,[18] including those displaying functional film gradients.[27], [28]

The role of the CVD coatings is the presentation of chemically addressable functional groups for targeted biomolecular immobilization. To obtain a stable interface, covalent bonding of biomolecules with reactive groups present at the surface is the preferred strategy. The functional groups, natively or synthetically present on the biomolecules, may be exploited as reactive partners for immobilized ligands. Such biomolecular immobilization benefits from chemical reactions that are quantitative, highly specific, and tolerant to many functional groups, such as click reactions.[58] Click chemistry was introduced by Sharpless and co-workers in 2001[59] and has since been widely used by material scientists for surface modification.[60]–[62] There are numerous click reactions including, but not limited to, Huisgen 1,3-dipolar cycloaddition, Diels–Alder, Staudinger, thiol–ene, and Aza-Wittig reactions.[63] However, the most commonly used click chemistry reaction is the copper(I)-catalyzed Huisgen 1,3-dipolar cycloaddition between azido- and ethynyl-terminated compounds. As a result of this coupling reaction, triazoles are formed, which are stable linkers under physiological conditions.[64] For instance, immobilization of azido-terminated sugars has been successfully achieved onto ethynyl-functionalized self-assembled monlayers (SAMs) via Huisgen cycloaddition.[65]–[69] Other recent studies reported spatially directed immobilization by Huisgen cycloaddition

of biotin[58], [70], carbohydrate[71], and peptide[16] derivatives. To consider surface functionalization by click chemistry on a broader range of substrates, CVD polymerization of ethynyl-substituted [2.2]paracyclophanes has been studied.[58] Azido-functionalized biotin was successfully immobilized on poly(4-ethynyl-*p*-xylylene-*co*-*p*-xylylene) and the spatially controlled copper-catalyzed Huisgen cycloaddition has also been enabled by dip-pen nanolithography (DPN).[33] This process led to nanostructuring of a broad range of substrates, including soft polymers. Copper-free click chemistry has also been investigated on CVD coatings for bio-orthogonal "double-click" reactions;[70] thereby combining copper-catalyzed and copper-free click chemistry for the immobilization of biotin and Oregon 488 on a single multifunctional surface. Very recently, a copolymer coating containing ethynyl and aldehyde groups for the coimmobilization of two different biomolecules has been synthesized by CVD polymerization.[72] However, to date, no study has combined spatio-selective microstructuring with multiple, distinct click chemistry reactions on a single CVD coating.

Herein, we first prepared ultrathin poly(4-ethynyl-*p*-xylylene-*co*-*p*-xylelene) films by CVD polymerization as a proof of principle of using homogeneous coatings to explore the effect of single biomolecules on a specific biological event. For this purpose, we tuned the thickness of the polymer coatings in a controlled fashion and established the dependence of the film thickness on the monomer feed amount. In order to show the functionality of such thin films, several biomolecules were immobilized on CVD coatings including azido-terminated

saccharides and peptides. Their influence on lectins conjugation and cell adhesion respectively has been investigated. Then, we produced microstructured coatings combining two types of functional parylenes on the same substrate that may undergo subsequent, orthogonal click reactions. The micropatterning of the CVD coatings has been performed by sequential deposition of poly(4-ethynyl-*p*-xylylene-*co*-*p*-xylelene) and poly(4-formyl-*p*-xylylene-*co*-*p*-xylylene) *via* vapor-assisted micropatterning in replica structures (VAMPIR).[73] Finally, the orthogonal reactivity of the CVD coating was confirmed by the selective bonding of saccharides through Huisgen cycloaddition and aldehyde-hydrazide coupling. This work is an important demonstration of the immobilization of various biomolecules on a microstructured CVD coating via multiple orthogonal click chemistry reactions. The selective immobilization of different sugars may be a promising means of assessing ligands/cell receptor interactions and synergic effects of a cascade of reactions on biological events.

2.2.2 Experimental Methods

CVD Polymerization

4-Ethynyl[2.2]paracyclophane[74] and 4-formyl[2,2]paracyclophane[57] precursors were synthesized as described elsewhere. Both precursors were sublimated at 90–110 °C under low pressure (<0.07 Torr) before entering the pyrolysis furnace, maintained at 660 °C, at an

argon flow rate of 20 sccm. Polymerization of the precursors occurred by vapor-deposition on the substrate, kept at 15 °C, in the deposition chamber. Micropatterns containing two different CVD coatings were prepared via the previously developed VAMPIR technique.[73] Briefly, a layer of poly(4-formyl-*p*-xylylene-*co*-*p*-xylylene) was first homogeneously coated on the substrate. Then a patterned PDMS microstencil (squares of 200 μm × 200 μm), fabricated as previously described[73] was placed on the coated substrate, and a second layer of poly(4-ethynyl-*p*-xylylene-*co*-*p*-xylylene) was subsequently deposited onto the surface not covered by the microstencil to generate the micropatterns.

Characterization of CVD Films

Fourier transform infrared spectroscopy (FTIR) was performed on a Nicolet 6700 spectrometer at a grazing angle of 85°. The thicknesses of the polymer layer were measured using an EP^3–SW imaging ellipsometer (Nanofilm AG, Germany) at a wavelength of 532 nm and at an angle of incidence of 65°. An anisotropic Cauchy parametrization model was used for curve fitting. The error bars on the thickness of the polymer films were calculated from three different CVD experiments, where each experiment was based on three parallel samples. For the mapping mode, data was recorded by an imaging scanner with a lateral resolution of 1 μm with a field of view of about 100 μm × 500 μm.

Poly(4-ethynyl-*p*-xylylene-*co*-*p*-xylylene):[58] FTIR (cm^{-1}) = 833, 894, 1158, 1251, 1411, 1454, 1493, 1513, 1605, 1699, 1900, 2102, 2859, 2926, 3015, 3286.

Poly(4-formyl-*p*-xylylene-*co*-*p*-xylylene):[57] FTIR (cm^{-1}) = 839, 905, 1158, 1235, 1453, 1500, 1567, 1608, 1688, 2732, 2922.

Immobilization of Azido-Functionalized Biomolecules by Microcontact Printing

A solution containing azido-saccharides (1-azido-1-deoxy-β-D-glucopyranoside or 1-azido-1-deoxy-β-D-galactopyranoside, 10 μg/mL) or azido-peptides (YIGSR-N_3, 20 μg/mL) and sodium ascorbate (1 mM) in a 2:1 mixture of water:tert-butyl alcohol was prepared. These azide solutions were spread on poly(4-ethynyl-*p*-xylylene-*co*-*p*-xylylene) coatings and the substrates were dried using N_2. Patterned PDMS stamps (squares of 50 μm x 50 or 250 μm × 250 μm) were created as previously described.[12] Stamps were oxidized for 20 min using a UV-ozone cleaner (Jelight Co. Inc., Irvine, CA) before use and inked with $CuSO_4$ solution (1 mM in methanol). The stamps were then kept in contact with the CVD coating for 12–18 h for the saccharides and for 3 h for the peptide.

For the peptide-patterned substrate, a similar microcontact printing procedure was repeated (after peptide microcontact printing) with an unpatterned flat PDMS stamp to immobilize azido-functionalized poly(ethylene glycol) (PEG-N_3, M_W = 5000 g/mol, 50 μg/mL)

on the remaining areas. Substrates were then washed with aqueous phosphate buffer (PBS) containing 0.02% (v/v) Tween 20, PBS and distilled water.

Immobilization of Mannobiose and Azido-Saccharide on Patterned CVD Coatings (obtained via VAMPIR)

The patterned substrate was first incubated in an aqueous solution containing adipic acid dihydrazide (100 mM, pH 4–5) overnight. After washing, the surface was incubated in an aqueous solution (pH 4–5) of mannobiose (10 mM) and sodium periodate (40 mM) for 5 h, followed by repeated washing with distilled water. Subsequently, the substrate was incubated in an aqueous solution containing 1-azido-1-deoxy-β-D-galactopyranoside (1 mg/mL), $CuSO_4$ (1 mM), and sodium ascorbate (3 mM) overnight, followed by repeated washing with distilled water.

Lectin Conjugation

For lectin conjugation of β-glucose- or β-galactose-patterned substrates obtained by microcontact printing, samples were incubated for 1 h in buffer solution (PBS with 0.02% (v/v) Tween 20 and 0.1% (w/v) bovine serum albumin) containing respectively fluorescein-

conjugated concanavalin A (FITC-Con A, 50 μg/mL) and rhodamine-labeled peanut agglutinin (TRITC-PNA, 50 μg/mL). For lectin conjugation of mannobiose- and β-galactose-patterned substrate obtained via VAMPIR technique, the sample was incubated in a buffer solution containing either rhodamine-labeled concanavalin A (TRITC-Con A) or fluorescein-conjugated peanut agglutinin (FITC-PNA) for 3 h. The buffer solution consisted of 4-(2-hydroxyethyl)-1-piperazineethanesulfonic acid (HEPES) buffer solution (10 mM) with MnCl (1 mM), $CaCl_2$ (1 mM), and NaCl (0.15 M). Substrates were then washed with the incubating buffer, PBS and distilled water. Fluorescence micrographs were captured using a Nikon TE200 fluorescence microscope.

Human Endothelial Cell Culture

Cryopreserved human umbilical vein endothelial cells (HUVECs) were purchased from Lonza (Walkersville, MD) and cultured in complete Endothelial Growth Medium (EGM) containing 2% fetal bovine serum. Cells were cultured in 75 cm^2 tissue culture-treated polystyrene flasks, maintained at 37 °C in a humidified atmosphere of 5% carbon dioxide and cell culture medium was replaced every other day until 80% confluence was attained. Cells were harvested from the flasks using 0.25% trypsin/ethylene-diaminetetraacetic acid solution and seeded on the substrates as needed.

For the cell patterning studies, peptide-patterned surfaces were rinsed with Dulbelcco's PBS (D-PBS) and placed in a multiwell plate. Cells were harvested from the flask and resuspended at a density of 1×10^4 cells/mL in endothelial basal medium (EBM) without serum and 1 mL was added to each well. They were allowed to adhere for 1 h without serum at 37 °C. Subsequently, this media was replaced with medium containing serum (EGM) and cells were maintained for 10 h. Substrates were washed with D-PBS, fixed with formaldehyde (4% v/v in D-PBS), permeabilized with TritonX-100 (0.1% v/v in D-PBS) and stained with rhodamine-conjugated phalloidin. Samples were mounted with Prolong Gold containing DAPI. Substrates were imaged using an Olympus BX-51 fluorescence microscope (Microscopy and Image Analysis Laboratory, University of Michigan, Ann Arbor).

2.2.3 Results and discussion

The polymerization of 4-ethynyl[2.2]paracyclophane was performed by the Gorham method in a custom-designed CVD system. As described in Scheme 2-1, the precursor was sublimated before being pyrolyzed under vacuum in order to form quinodimethane intermediates. Poly(4-ethynyl-*p*-xylylene-*co*-*p*-xylylene) was then deposited by spontaneous polymerization of these intermediates in the deposition chamber at 15 °C. As confirmed by a scotch tape test[57] and by solubility tests in various media,[58] the polymer films coated on

silicon and gold wafers adhered to the substrates. FTIR analyses confirmed the presence of ethynyl groups on the CVD surface, as indicated by strong stretching modes of the C–H bonds at 3286 cm^{-1} and the carbon/carbon triple bonds at 2102 cm^{-1}.

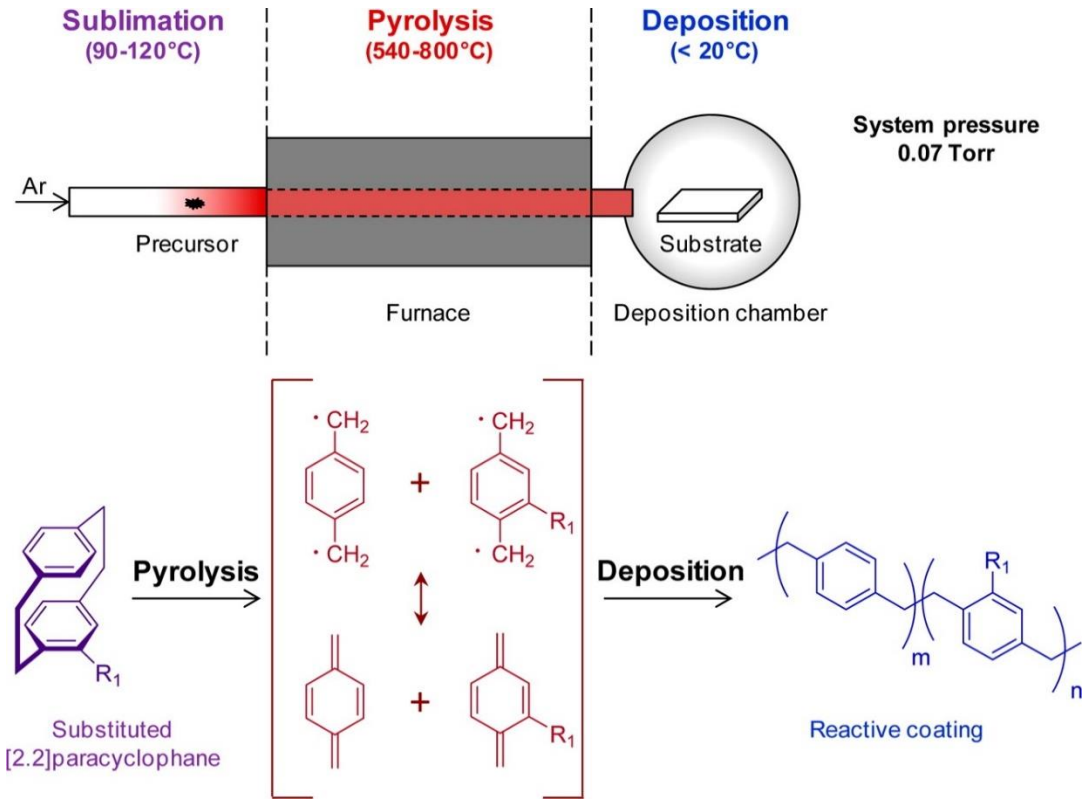

Scheme 2-1: CVD Polymerization Process of Functional Poly(p-xylylene) Polymers

Depending on the amount of precursor (3–80 mg) used for CVD polymerization, poly(4-ethynyl-*p*-xylylene-*co*-*p*-xylylene) films (Figure 2-1a) with various thicknesses were obtained. The experimentally observed thicknesses ranged from 2.7 to 90 nm, as shown in Figure 1b. The coating thickness was determined by ellipsometry and the reproducibility of the process resulted

in remarkably small error bars. The thickness of the polymer film increased linearly with the amount of precursor used for CVD polymerization. This observation allows for facile fine-tuning of the coating thickness for the requirements of a given application. Furthermore, ultrathin reactive films of few nanometers can be produced, which may further increase the potential applications of this CVD technique, for instance for coating of biosensors. Even below 20 nm, the thickness of the coating can be adjusted by the precursor amount.

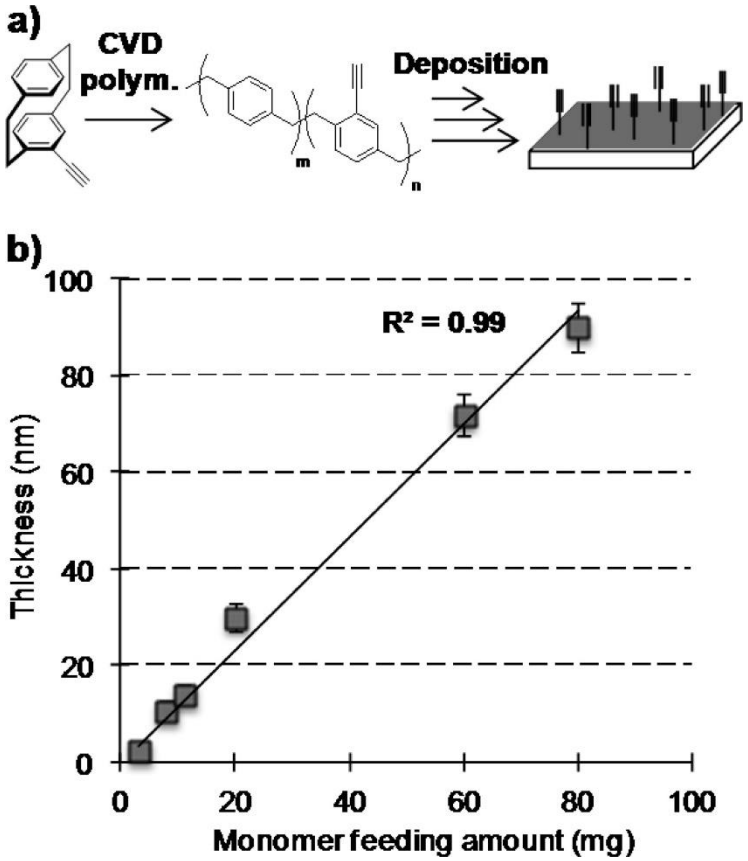

Figure 2-1: CVD polymerization process for the poly(4-ethynyl-p-xylylene-co-p-xylylene) preparation: (a) illustration of the coating process and (b) polymer film thickness as a function of the feeding amount of precursor.

The reactivity of poly(4-ethynyl-*p*-xylylene-*co*-*p*-xylylene) was confirmed by spatially directed biomolecular immobilization as described in Scheme 2-2. The ethynyl functionality was tested against an azido-terminated biomolecule, in the presence of copper(II)sulfate and sodium ascorbate at room temperature. Under these conditions, copper(I)-catalyzed Huisgen 1,3-dipolar cycloaddition was expected to occur on the substrates and bind biomolecules onto the surface through the formation of five-membered heterocyclic triazoles. For this purpose, a poly(4-ethynyl-*p*-xylylene-*co*-*p*-xylylene) coating was exposed to azido-functionalized saccharides (1-azido-1-deoxy-β-D-glucopyranoside and 1-azido-1-deoxy-β-D-galactopyranoside) or azido-functionalized peptides (YIGSR-N_3) solutions. The spatial selectivity of the Huisgen cycloaddition was ensured by microcontact printing of a Cu(I) catalyst. A square-patterned PDMS stamp was inked with copper sulfate and kept in contact with the substrates for several hours. Saccharide-pattering was then evidenced by incubation of the substrates with fluorescently labeled lectins and subsequent imaging by fluorescence microscopy. As shown in Figure 2-2a, fluorescein-conjugated concanavalin A (FITC-Con A), a β-glucose-binding lectin, was successfully immobilized on β-glucose-modified square islands patterned on the substrate, because fluorescence intensity is higher in the regions where saccharides were previously immobilized. Similarly, Figure 2-2b confirms the immobilization of β-galactose on the square islands of the patterned substrate, because rhodamine-labeled

peanut agglutinin (TRITC-PNA), a specific lectin for β-galactose, was primarily visualized. The slight fluorescence observed outside the square islands probably originates from free residual fluorescently labeled lectin that was not removed by rinsing.

As previously described, patterned peptide-immobilization was also performed by microcontact printing of a laminin-derived peptide (YIGSR) on poly(4-ethynyl-*p*-xylylene-*co*-*p*-xylylene) coatings. Ellipsometry images shown in Figure 2-2c reveal a slightly higher thickness of the bioactive coating outside the square islands, which demonstrates a successful immobilization of YIGSR. A thickness difference of about 1 nm in ellipsometry can correspond to a peptide monolayer immobilized on a substrate.[58] This result has been confirmed by the selective adhesion of human endothelial cells (HUVECs). As depicted in Figure 2-2d, the presence of HUVECs was observed, where the cell-adhesive peptide (YIGSR) was immobilized. These findings confirm an efficient patterning by microcontact printing and good selectivity of the click reaction for spatially directed immobilization of peptide. To avoid uncontrolled cell adhesion, when proteineaceous serum is used, we also immobilized azido-PEG on the remaining ethynyl-terminated areas by microcontact printing prior to cell culture experiments being conducted. As expected, minimal cell attachment was observed on PEG-modified regions.

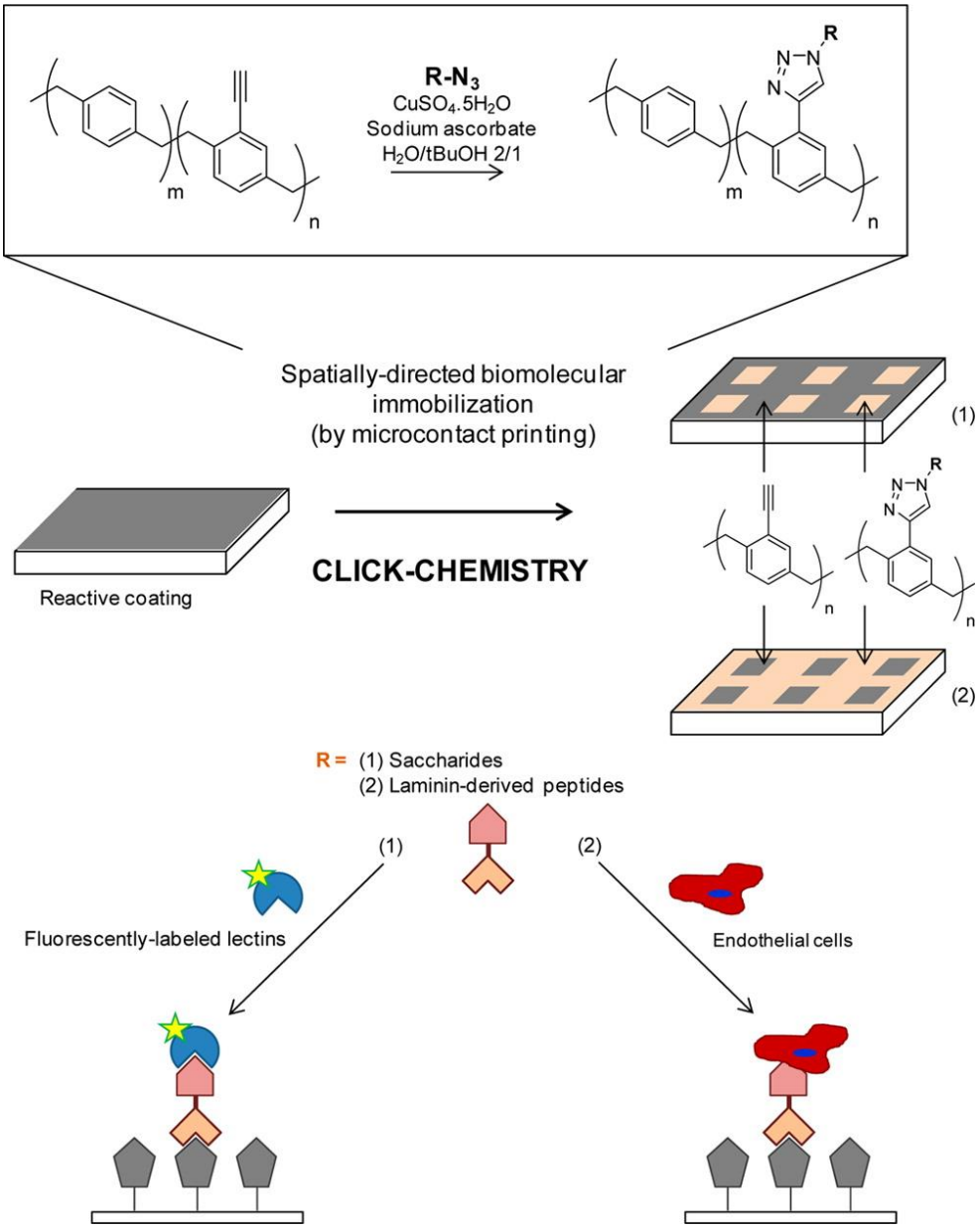

Scheme 2-2: Schematic Illustration of the Strategy Used for Spatially-Directed Biomolecular Immobilization by Microcontact Printing via Click Chemistry

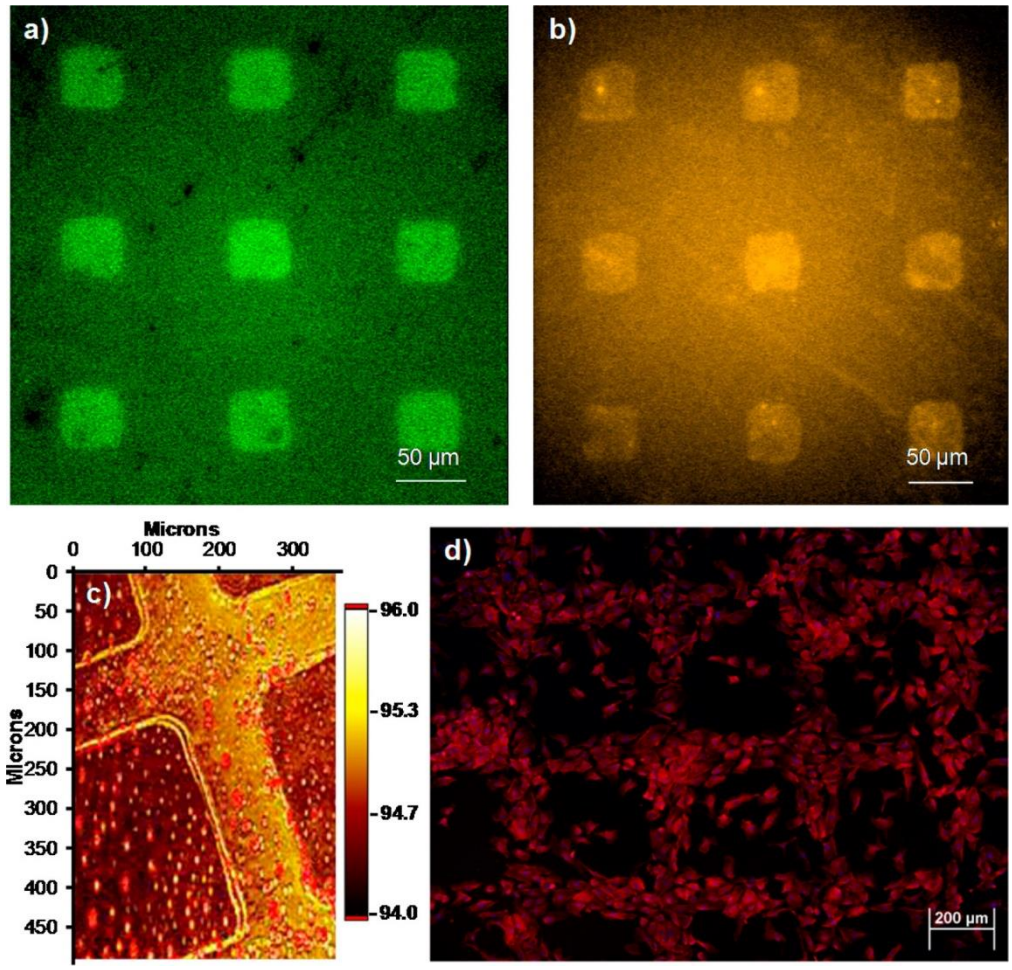

Figure 2-2:(a, b) Fluorescence micrographs of samples prepared by immobilization of saccharides and fluorescently labeled lectins on the square islands; (c) ellipsometry imaging of samples prepared by immobilization of peptides outside the square islands and (d) f luorescence micrographs of subsequent adhesion of HUVECs. Immunostaining with rhodamine-conjugated phalloidin (for actin) and DAPI (for nucleus) was carried out.

The microstructuring of different functional groups that can engage in orthogonal click reactions on the CVD substrate was attempted. For this purpose, two successive CVD steps were performed to generate a pattern with multiple functional parylenes through the VAMPIR technique.[73] The CVD coatings were selected to subsequently undergo different click

chemistry reactions. First, the sample was homogeneously coated with poly(4-formyl-*p*-xylylene-*co*-*p*-xylylene). The second CVD step then creates the functional pattern by polymerization of poly(4-ethynyl-*p*-xylylene-*co*-*p*-xylylene). To confirm the presence and the reactivity of both functional groups that can undergo subsequent click chemistry reactions, we immobilized two different sugars, mannobiose and azido-terminated galactose, on the microstructured CVD coating, as depicted in Scheme 2-3.

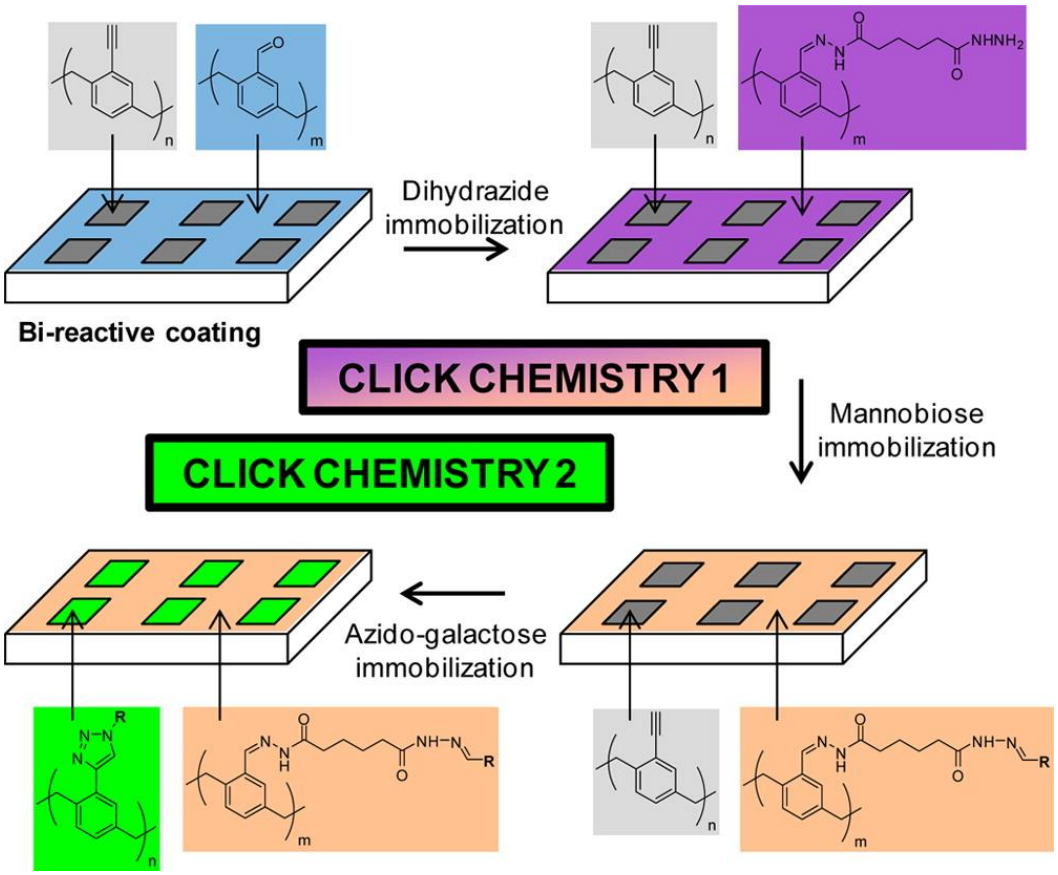

Scheme 2-3:Schematic Illustration of the Strategy Used for Successive Immobilization of Two Saccharides on Microstructured CVD Coatings; Mannobiose Underwent Aldhehyde–hydrazide Coupling (click chemistry 1) with a Dihydrazide Linker Previously Anchored on the Reac tive Coating and Azido-Galactose Was Bound via Huisgen Cycloaddition (click chemistry 2)

Mannobiose was first immobilized outside the square islands by reacting it to the aldehyde groups on the coating via aldehyde-hydrazide coupling. This aldehyde-hydrazide coupling was made possible with the help of dihydrazide linkers. We chose adipic acid dihydrazide as the linker because we hypothesized that it has an intermediate chain length that allows just one of the hydrazide moieties to bind to the aldehyde groups present in the CVD coating and the other hydrazide moiety can serve to immobilize mannobiose onto the substrate. The substrate was then immersed in an aqueous solution containing 1-azido-1-deoxy-β-D-galactopyranoside and copper catalyst. Under these conditions, Huisgen cycloaddition occurred with the ethynyl groups present on the square islands of the microstructure.

The spatial distribution of the two saccharides was then investigated by immersing the substrate in a solution containing a fluorescently labeled lectin with selective affinity to one of the two sugars. Figure 2-3 depicts fluorescence micrographs after conjugation of FITC-PNA with galactose (Figure 2-3a) and of TRITC-Con A with mannobiose (Figure 2-3b). The higher fluorescence of FITC-PNA in the squares, where galactose was previously immobilized, and of TRITC-Con A outside the squares, where mannobiose was bound, confirms the selectivity and efficiency of the click chemistry reactions.

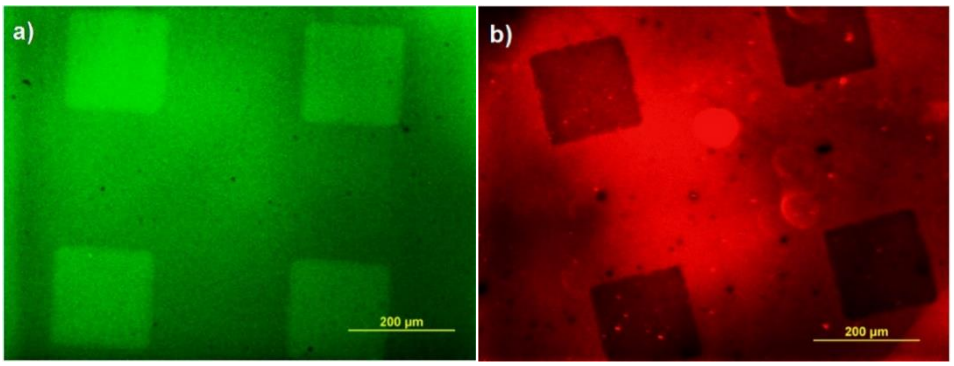

Figure 2-3: Fluorescence micrographs of microstructured CVD coatings after conjugation of (a) FITC-PNA with galactose and (b) TRITC-Con A with mannobiose; the saccharides being immobilized via click chemistry reactions.

2.2.4 Conclusion

CVD polymerization is a versatile process that can be used to tailor reactive polymer coatings, in terms of chemical functionalities as well as coating thicknesses. Stable, ultrathin reactive polymer coatings can be obtained providing desired functionality while preserving properties inherent to the bulk material. Copper-catalyzed Huisgen cycloaddition was performed on the reactive coatings by microcontact printing and saccharides and peptides alike can be immobilized. In addition, microstructured coatings provide a versatile route toward the immobilization of various saccharides through multiple click chemistry reactions. As an exemplary demonstration, substituted poly(*p*-xylylene) coatings in conjunction with multiple, orthogonal click reactions were successfully used for spatially directed surface modification and biomolecular immobilization. The strategy developed in this work for surface engineering is versatile enough to be adapted to other anchoring chemistries and also to other biomolecules.

The combination of various orthogonal chemistries in a microstructured manner is also a step forward in the development of biomimetic interfaces. Numerous potential applications in biotechnology can be considered from the results of this study. For instance, synthetic substrates for cell co-culture, structured micro-sensors or more generally platforms for biomolecular screening may benefit from selective and multiple immobilizations of biomolecules via orthogonal click reactions, as outlined in this work.

2.3 Multi-Growth Factor Delivery via Immobilization of Gene Therapy Vectors

2.3.1 Introduction

The fundamental goal of tissue engineering and regenerative medicine (TE/RM) is to promote formation, organization, and integration of tissue formation to produce functional organs or structures. Key components of TE/RM for clinical application include putative regenerative cells, signaling growth factors, three-dimensional scaffolding matrices and a vascular or nutrient supply to allow tissue neogenesis and homeostasis.[75] Of these, growth factors play very important roles in regulating all the biological activities of cells, such as migration, proliferation, differentiation, maturation and apoptosis A major clinical challenge for oral and craniofacial TE/RM is the controlled and efficient delivery of growth factors for tissue regeneration of multi-tissue interfaces (i.e., bone, ligaments and oral mucosal soft tissues) due to rapid degradation of the proteins and safety considerations of gene-mediated local delivery platforms. In this study, we demonstrate for the first time the efficacy of multi-growth factor gene delivery using adenoviral vectors chemically conjugated onto the surfaces of PLGA, PCL, and titanium, which indicates the feasibility of currently available FDA-approved biomaterials in TE/RM clinical applications**.**

Biodegradable and biocompatible scaffold materials, such as PCL and PLGA, are approved by the FDA for several clinical applications and promote tissue regeneration in

numerous biomedical studies.[76]–[78] Several methods for attachment of biomolecules to material surfaces depend on physical adsorption, which lacks the ability to target and immobilize biomolecules or release them in a controlled manner.[28] Reactive polymer coating prepared via chemical vapor deposition (CVD) polymerization of substituted paracyclophanes presents a broadly applicable strategy for covalent immobilization of biomolecules onto a variety of solid materials.[11] In addition, the polymer coatings can be applied conformally onto 3D complex structures, such as tissue scaffolds, which enables direct conjugation of biomolecules on tissue scaffolds and allows for localized delivery of genes and proteins to cells, and minimizing infection of surrounding tissues.[28], [32] Previous studies have reported the potential of CVD polymerization for immobilization of adenovirus to polymer films for up-regulated growth factor expression and cellular differentiation. [79], [80]

For clinical use, bone morphogenetic protein-7 (BMP7) for bone regeneration and platelet-derived growth factor-BB (PDGF-BB) for soft-tissue regeneration (two FDA-approved growth factors used for craniofacial applications) provide a matrix for restoring tissue lost due to oral disease. In contrast to direct protein-based or plasmid therapies, virus-mediated gene therapy has the advantage of sustained and localized production of therapeutic proteins. One of the main benefits of utilizing adenoviral vectors for gene delivery is that, in theory, adenovirus can infect many human cells due to the presence of the classical adenoviral receptor, coxsackie and adenovirus receptor (CAR), which is present in fibroblasts, endothelial, epithelial and

smooth muscle cells. The CVD coating methodology tethers the virus to the material, thereby reducing the acute toxicity and hepatic pathology caused by direct systemic administration of adenoviral vectors.[81] In the present study, we utilized CVD coatings on three distinct materials for direct gene delivery to orally derived progenitor cells (primary human periodontal ligament (hPDL) fibroblasts). Our findings revealed that the immobilized adenovirus transduced hPDL cells and induced sustained production of bioactive PDGF-BB and BMP7 protein on all tested materials (PCL, PLGA, and titanium). No cytotoxic effects were observed due to the polymer coating. We found that the adenoviral load could easily be modified to ensure that the resulting growth factor concentration is optimal for tissue formation for subsequent in vivo applications. This work establishes a general strategy for safe and efficient cell transduction and growth factor protein production because it is immobilized and controllable.

Several scaffold materials are available, but currently a technique to customize polymer surfaces for specific gene delivery applications is needed. [82] PLGA is a copolymer prepared from different ratios of lactic (LA) and glycolic acid (GA) monomers. There is great interest in PLGA due to its modifiable surface properties, biodegradation rate, and biocompatibility and it has been widely used for tissue engineering as scaffolds, fibers, hydrogels, microspheres, and in composite constructs. [83] Titanium is the standard for dental and biomedical implant applications requiring osseointegration. We will use these materials to mimic the normal

periodontal structure (bone- ligament- cementum). Bioactive agents have been applied to titanium surfaces to further improve bone-to-implant contact and accelerate healing. [84] Our strategy could be applied to a multilayered scaffold that aims to regenerate several tissues simultaneously by immobilizing different viral vectors for gene therapy onto different regions of the scaffold, thereby reducing interference between different biomolecules compared to other methods of delivery in which unbound virus can dissipate into surrounding tissue.

2.3.2 Experimental Methods

Materials

PLGA (MW: 31-52 kDa), 75:25 ratio of Lactic Acid to Glycolic Acid monomers was purchased from Evonik Industries. PCL (MW: 43-50kDa) was purchased from Polysciences, Inc. (Warrington, PA). 6AL-4V titanium discs were obtained from the University of Michigan Engineering department.

Polymer and titanium disc fabrication

Selective laser sintering (SLS) was used to fabricate 5mm dia. x 1mm discs using PCL and 4% hydroxyapatite. The PLGA discs were prepared on 2-layer silicone molds, prepared following instructions of SYLGARD 182 Silicone Elastomer Kit and poured into aluminum-lined glass

petri dishes to create a lower 10 mm x 90 mm diameter mold of uniform thickness. The upper mold layer is 1 mm thick with 5 mm diameter holes created with a biopsy punch. PLGA crystals were melted into the mold at 90-130 °C and flattened, resulting in PLGA discs 1 mm x 5 mm in diameter. Titanium discs were manufactured from 0.040" x 2.0" x 2.0" 6AL-4V titanium sheets by slicing 1mm x 5 mm diameter discs using a Computerized Numerical Control (CNC) machine.

Chemical vapor deposition (CVD) polymerization:

PCL, PLGA and titanium discs were coated with a layer of amine-reactive polymer using a custom-built CVD system previously reported [85]. During the coating process, discs were fixed inside the deposition chamber at 15 ^{o}C. The starting material (synthesis is described elsewhere [85]) was sublimated at 120 ^{o}C, which was then pyrolyzed at 540 ^{o}C to form into a stream of reactive di-radical vapor. The stream of reactive di-radicals then entered the deposition chamber where they deposited and polymerized simultaneously on the discs. The whole process operated at a pressure of 0.1 mbar using argon as carrier gas.

Chemical Characterization via x-ray photoelectron spectroscopy (XPS)

XPS data were recorded with an Axis Ultra X-ray photoelectron spectrometer (Kratos Analyticals, UK) outfitted with a monochromatized Al Kα X-ray source at 150 kW. Survey and high-resolution XPS spectra were taken at 160 and 20 eV, respectively. All spectra were calibrated with respect to the non-functionalized aliphatic carbon with a binding energy of 285 eV. The averaged experimental composition obtained on the three types of polymer-coated materials is listed in Figure 1b and compared to the theoretical composition of the polymer.

Adenovirus immobilization to the polymer (performed by Jie Hao)

After CVD coating, discs were sterilized in 70% ethanol for 1 hour, followed by virus immobilization and cell seeding. A 10 ug/ml solution of Goat anti-Adenovirus (AbD Serotec; 0151- 9004) polyclonal antibody was prepared in PBS. Ten discs were added to 12ml antibody solution and incubated overnight at 4 ℃ on a rotating mixer. Discs were rinsed 5 x 5 minutes with PBS. Adenoviruses containing GFP, PDGF, BMP7 genes were prepared by University of Michigan Vector Core. Discs were incubated in 12ml cold adenovirus solution (10^{11} or 10^{12} PN/ 10 discs) for 4 hours at 4 ℃, followed by 5 x 5 minute PBS rinses.

Verification of anti-Adenovirus antibody binding

After incubation in anti-Adenovirus antibody, polymer-coated and as-received discs were incubated in PBS containing 10 ug/ml AlexaFluor647 Rabbit anti-Goat IgG secondary

antibody (Invitrogen, Inc.), 0.02% (v/v) Tween20 and 0.1% (w/v) bovine serum albumin (Sigma-Aldrich, Inc.) for 1 hour, followed by PBS rinses. Subsequently, fluorescence microscopy (Nikon E800) and ImageJ were used to quantify and compare the fluorescence signals obtained on polymer-coated and uncoated discs.

SEM imaging and quantification of adenovirus (performed by Jie Hao, Laura Kruger, Lena Larsson and James Sugai)

The viral particle distribution was determined by scanning electron microscopy (SEM). PCL, PLGA and Ti discs with immobilized AdGFP were fixed in 2.5% glutaraldehyde in PBS for 30 minutes. After two washes with distilled water and dehydration with ethanol, samples were desiccated under vacuum overnight. SEM images were captured using the AMRAY 1910 FE Field Emission Microscope and SEMTech Solutions SEM interface version V1.0.4.179. Samples were mounted for AMR using Graphite Conductive Adhesive from Electron Microscopy Sciences and coated with gold using the Polaron SEM Coating System for 100-120 seconds. All images were taken at 10,000x magnification. Viral particles were counted by two independent investigators using 10 SEM images of each material (Ti, PCL, PLGA) at each viral concentration (10^{11}, 10^{12}) resulting in a total of 60 images. Investigators counted bright particles approximately 70-100 nm in diameter towards the number of Adenovirus attached to the surface. [86]

2.3.3 Results and Discussion

A schematic illustrating the polymer coating and conjugation of antibody and adenovirus on the three materials is shown in Figure 2-4. First, a thin layer of polymer film containing pentafluorophenol (PFP)-ester groups was coated on the three materials via CVD polymerization. Goat anti-adenovirus antibody was immobilized on the polymer-coated materials. Subsequently, adenoviruses were immobilized on the materials via antibody–antigen interaction.

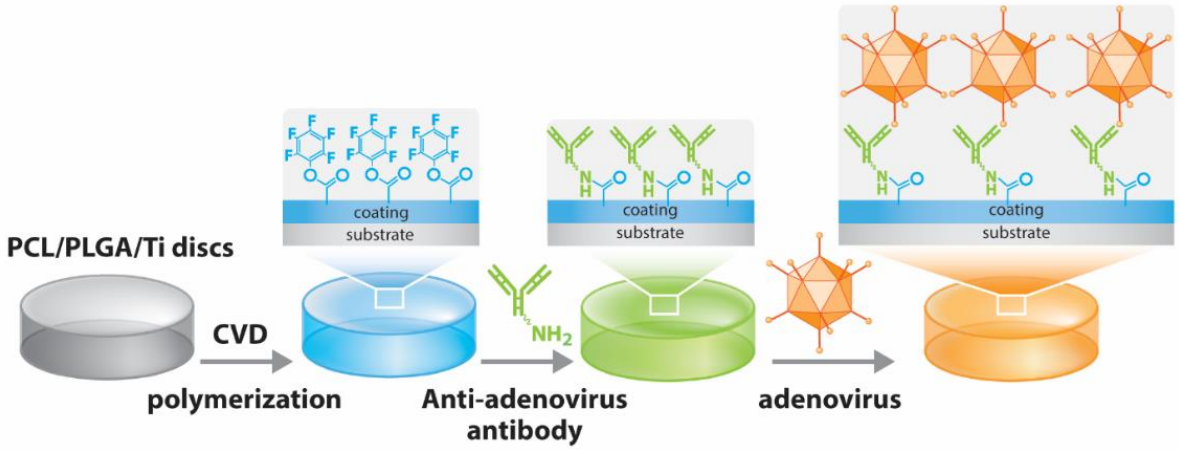

Figure 2-4: A schematic showing the process for attaching adenovirus onto PCL, PLGA, and titanium discs [87].

X-ray photoelectron spectroscopy (XPS) and immunofluorescence were used to verify the presence of polymer and binding of anti-adenovirus antibody on the three polymer-coated materials. XPS is capable of detecting the elemental composition of the top 10nm of a specimen. Table 2-1 summarizes the elemental composition of the three types of materials coated with the

polymer. The characteristic elements of the polymer coating were detected on all three materials and the composition of these elements are in good agreement with the calculated elemental composition of the polymer coating based on the structure of the polymer, confirming the presence of the polymer coating on all three materials. AlexaFluor647-conjugated anti-Goat IgG secondary antibody was used to verify binding of anti-adenovirus antibody on the three polymer-coated materials via immunofluorescence. Mean fluorescence intensity on the polymer-coated materials was higher than on the uncoated materials, confirming successful binding of anti-adenovirus antibody on the polymer-coated materials (Figure 2-5).

Table 2-1: XPS analysis of PCL, PLGA, and titanium discs coated with polymer. The values in brackets are the theoretical values of the polymer coating [87].

Elements	**C (1s)**						**O (1s)**	**F (1s)**
(Chemical states)	**C-C/H**	**C-C=O**	**C-O**	**C-F**	**O-C=O**	**$\pi \rightarrow \pi^*$**		
B.E [eV]	**285.0**	**285.7**	**286.6**	**288.1**	**289.2**	**291.5**	**533.0**	**688.0**
Average experimental values [at%]	47.0 ± 1.7	3.4 ± 0.1	3.4 ± 0.1	16.8 ± 0.3	3.6 ± 0.1	2.7 ± 0.7	5.7 ± 0.3	17.3 ± 0.9
Calculated values [at%]	50	3.3	3.3	16.7	3.3	-	6.7	16.7

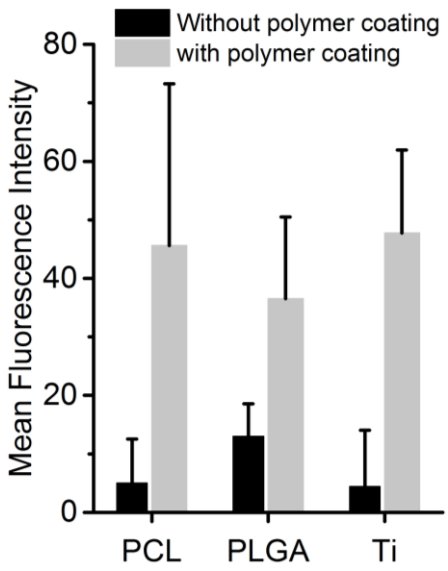

Figure 2-5: Mean fluorescence intensity per ROI of polymer-coated and non-coated discs following incubation in anti-adenovirus antibody and Alexafluor647 (or FITC)-conjugated anti-goat IgG secondary antibody (n = 9). ROI = 0.394 mm^2 [87].

To ensure successful covalent immobilization of adenovirus to the three material surfaces after CVD coating, a GFP-expressing adenovirus was conjugated to antibody and viral particles were quantified using SEM images (Figure 2-6 & Figure 2-7). Two concentrations of virus were used for immobilization to the respective surfaces. For transduction, the hPDL cells were directly seeded onto the coated samples. Fluorescence microscopy showed that maximal GFP protein expression was seen at 72 h for all coated materials, indicating excellent transduction efficiency of the surface-bound adenovirus (**Error! Reference source not found.**). T

o highlight the potential uses of CVD in oral tissue engineering, we tested three additional cell types in addition to hPDL (**Error! Reference source not found.**).

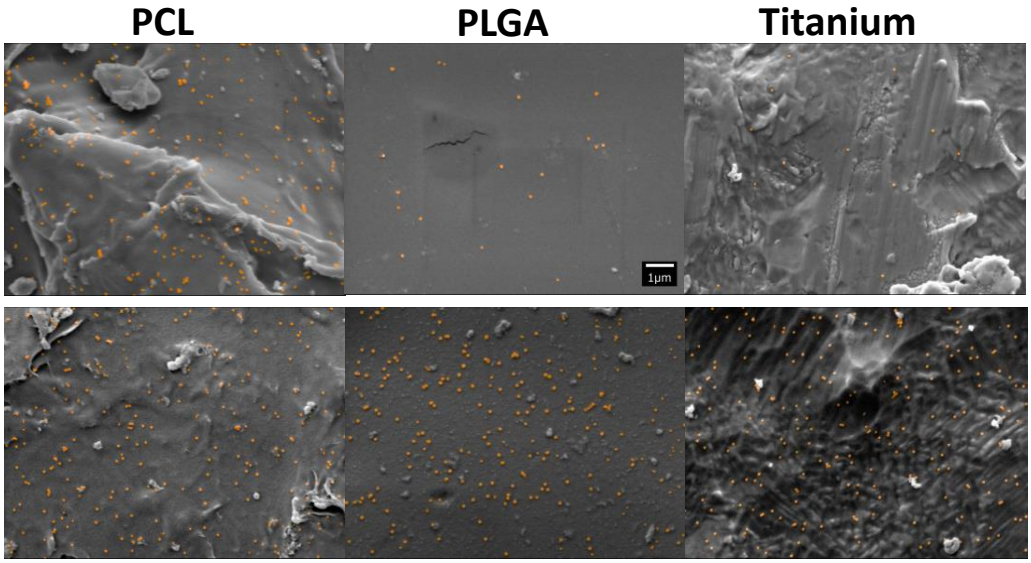

Figure 2-6: Scanning Electron Microscopy (SEM) images of PCL, PLGA, and titanium discs with 10^{11} and 10^{12} PN of GFP-adenovirus immobilized onto the surfaces. Viral particles have been colorized to enhance contrast [87].

Figure 2-7: Quantification of viral particles within ROI (n = 10). ROI = 101.4 μm^2 [87].

After confirming the successful immobilization of adenovirus onto different CVD-coated substrates (i.e. PCL, PLGA and titanium), the Giannobile Research group (Dentistry, Univ. of Michigan) further examined the use of surface-bound adenoviruses for protein delivery via in-vitro studies. Specifically, surface-bound adenoviruses encoded with either platelet-derived growth factor-BB (PDGF-BB; for soft-tissue regeneration) or bone morphogenetic protein-7 (BMP7; for bone regeneration) provided highly transduction of bioactive PDGF-BB and BMP7 protein production over 14 days, as confirmed with ELISA. The adenovirus-derived BMP7 protein promoted cell differentiation and induce mineralization, while the adenovirus-derived PDGF-BB protein induced the same level of cellular proliferation as recombinant PDGF-BB did. Furthermore, the CVD-based polymer coatings did not induce any cytotoxic effect and could be coated on 3D complex geometries. The CVD-based polymer coatings also enabled the co-immobilization of PDGF-BB and BMP-7 encoded adenoviruses to the same substrate for co-delivery of genes. Both gene delivery vectors remained fully compartmentalized on the substrate such that gene delivery can remain localized on the respective compartment. Details of the experimental procedures and results can be found in [87].

2.3.4 Conclusion

In summary, this multi-gene delivery strategy using CVD coating and adenovirus has several key advantages over other methods for gene therapy or protein delivery. Our system

produces much more prolonged and sustained levels of protein than recombinant protein delivery. This would provide a distinct advantage because recombinant proteins would need to be delivered every 24-48 hours to achieve a similar level, requiring many more office visits for clinical applications. Additionally, recombinant protein is not localized to the regeneration region and can escape into the surrounding tissues. The CVD method would reduce the number of office visits required for clinical application and protein would be expressed by the cells in the area of regeneration. In addition, compared to other gene therapy methods involving adenovirus, the CVD method localizes the adenovirus onto theoretically any scaffold material allowing for a variety of applications. Because the viruses are immobilized on the scaffold material, this method does not require scaffold to be seeded with a patient's cells prior to implantation. Native cells can infiltrate the scaffold and, once there, be transduced by the immobilized vectors. This would reduce the time, cost, and regulatory burden for clinical applications of these scaffolds as a patient's cells would not need to be harvested, expanded in culture, transduced with virus, and seeded onto a scaffold before the scaffold could be implanted in a patient. Furthermore, because the viruses are immobilized, they cannot spread into the surrounding tissues and infect cells outside the area to be regenerated. This is particularly helpful for regenerating tissues in a compartmentalized manner and creating delineation between regions. Future work aims to regenerate multiple tissue types simultaneously using this method with different adenoviral vectors in each region.

CHAPTER 3 Organized Assemblies of Shape-Controlled Nanofibers via Chemical Vapor Deposition into Thin Films of Liquid Crystals

The materials in this chapter were adapted from the following journal articles:

- **Cheng, K.***, Bedolla, M.*, Gregory, J., Kim, Y., de France, A., Vargas, D., Abbott, N.L., Lahann, J., "Templated Synthesis of Shape-Controlled Polymeric Nanofibers by Chemical Vapor Deposition (CVD) In Liquid Crystals". *To be submitted.* [*equal contribution]

3.1 Overview

Surfaces decorated with oriented arrays of fibers are ubiquitous in the natural world, because they can provide functionalities such as sensing (hair cells [88], [89]), thermal insulation (polar bear fur [90]), enhanced mass transport (microtubules [91]), extreme wetting behaviors (lotus leave [92]) and remarkable adhesive properties (gecko foot [93]). Few synthetic methods exist, however, to fabricate organized arrays of surface-supported fibers to engineer comparable functionalities [91], [93]–[96]. In principle, nanofibers can be prepared using nanofabrication [94], [95], surface-catalyzed growth [94], [97], supramolecular assembly

[98], [99] or polymerizations in anisotropic media [100]–[102]. The idea of employing liquid crystalline media to control chemical reactions dates back to T. Svedberg in 1916 [103] and has since been used in a wide range of bulk transformations ranging from unimolecular reactions [104] and polymerizations [105] to the self-assembly of nanoparticles [100]–[102], [106]–[109]. In Chapter 3, we demonstrate that chemical vapor deposition into thin films of liquid crystals supported on surfaces can create polymer with unprecedented topological complexity.

3.2 Experimental Methods

Materials

The precursors for CVD polymerization, 4-hydroxymethyl[2,2]paracyclophane **1a** and 4-ethynyl [2,2]paracyclophane **1b**, were synthesized using previously-reported procedures [74], [110]. [2,2]Paracyclophane **1d** was purchased from Kisco Conformal Coating LLC (San Jose, CA). LC materials, 5CB (4-pentyl-4'cyanobiphenyl), E7 (a nematic mixture of cyanobiphenyls and terphenyls), TL205 (a nematic mixture of halogenated biphenyls and terphenyls) and 4-{[(1-methylheptyl)oxy]carbonyl}phenyl-4-(hexyloxy)benzoate (chiral dopant S-/R-811), were obtained from EMD Millipore (Billerica, MA). Toluene (99.5% purity), acetone, hexane (CHROMA SOLV ® grade), TWEEN® 20 surfactant, copper (II) sulfate, sodium ascorbate and octyltrichlorosilane (OTS) were purchased from Sigma-Aldrich (St. Louis, MO) and used

as received. Ethanol (anhydrous, 200 proof) was purchased from Pharmco-AAPER (Brookfield, CT) and used as received. Monodisperse or "discrete" polyethylene glycol (dPEG®)-biotin acid was obtained from Quanta Biodesign (Plain City, OH). 1-Ethyl-3-(3-dimethylaminopropyl)carbodiimide (EDC), N-hydroxysulfosuccinimide (NHS), phosphate-buffered saline (PBS) solution, sulfuric acid and hydrogen peroxide were obtained from ThermoFisher Scientific (Waltham, MA). Streptavidin-alexafluor647 and azide-Alexafluor596 conjugates were obtained from Life Technologies (Waltham, MA). TEM copper grids and quartz slides were purchased from Electron Microscopy Sciences (Hatfield, PA). SU-8 photoresist was purchased from MicroChem Corp. (Newton, MA).

Sample Preparation: Preparation of LCs

5CB, E7 and TL205 were used as received from the vendor. Cholesteric LCs were prepared by adding 5wt% of S-/R-811 into the LC. Specifically, 3.5 mg of S-/R-811 was first dissolved in a small amount of toluene (~7 mg). Then, the solution was added into 67 mg of LC, and the entire mixture was left in vacuum overnight to allow the toluene to evaporate.

LC Sample Preparation

Solutions containing various concentrations of SU-8 photoresist were spin-coated onto glass slides to obtain films of the desired thickness between 5.6 ± 1.1 and 21.7 ± 0.5 μm. Pre-

exposure bake, UV-exposure and post-exposure bake were carried out according to the specifications provided by the manufacturer. Prior to development of the photoresist with solvent, the films of cross-linked SU-8 were exposed to oxygen plasma and functionalized with a fluorinated monolayer. The samples were then sonicated in a solution of SU-8 developer, obtained from the manufacturer, for 3-5 minutes. A final baking step was carried at 95 °C for 10 minutes to remove any remaining solvent. The thicknesses of the resulting microwells were measured using a surface profilometer (Tencor, AlphaStep). A 5 μL droplet of the LC was spincoated onto the microwell arrays. The thicknesses of the LC were characterized by first measuring the retardance of the layer using a Berek compensator purchased from Olympus America Inc. (Melville, NY) and are based on the value of the birefringence of the LC films obtained from literature [111]. To create a layer of LC with uniform homeotropic alignment, clean glass slides were functionalized with OTS according to previously reported procedures [112]. The fabrication of the microwells was then carried out according to the procedure outlined above.

Alternatively, glass substrates were first sonicated in isopropanol and were then rinsed with ethanol. A TEM grid was subsequently placed on a cleaned glass substrate, and a ~1uL droplet of LC was placed on top of the grid, allowing the LC to fill the whole grid. Excess LC

was then removed from the grid using a capillary tube, yielding a ~18um thick LC layer [112], [113].

Stainless steel meshes were sonicated in isopropanol, followed by a quick rinse in ethanol prior to use. A droplet of LCs was spread across the clean mesh using a pipette tip such that the LCs formed hanging droplets within the pores of the meshes.

10 uL or 50 uL glass capillaries were first sectioned into ~1 cm long tubes. The tubes were then incubated in piranha solution (3 sulfuric acid: 1 hydrogen peroxide volume ratio) for 30 minutes, followed by thorough rinse in deionized water (DI-H_2O). Subsequently, a drop of LC was either spread along the surface of the outer or inner glass capillary to form into a thin layer on the outer or inner surface of the tubes, or was filled into the entire capillary tube.

Microparticles immersed in LC

Polystyrene (PS) microparticles with an average diameter of 10.0 ± 0.2 μm were obtained from Sigma-Aldrich. CVD polymerization was performed into films of E7 containing these microparticles. The films were supported on OTS-treated substrates using TEM grids with thickness of 18 μm.

Chemical vapor deposition (CVD) polymerization

CVD polymerization was carried out in a custom-built CVD system that consists of a sublimation zone, a pyrolysis zone and a deposition chamber. Specimens (LC supported in microwells, pores of TEM grids or on complex geometries) were placed on a rotating stage inside the deposition chamber and were pumped to reduced pressure slightly above 2 mbar. The rotating stage was subsequently cooled to a temperature within the liquid crystalline phase of the LC and the pressure inside the deposition chamber was further reduced to 0.1 mbar. Under these conditions, we did not observe any significant evaporation of LCs. For 5CB at 23 °C, for example, the partial pressure is 0.0007 mbar. Subsequently, the precursor **1a**, **1b**, **1c (**combination of **1a** and **1b**) or **1d** was sublimed at a temperature of 120 ^{o}C and pressure of 0.1 mbar inside the sublimation zone, and was then transferred to the pyrolysis zone by a stream of argon flow. Pyrolysis of the precursor was performed at 550 ^{o}C and resulted in a stream of reactive molecules. Following pyrolysis, the molecules were transferred into the deposition chamber where they were deposited into the LC. After the CVD process, the specimens were either rinsed with solvents, such as ethanol, acetone or hexane, or heat-treated at 75^{o}C under 0.1 mbar to remove the LC from the specimen.

To disperse the nanofibers from the supporting substrate after the CVD process, we first removed the LC by repeatedly rinsing the specimen with ethanol and acetone. The specimen

was then incubated in either methanol or ethanol and was placed in a bath sonicator for ~1-2 minutes. The nanofibers were then removed from the supporting substrates and dispersed into the solvent that the specimen was incubated in.

To fabricate square islands of polymer **2c** nanofiber array on a glass surface, we first place a TEM copper square grid on the glass surface, and a ~1 uL droplet of LC was then placed on top of the grid, allowing the LC to fill the whole grid. Excess LC was then removed from the grid using a capillary tube. Subsequently, the specimen was coated with polymer **2c** by CVD, where the polymer will form into nanofibers inside the LC layers filled inside the TEM grid. Following the CVD process, the sample was rinsed with ethanol to remove the LCs and the copper grid was peeled off from the sample, leaving the surface with square islands of polymer **2c** nanofiber array.

Sample Characterization

The morphology and sizes (diameter and length) of the nanofibers were analyzed using scanning electron microscopy (SEM) (FEI Helios NanoLab). A thin layer of gold was sputtered onto the samples prior to SEM imaging to minimize surface charging. For length and diameter measurements, over 100 images were analyzed. The diameter of the nanofibers was also confirmed with transmission electron microscopy (TEM). The birefringent of the nanofibers

were characterized using cross-polarized light microscopy (PLM). The chemical composition of the polymer nanofibers was characterized via X-ray photoelectron spectroscopy (XPS) and Fourier transform infrared spectroscopy (FTIR). XPS data were obtained using an Axis Ultra X-ray photoelectron spectrometer (Kratos Analyticals, UK) equipped with a mono-chromatized Al Kα X-ray source at a power of 150 kW. The survey and high-resolution spectra were taken at 160 eV and 20 eV, respectively. All spectra were calibrated with respect to the non-functionalized aliphatic carbon with a binding energy of 285 eV. FTIR spectra were obtained on a Nicolet 6700 spectrometer with grazing angle accessory (Smart SAGA) at a grazing angle of 80°. A total of 128 scans were taken for each specimen. Circular dichroism (CD) and ultraviolet–visible (UV-Vis) absorption spectra of the helical nanofiber arrays anchored on quartz surfaces were obtained using a JASCO J-815 spectrometer.

Surface functionalization

2.5 mg of dPEG®$_{48}$-biotin acid and 2 mg of EDC were first added to 1mL PBS solution (1mM; pH7.4) containing 0.02% (v/v) Tween 20, and the solution was mixed for 10 minutes. Subsequently, 0.2 mg of NHS was added into the solution, and the entire solution was mixed for another 10 minutes. A glass coverslip with square islands of polymer **2c** nanofiber array (as shown in Fig. 4I) was incubated in the mixture for 2 hours. Upon completion, the specimen was rinsed with PBS with 0.02% (v/v) Tween 20 to remove unbound molecules. Following the

rinsing step, the specimen was incubated in an aqueous solution containing 10ug/ml azide-Alexafluor596, 0.1mM copper sulfate, 100 mM sodium ascorbate and 0.02% (v/v) Tween 20 for 1 hour, and was subsequently rinsed with DI-H_2O containing 0.02% (v/v) Tween20. Afterwards, the specimen was incubated in a PBS solution containing 0.1% (m/v) bovine serum albumin and 0.02% (v/v) Tween 20 for 10 minutes, and was then transferred to another PBS solution with 10 ug/ml Alexafluor647-strepavidin, 0.1% (m/v) bovine serum albumin and 0.02% (v/v) Tween20. The specimen was kept in the solution for 1 hour. After the incubation, the specimen was rinsed in PBS multiple times and analyzed with a Nikon Eclipse E800 epifluorescence microscope (Nikon Instruments, Japan).

3.3 Results and Discussion

Chemical vapor deposition (CVD) involves the thermal activation of molecules such as [2.2]paracyclophanes to form diradical species (Fig. 1B) and their subsequent polymerization at surfaces to form polymeric films [7], [8], [34], [38], [42], [87]. We found that CVD of compound **1a** onto glass surfaces covered with a micrometer-thick film of the nematic liquid crystal (LC) called 5CB (Figure 3-1), and subsequent removal of the LC (confirmed by FTIR spectroscopy, Figure 3-3), resulted in the formation of a surface decorated with an aligned array of nanofibers (Figure 3-2). The polymer nanofibers were anchored at one end to the surface,

and were determined to be structurally amorphous (Figure 3-2), yet optically birefringent, as confirmed by cross-polarized light microscopy (PLM, Figure 3-4). Insertion of a quarter wave plate (Figure 3-5) confirmed that the refractive index was greatest along the fiber axis, consistent with the alignment of polymer chains along the main axis of the nanofibers [114].

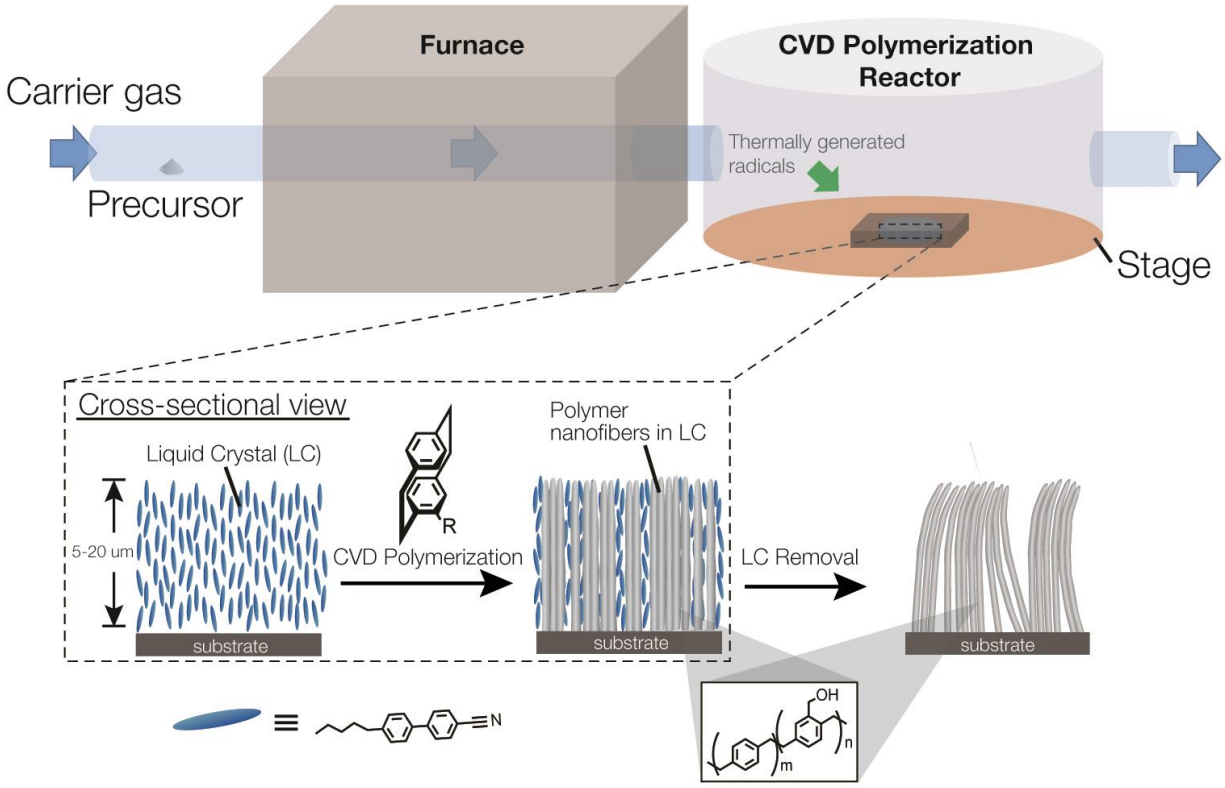

Figure 3-1: Graphical illustration of the CVD polymerization of substituted [2.2]paracyclophane in a thin film of LC layer decorated on a flat substrate and the subsequent removal of LC to create oriented poly-p-xylylene nanofibers anchored a flat substrate.

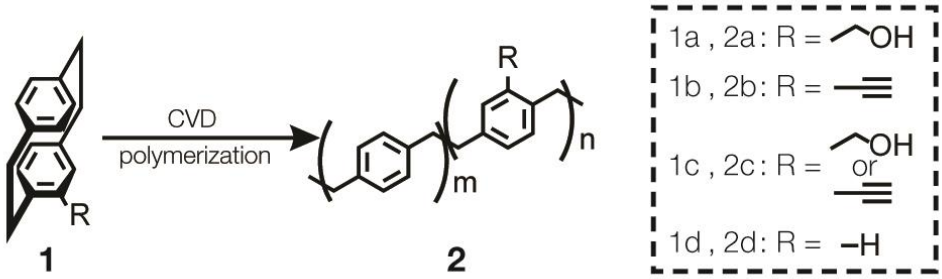

Scheme 3-1: CVD polymerization of [2.2] paracyclophanes 1a, 1b, 1c, 1d into poly-p-xylylenes with the corresponding functional groups (2a, 2b, 2c, 2d).

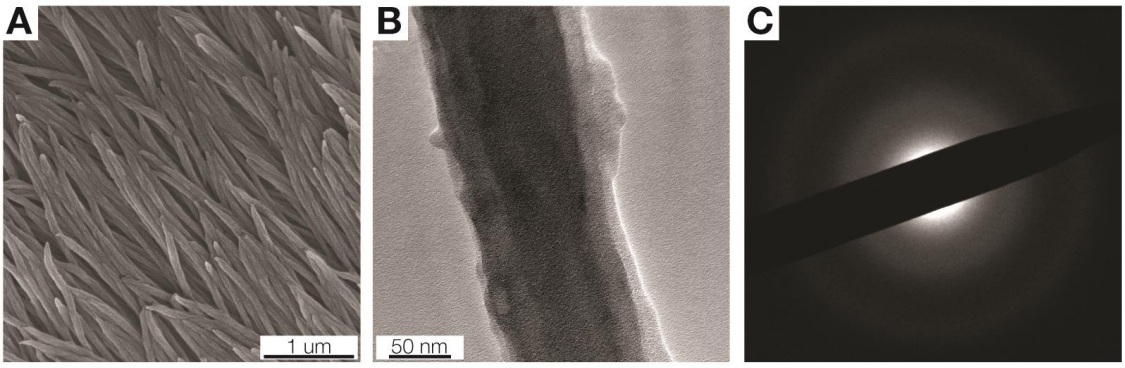

Figure 3-2: (A) A representative SEM image of the resulting surface-anchored 2a nanofibers prepared by CVD polymerization of 1a into a 18um-thick film of 5CB. LC was removed prior to imaging. (B) A TEM image taken on a 2a nanofibers prepared by CVD polymerization of 1a into a 18um-thick film of 5CB, and (C) the corresponding diffraction pattern taken on the nanofiber in (B). The halo ring diffraction pattern indicates that the polymer nanofibers are amorphous.

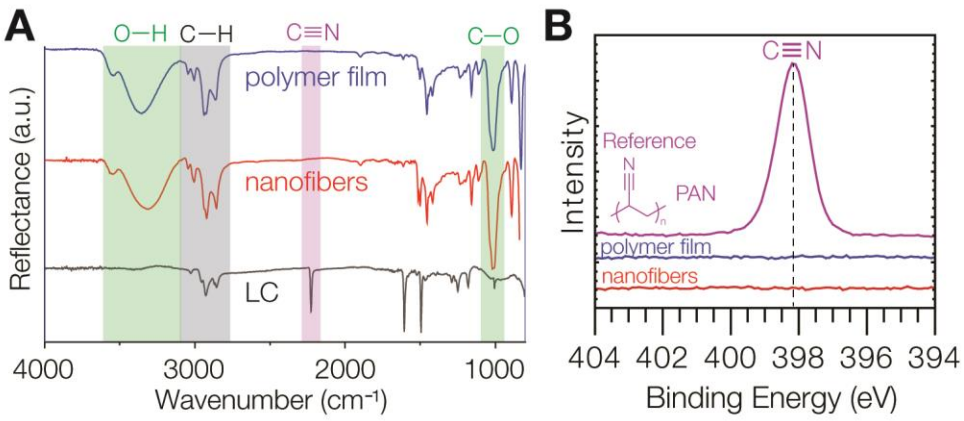

Figure 3-3: (A) FTIR spectra of a film of polymer 2a (blue), nanofiber assemblies of polymer **2a** (red) and a film of E7 (dark grey). The IR spectra of the nanofibers closely resemble that of the polymer thin film composed of the same polymer. Further, the absence of nitrile (~2200 cm^{-1}) on the nanofibers suggests the complete removal of the LC film during the LC removal step and that the nanofibers were composed of purely the polymer. (B) XPS survey spectra of a film of polymer **2a** (blue) and nanofiber assemblies of polymer **2a** (red). (**C**) XPS high-resolution N1s spectra of a film of polymer **2a** (blue), nanofiber assemblies of polymer **2a** (red) and reference, polyacrylonitrile (PAN) containing 25 at% of nitrogen (purple). The absence of nitrogen signal on the nanofibers indicates that the LC was completely removed, supporting the FTIR result.

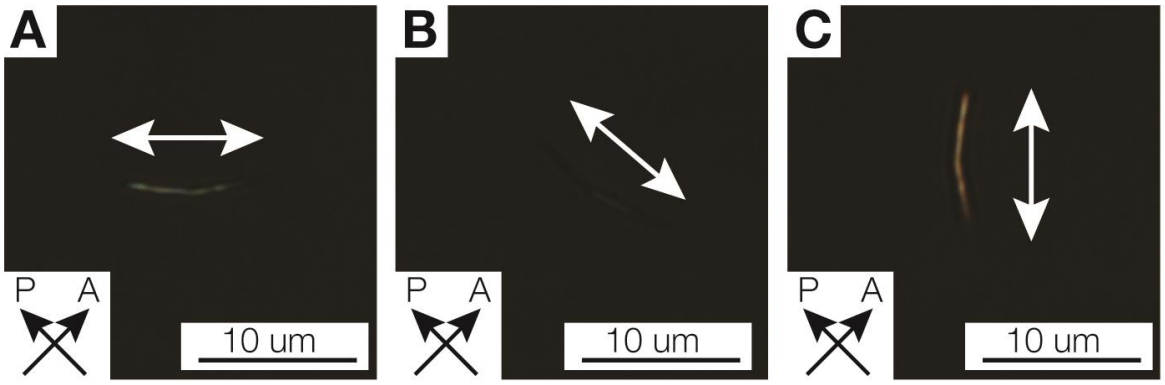

Figure 3-4: Polarized light micrograph (PLM) of an individual **2a** nanofiber oriented at different angles with respected to the polarizer. The PLM indicates that the nanofiber is birefringent. The birefringence is strongest when the nanofiber is oriented 45° with respect to the polarizer (P) and analyzer (A), and weakest when oriented along the polarizer (or the analyzer).

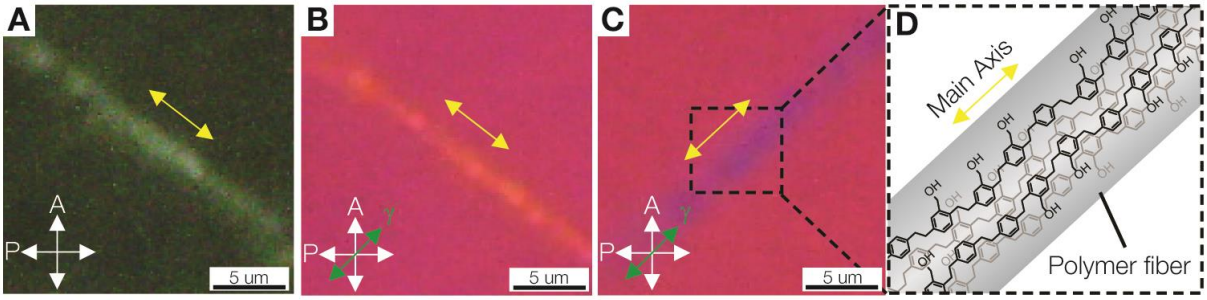

Figure 3-5: To better understand the cause of the birefringence, we analyzed individual nanofibers using a cross-polarized light microscope. The orientation of the analyzer (A) and polarizer (P) is shown in the double-arrow cross. (G) Image of the polymer nanofiber in (F) that was viewed with a quarter wave plate: Orientation is perpendicular to the slow axis (γ) of the plate (red double-arrow); the decreased retardance results in lower order interference colors. (H) Image of polymer nanofiber viewed with a quarter wave plate: Orientation is parallel to the slow axis of the plate; the increased retardance causes higher order interference colors. (I) Analysis of the nanofiber in (G) and (H) indicates orientation of the polymer chains aligned along the optical axis.

Nematic LCs are structured liquids within which the molecules exhibit long-range orientational order [115]. We found that CVD into films that lack this long-range order, e.g., solid crystalline 5CB, isotropic 5CB or silicone oil (Figure 3-6) did not yield nanofibers, indicating that the ordered, yet fluid properties of the nematic LC was necessary for the shape-controlled synthesis of nanofibers. Replacement of 5CB with a nematic LC called E7, which is a mixture of cyanobiphenyls that is nematic over a wider temperature range than 5CB, or TL205, which is a halogenated LC with a lower solubility for hydrocarbon compounds than 5CB or E7, also yielded organized assemblies of nanofibers. The diameters of the nanofibers,

however, were dependent on the LC (67 ± 9 nm in TL205, 86 ± 9 nm in E7, and 141 ± 11 nm in 5CB (

Figure 3-7)). In contrast to 5CB and E7, nanofibers synthesized using TL205 displayed a broadening of the fiber tip furthest from the surface (Figure 3-8), which indicates preferential polymer fiber growth near the surface of the LC film due to lower solubility of monomer **1a** in TL205, as compared to the non-halogenated LCs (Figure 3-8). Overall, these results are consistent with a mechanism of growth in which the thermally generated radicals partition into the structured LC fluid, adsorb to the solid-LC interface, and initiate growth of the nanofibers. The polymer chains preferentially grow along the alignment direction of the LC molecules, creating well-organized nanofibers inside the structured fluid.

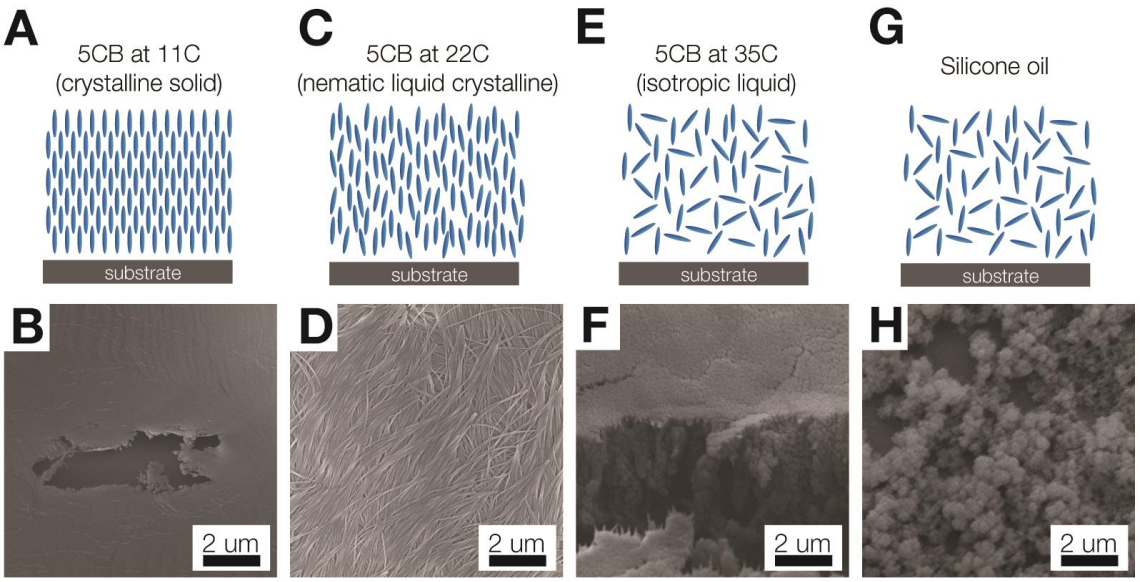

Figure 3-6: Schematic of (A) crystalline 5CB solid at 11C, (C) nematic liquid crystalline 5CB at 22C, (E) isotropic 5CB liquid at 35C, and (G) isotropic silicone oil at 22C. The resulting polymer structure templated in (B) crystalline 5CB solid at 11C, (D) nematic liquid crystalline 5CB at 22C, **(F)** isotropic 5CB liquid at 35C, and **(H)** isotropic silicone oil at 22C.

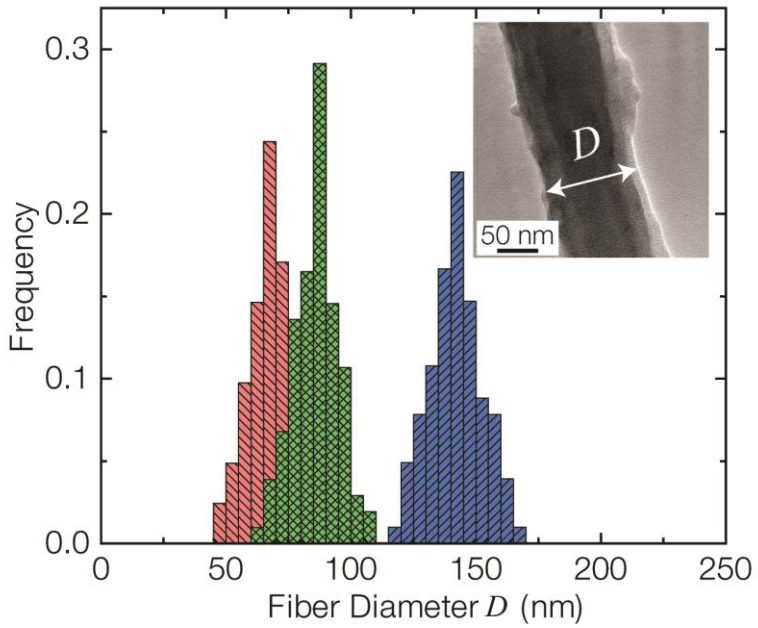

Figure 3-7: Diameter distribution of polymer 2a nanofibers templated in (blue) 5CB, (green) E7, and (red) TL205.

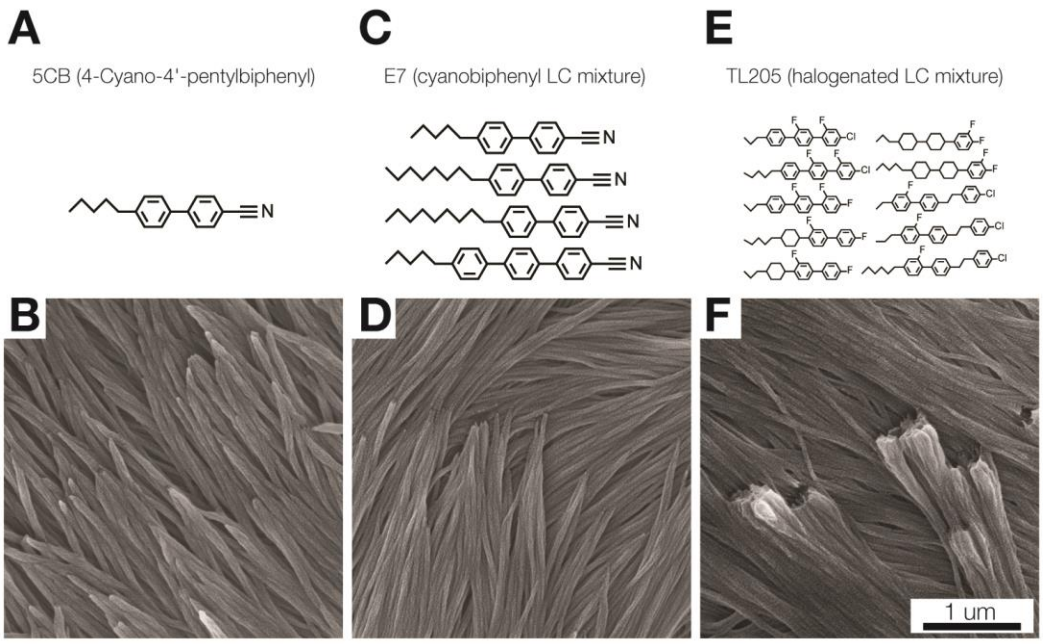

Figure 3-8: The chemical structures of (A) 5CB (C) E7 and (E) TL205 and the resulting polymer 2a nanofibers templated into (B) 5CB, (D) E7 and (F) TL205.

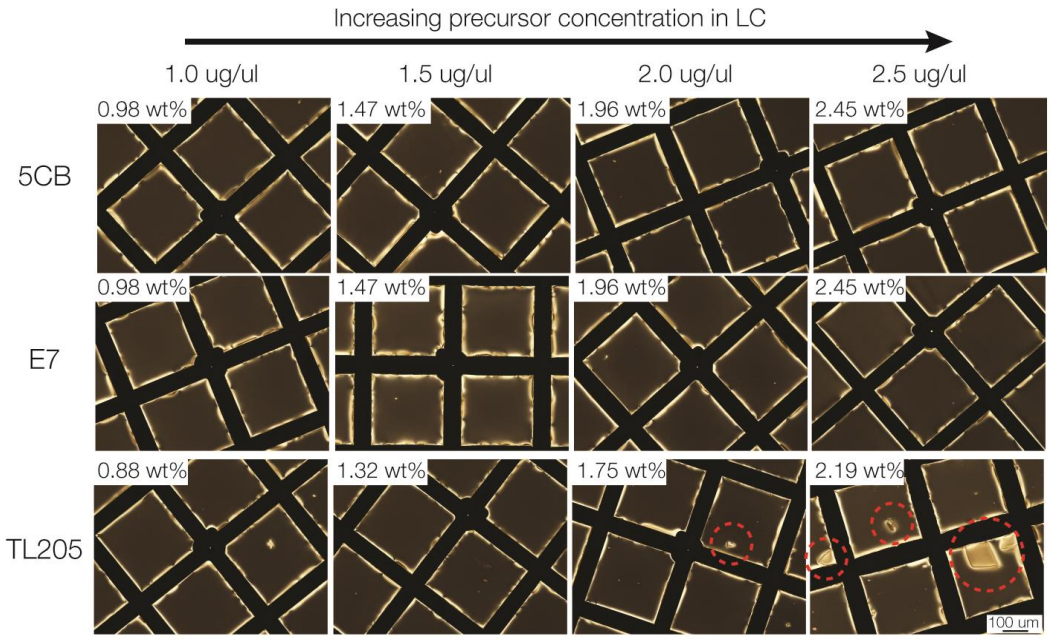

Figure 3-9: Polarized light micrographs of 5CB, E7 and TL205 LCs doped with varying amount of 1a. 1a remained fully dispersed from 0.98 to 2.45 wt% in 5CB and E7. Conversely, 1a began to phase separate in TL205 and agglomerate into crystals (red dashed circles) above 1.75 wt%, suggesting that 1a is not as soluble in TL205 as it is in 5CB or E7.

We then investigated the effect of the deposition amount on the resulting nanofiber length. Below 1 mg, the process becomes mass-limited resulting in shorter fibers with broad size distributions (Figure 3-10). Above 1 mg, the nanofibers are constrained at ~22 um, suggesting that the formation of nanofibers fully extend throughout the entire LC film (~22 um). As we introduce more precursor, the nanofiber length does not increase beyond 20um. Instead, the population of nanofibers grown inside the LC film increase (Figure 3-11). Please note that at 8 mg of deposition, the resulting nanofibers corresponds to only 1.7 ± 0.6 % (wt/wt) of the LC template. Because of such small weight fraction, we expect that the thickness of the LC remained roughly constant throughout the CVD polymerization.

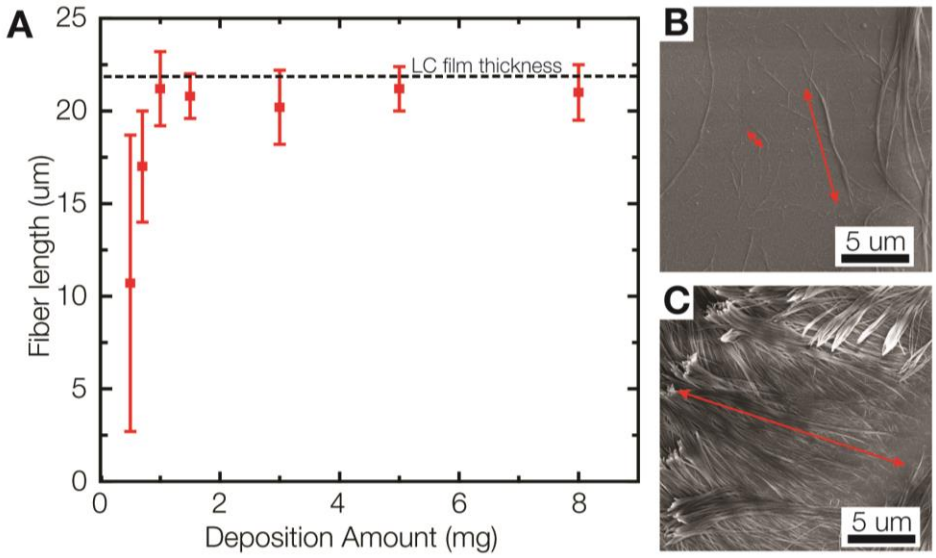

Figure 3-10: (A) The length of resulting polymer 2a nanofibers as a function of the deposition amount used during CVD polymerization of 1a into a set of 22um thick E7 film. The nanofiber length increase that the deposition amount increase but plateaus out once the length reaches ~22 um long. (B) Representative SEM image obtained on the resulting nanofibers after 0.5 mg of deposition. (C) Representative SEM image obtained on the resulting nanofibers after 5 mg of deposition.

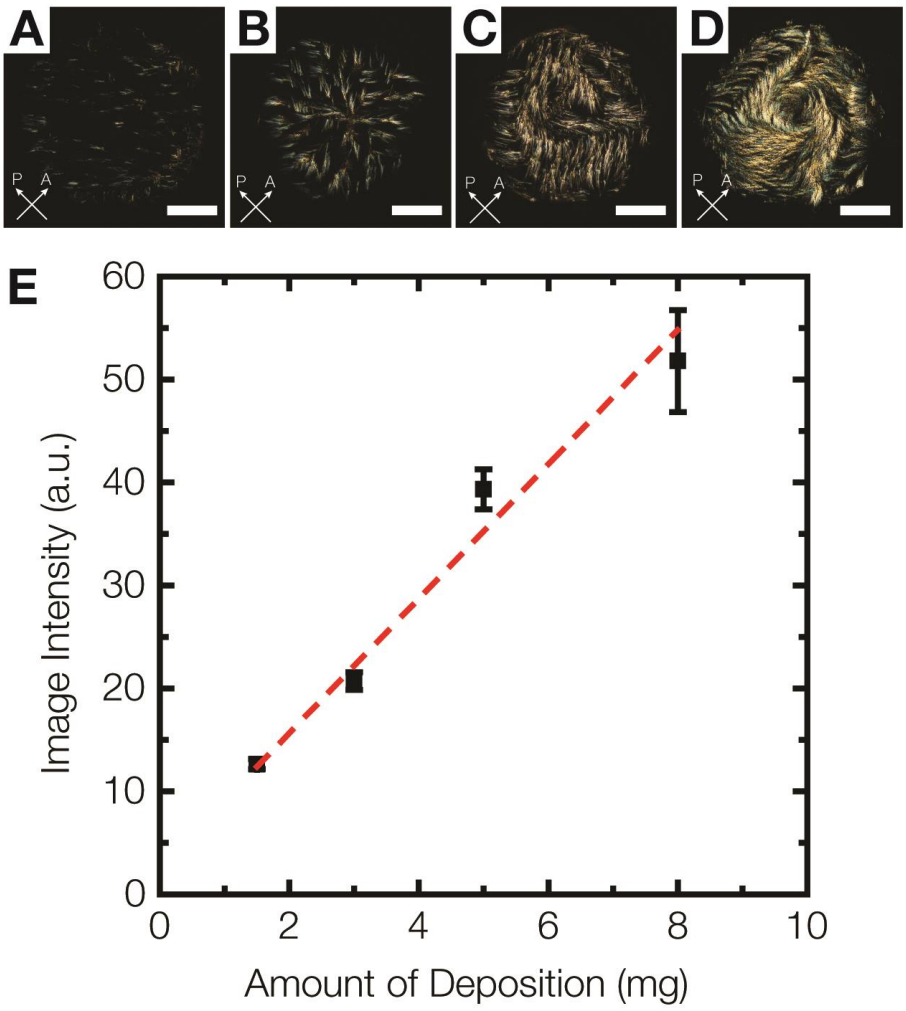

Figure 3-11: PLM images of nanofiber arrays formed by CVD polymerization of 1a into films of E7 homeotropically anchored on OTS-treated glass surfaces. The amount of the 1a used during CVD polymerization was different for each sample: (A) 1.5 mg, (B) 3 mg, (C) 5 mg, and (D) 8 mg. These images suggest that as the amount of precursor increases, the nanofiber population grown inside the LC film increases, leading to an increase in optical intensity of the PLM images. E7 was removed prior to imaging by submerging the sample in ethanol. The thickness of the LC films was 21.7 ± 0.5 μm. Scale bar = 50 μm. (E) A plot of the optical intensity of images presented in (A-D) as a function of the amount of 1a introduced during CVD polymerization. Image intensity was measured using ImageJ.

Using a deposition amount of 2mg, we performed CVD polymerization of **1a** using E7 films with thicknesses ranging from 5 to 22 μm and found that the lengths of the resulting polymer **2a** nanofibers closely matched the LC film thicknesses (Figure 3-12).

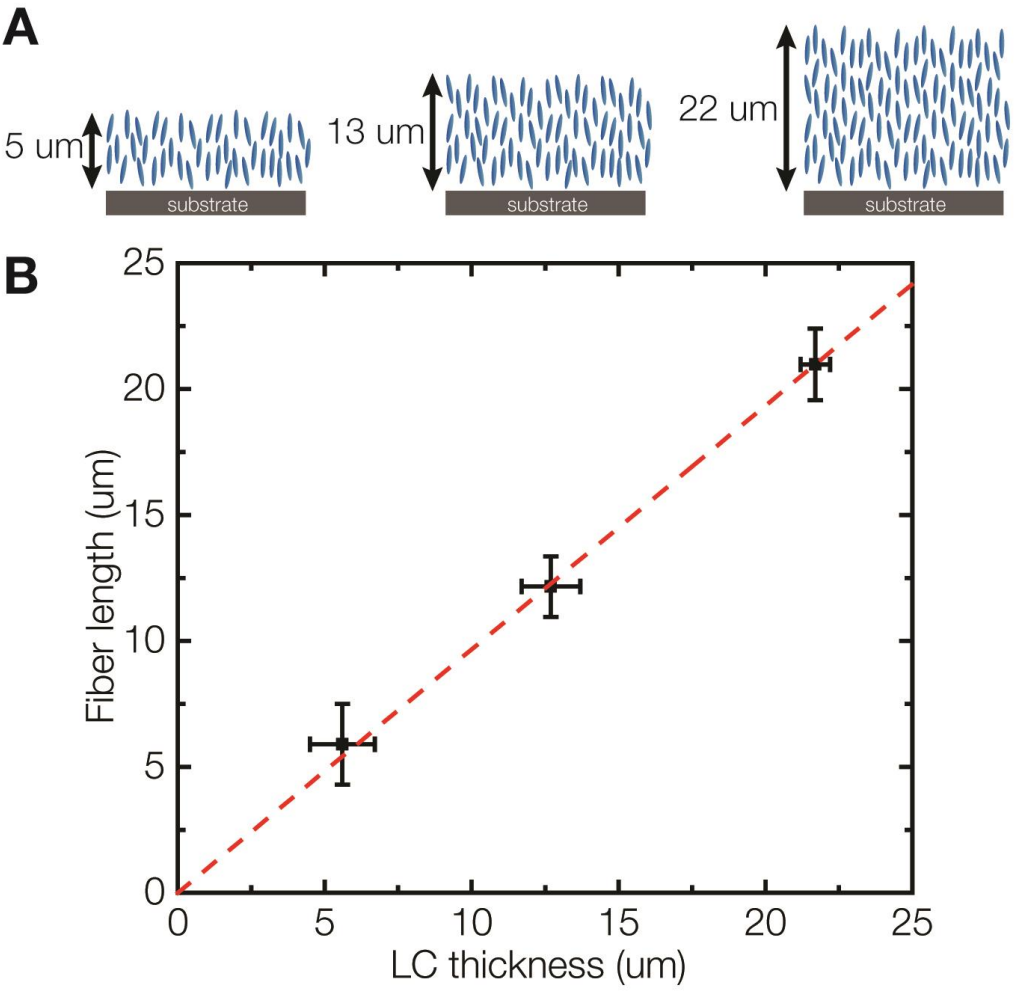

Figure 3-12: (A) Graphical illustration of LC films with different thickness (5 um, 13 um and 22 um) anchored on a flat substrate. (B) Nanofiber length as a function of the LC film thickness used during the polymerization process. The length of the resulting nanofibers is in agreement with the thickness of the LC film.

We then demonstrated that CVD of chemically functionalized [2.2]paracyclophanes [32] can be used to synthesize (i) ethynyl-functionalized nanofibers for reaction with azide derivatives (**2b**), (ii) nanofibers that simultaneously present ethynyl and hydroxyl groups for reaction with azides and activated carboxylic acids (**2c**), and (iii) nanofibers without functional groups (**2d**) that can act as a non-reactive reference. When grown into TL205, these nanofibers were morphologically identical (Figure 3-13) yet displayed the spectroscopic signatures of the respective functional groups, as measured by FTIR spectroscopy (Figure 3-13). The FTIR data suggest that the chemical functionality of shape controlled nanofiber assemblies can be altered, while maintaining their original morphology. The latter is a powerful concept, when surface decoration of complex topologies is attempted, such as the controlled presentation of high-density protein arrays (see Figure 3-27, Figure 3-28 and Figure 3-29 for an illustrative example).

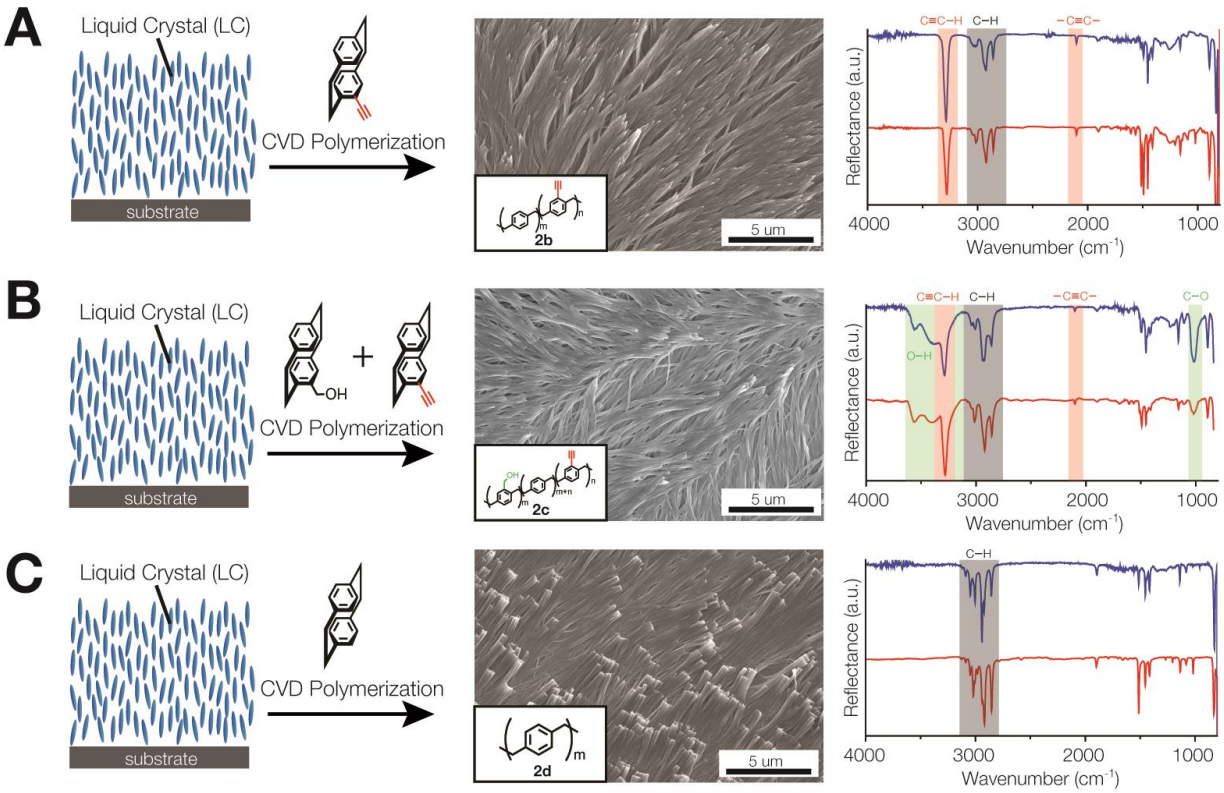

Figure 3-13: CVD polymerization of (A) 1b, (B) 1c and (C) 1d into a thin film of TL205 and the representative SEM images and FTIR spectra of the resulting nanofibers. TL205 was removed prior to imaging and IR analysis. IR spectra of the nanofibers (red) are compared to the corresponding polymer films synthesized without the LC phase (blue). The IR spectra of the nanofibers is in accordance to that of the polymer thin films, indicating the successful formation of nanofibers with different chemical functionalities.

The internal ordering of LC films can be manipulated by changing surface interactions, topology or chirality, thus offering a diverse range of nanofiber templates [115]. We added 5% (wt/wt) of either enantiomer (R or S) of a chiral dopant to E7 to create cholesteric LC films in which the helical axes were opposite in handedness (Figure 3-14 & Figure 3-15).

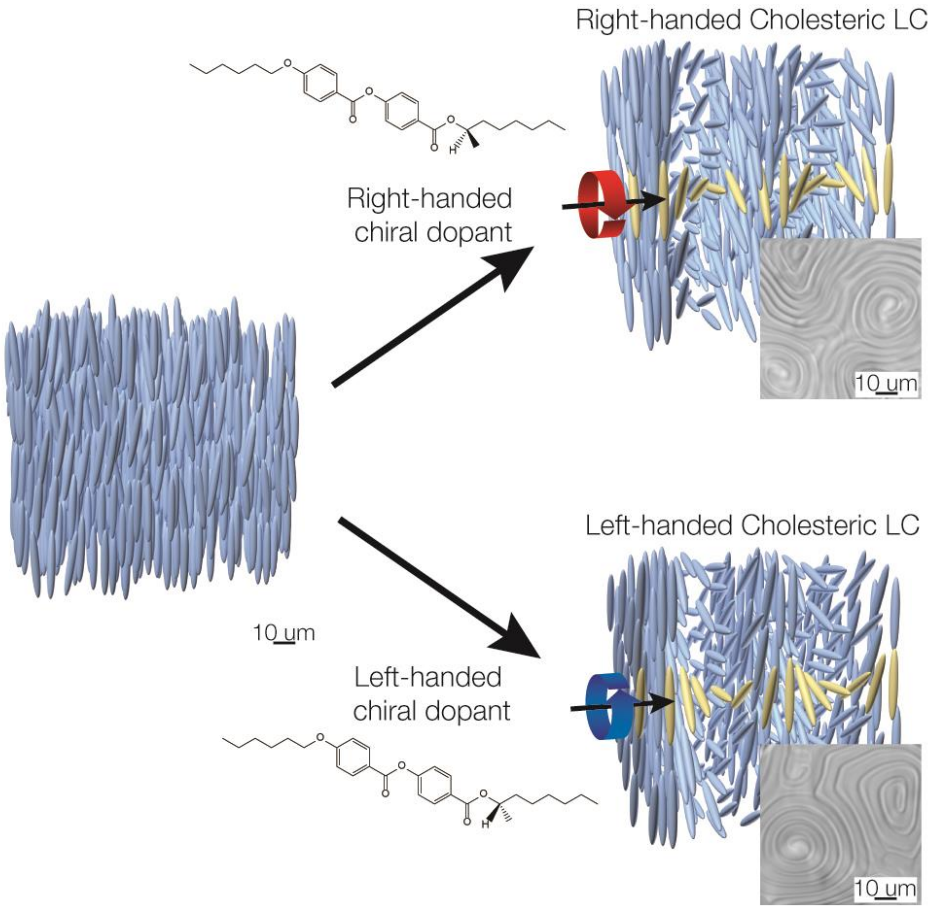

Figure 3-14: Schematics of nematic LCs, right-handed cholesteric LC and left-handed cholesteric LCs.

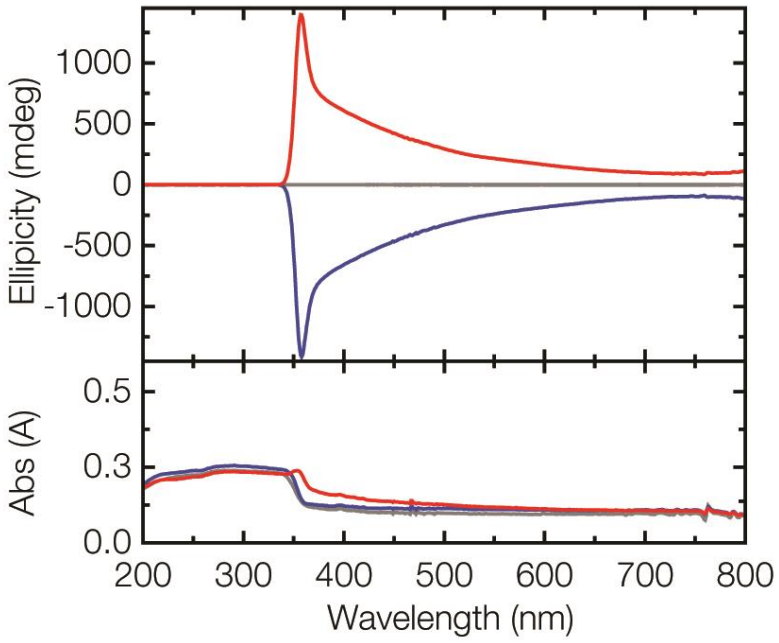

Figure 3-15: CD and UV-Vis absorption spectra of left-handed (blue) cholesteric, right-handed cholesteric (red) and non-cholesteric (grey) LCs (E7).

Templated CVD into the chiral LC films, and subsequent removal of the LC revealed shape-controlled nanofiber assemblies with micrometer-scale periodicities (4.7 ± 0.9 um and 4.9 ± 1.3 um for S- and R-templated nanofibers, respectively) and an organization consistent with the fingerprint pattern characteristic of the chiral LC films (periodicity of 4.4 ± 1.2 um and 4.7 ± 1.1 um for S- and R-handed cholesteric phase, respectively; Figure 3-16). The right-handed configuration of the cholesteric phase templated nanofibers into counterclockwise helices (S-configuration, red arrows in Figure 3-17) and, in contrast, the S-configured cholesteric phase resulted in R-configured nanofiber assemblies (blue arrows in Figure 3-17).

Circular dichroism spectroscopy of the R- and S-configured nanofiber helices reveals distinct bands below 280 nm for the polymer chains, such as the aromatic rings of polymer **2a** (Figure 3-17). Independent of the angle of incident light (Figure 3-18), the spectra further display broad bands between 300 to 800 nm, which vanish, when the nanofibers are dispersed in methanol (Figure 3-19), thus suggesting that they arise from cooperate effects of the helical nanofibers bundles [116], [117].

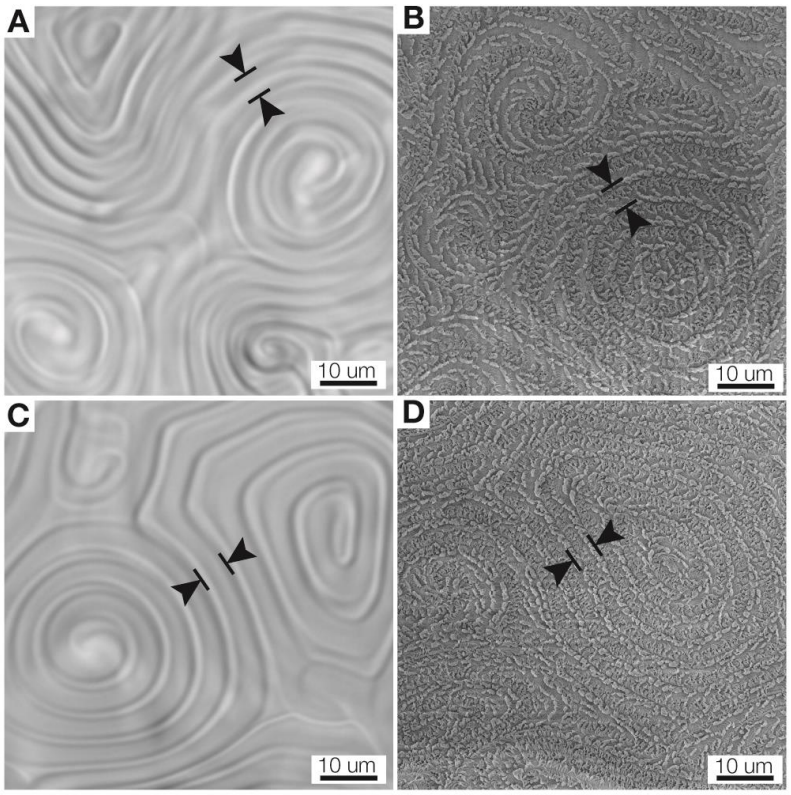

Figure 3-16: (A) PLM image of right-handed used in the CVD polymerization and (B) the representative SEM image of the resulting helical nanofiber bundles obtained from polymerization of 1a into a right-handed LCs. (C) PLM image of left-handed used in the CVD polymerization and (D) the representative SEM image of the resulting helical nanofiber bundles obtained from polymerization of 1a into a left-handed LCs.

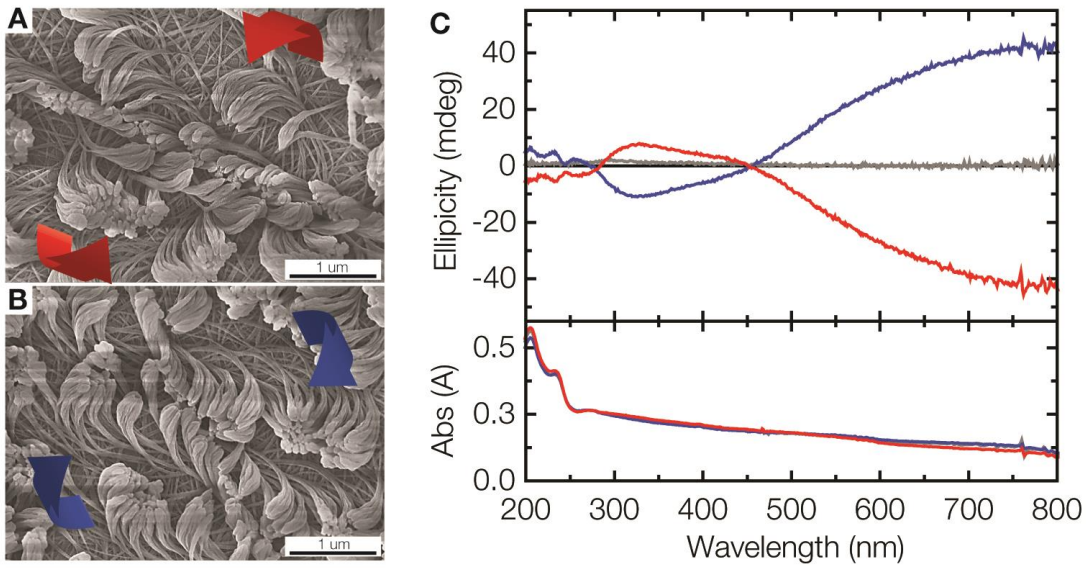

Figure 3-17: High-magnification SEM image of the helical nanofibers obtained by polymerization of 1a into right-handed (A) and left-handed (B) cholesteric LC. (C) CD and UV-Vis absorption spectra of helical nanofiber bundles prepared by polymerization of 1a into right-handed cholesteric (red), left-handed cholesteric (blue) and non-cholesteric (grey) LCs.

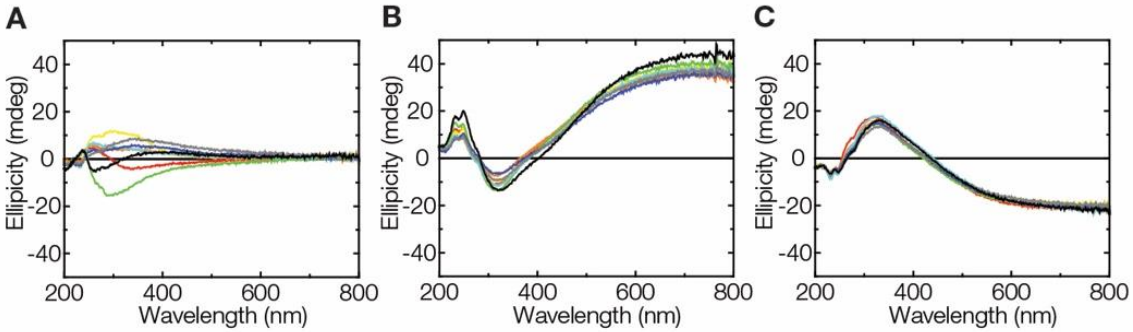

Figure 3-18: CD spectra of (A) non-helical, (B) R-configured helical and (C) S-configured helical nanofiber assemblies at different rotation along the beam axis. Red: 0o ; orange: 45o ; yellow: 90o ; green: 135o ; cyan: 180o ; blue: 225o ; grey: 270o ; black: 315o. Specimens were fabricated by CVD polymerization of 1a on (A) E7, (B) E7 with 5% wt/wt S-811 and (C) E7 with 5% wt/wt R-811. The LCs were homeotropically anchored on quartz surfaces and were ~18um in thickness. LC films were removed by rinsing the samples with ethanol and acetone prior to CD measurements. During CD measurements, the specimens were positioned such that the quartz surface was perpendicular to the beam axis. The specimen was rotated accordingly along the beam axis to obtain the 8 measurements.

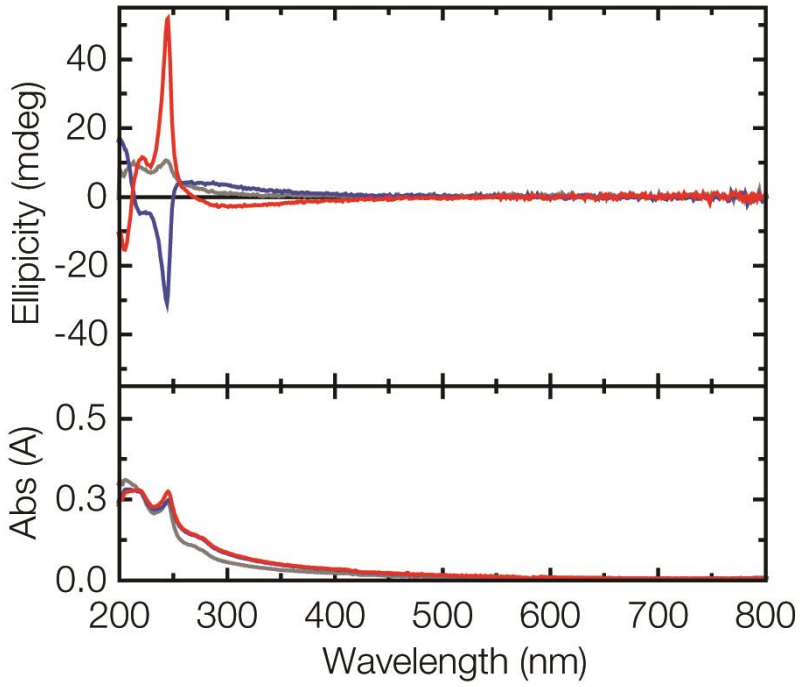

Figure 3-19: CD and UV-Vis absorption spectra of respective helical nanofiber bundles after removal from the surface and dispersion in methanol to ensure random alignment of the nanofibers. The nanofibers were prepared by polymerization of 1a into right-handed cholesteric (red), left-handed cholesteric (blue) and non-cholesteric (grey) LCs.

Next, we demonstrated the feasibility of LC-templated CVD in systems with complex topologies and interfacial interactions. In Figure 3-20, a conformally achiral LC film with a thickness of 5.1 ± 2.1 um was formed on the entire surface of a cylinder. After CVD polymerization and subsequent LC removal, a homogenous array of nanofibers (97.5 ± 17.5 nm diameter) decorated the curved surface of the cylinder, as indicated by the SEM images associated with representative regions 1-3 in Figure 3-20. Interestingly, CVD of **1a** into a thin film of E7 spread onto the luminal surface of a glass capillary also leads to templated nanofibers, where the density of the nanofibers decreases with increasing distance from the orifice.

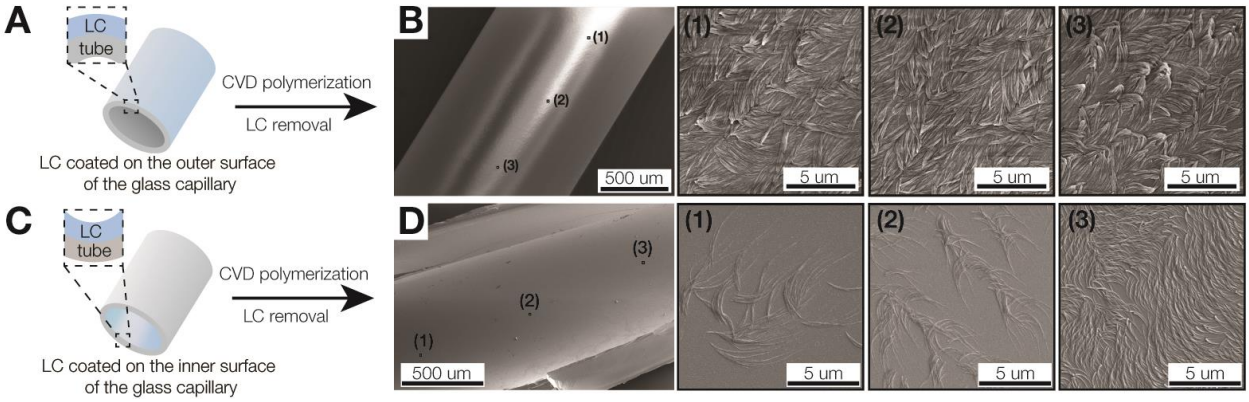

Figure 3-20: (A) CVD of 1a on the exterior surface of a glass tube coated with a 5.1 ± 2.1 um thick layer of E7 (blue) and (B) SEM images of corresponding nanofibers. (C) CVD of 1a on the luminal surface of a glass capillary coated with E7 and (D) SEM images ((3) indicates the region closest to the orifice).

As nanofibers assemble only on regions containing LC, it is possible to create patterned arrays of nanofibers by spatio-selectively patterning the LC film prior to LC-templated CVD. Figure 3-21A shows a flat substrate covered with ~18um thick patterned films of LC that are spaced apart by a 285 um by 285 um square grid. Following CVD polymerization and subsequent removal of LC and square grid, square islands of nanofibers arrays are patterned on the flat substrate (Figure 3-21B).

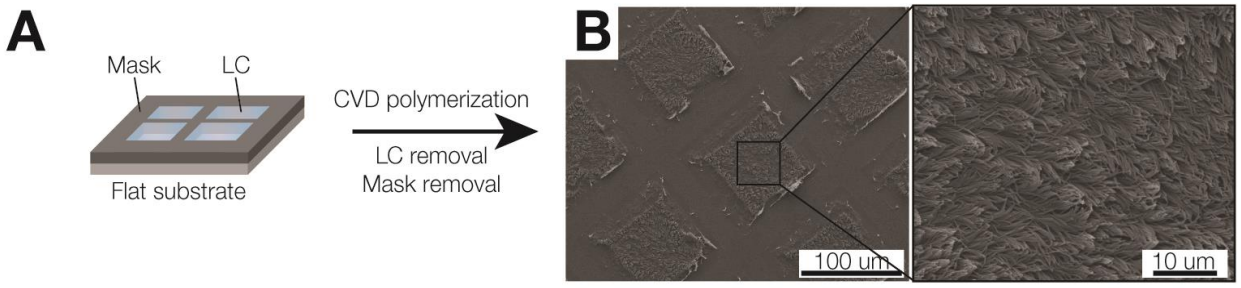

Figure 3-21: Graphical illustration of a flat substrate covered with patterned LC films spaced apart by a TEM grid. CVD polymerization of 1a onto the patterned LC films, followed by removal of LC and TEM grid, reveals an island of nanofiber arrays on the substrate surface.

A scalable approach towards mesoscopic nanofiber structures (Figure 3-22A) involved the deposition of micron-sized LC droplets onto a glass substrate using electro-spraying followed by CVD and removal of the templating phase. Figure 3-22B&C confirms that spherical nanofiber patterns can be prepared with micron-scale resolution.

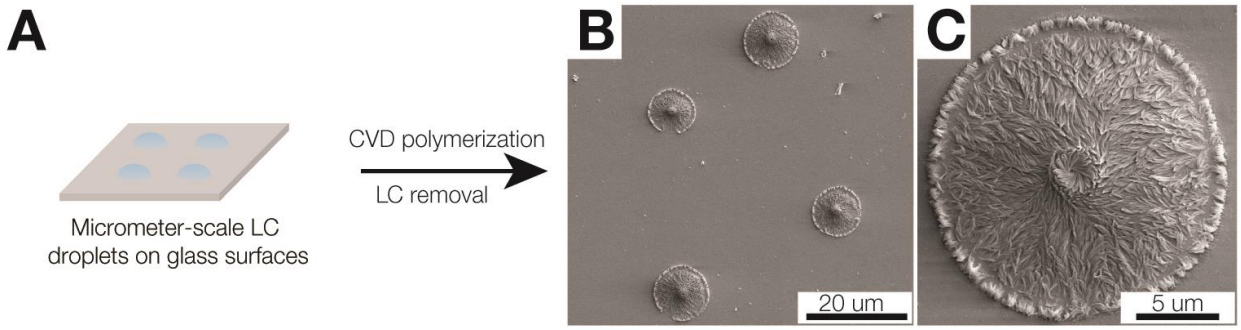

Figure 3-22: (A) CVD of 1a on a glass surface decorated with E7 microdroplets and (B-C) SEM images of the nanofiber assemblies. The E7 microdroplets were prepared via electrospraying onto a OTS-treated glass substrate. Electrospraying was performed by Jason Gregory, Lahann Research group, University of Michigan.

Figure 3-23A shows that a free-standing LC films can also templated aligned nanofiber assemblies. Figure 3-23B shows a metallic mesh with 110 μm-wide pores that are partially coated with a thin film of LC. After CVD polymerization and LC removal, highly aligned and uniform nanofibers are observed to span the LC-coated pores. In contrast, parts of the metal mesh that were not coated with LC were covered with a conformal polymer coating.

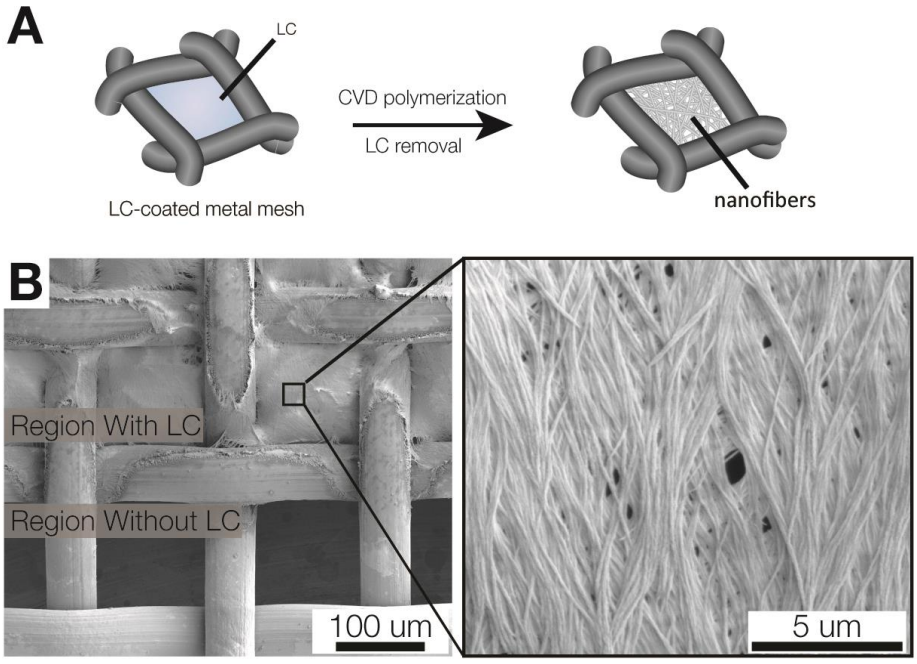

Figure 3-23: (A) CVD of 1a on a stainless steel (SS) mesh coated with E7 and (B) SEM image of suspended nanofiber film.

At a larger scale, Figure 3-24 confirms this finding for a glass capillary that was filled with LC prior to CVD polymerization. A free-standing film of nanofibers was formed at the orifice of the capillary. In contrast to Figure 3-23, the templated nanofibers are no longer aligned, suggesting that the LC phase lacked uniform order over extended areas.

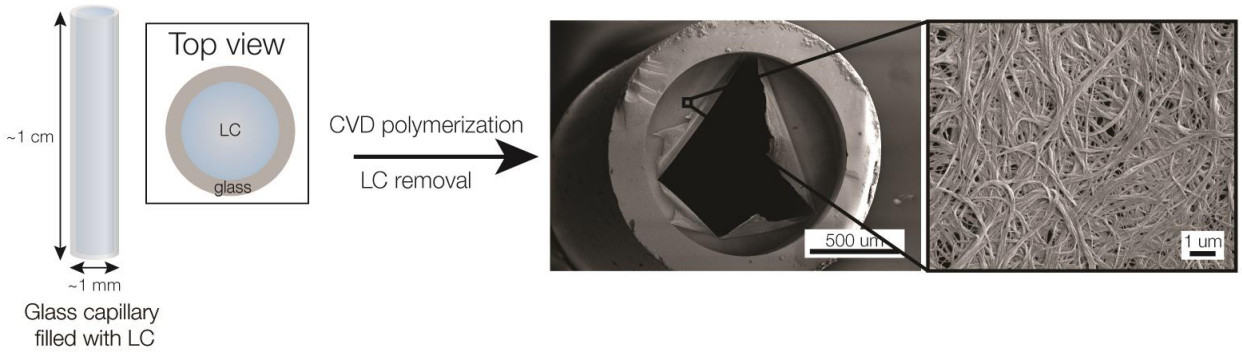

Figure 3-24: CVD of 1a on a glass capillary entirely filled with E7. SEM image of nanofiber membrane spanning the tip of a glass capillary, which was initially intact, but was opened during microscopy revealing an ultrathin nanofiber array.

When glass microbeads were dispersed in the LC fluid prior to CVD polymerization, complex fiber bundles were formed locally at various locations on the beads, suggesting that topological defects induced by the particles in the templating LC phase may influence fiber initiation and growth (Figure 3-25) [106], [107].

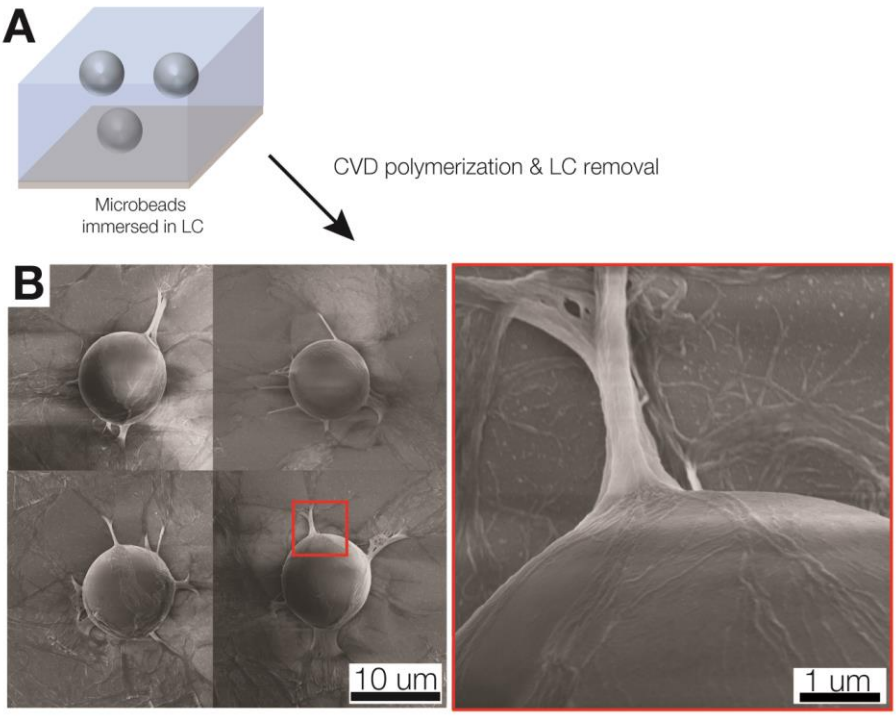

Figure 3-25: (A) Graphical illustration of the immersion of 10um dia. polystyrene microparticles into E7 prior to CVD and (B) SEM images of microparticles decorated with nanofiber bundles after CVD polymerization of **1a** onto the microparticles-dispersed E7 film (22 um thick), followed by LC removal.

The presence of chemically reactive side groups on the poly-p-xylylene enables post modification to immobilize a variety of biomolecules of interest to the nanofiber surface [118]. As a demonstration, streptavidin was immobilized onto a hydroxyl-functionalized **2a** nanofibers using a 2-step bio-conjugation strategy, as illustrated in Figure 3-26. Carboxylic acid-containing biotin linkers (COOH-PEG-biotin) were first immobilized onto the nanofibers via EDC chemistry [118]. During this reaction, carboxylic acid first reacts with EDC (1-Ethyl-3-(3-dimethylaminopropyl)carbodiimide) to form into an O-acylisourea intermediate that can be easily displaced afterwards by nucleophilic attack, from a primary amine group or hydroxyl

group to form an amide bond or ester bond. As the O-acylisourea intermediate can easily undergo hydrolysis in aqueous solution, the O-acylisourea is often reacted with N-hydroxysuccinimide (NHS), or Sulfo-NHS, to convert to an NHS ester to become more stable. This reaction chemically immobilizes COOH-PEG-biotin on the nanofibers, leaving the unreacted biotin groups exposed on the nanofiber surface. As biotin has very strong affinity to streptavidin, incubation of the biotinylated nanofibers in a phosphate buffered solution of streptavidin would immobilize streptavidin onto the nanofiber surface. Fluorescently-labelled streptavidin (streptavidin-Alexafluor647) was immobilized on the biotinylated nanofibers in order to visualize the binding of the streptavidin (Figure 3-27A).

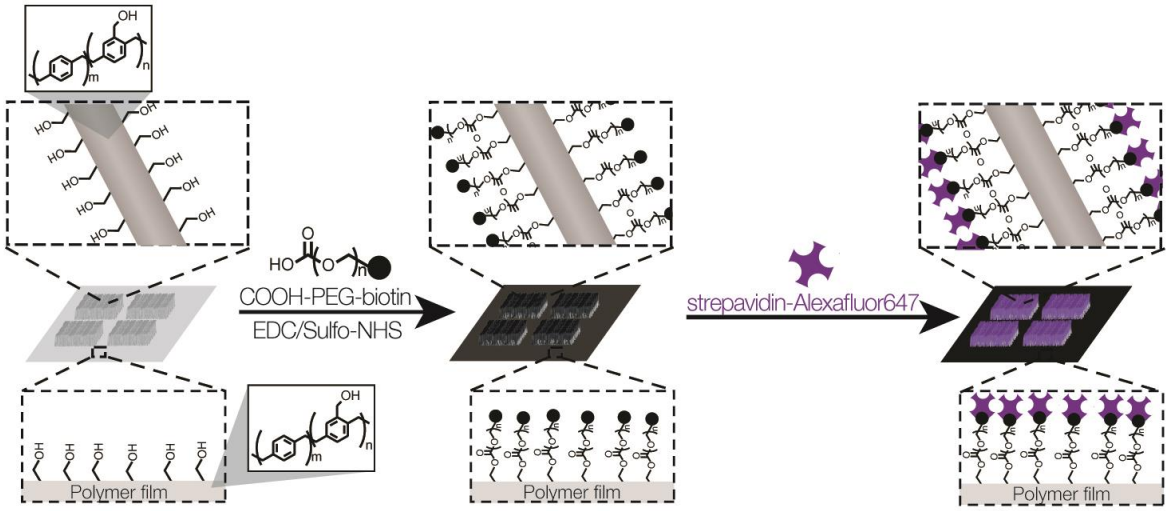

Figure 3-26: Graphical illustration of the immobilization of COOH-PEG-biotin via EDC chemistry and the subsequent immobilization of streptavidin-Alexafluor647 on a patterned surface of hydroxyl-containing **2a** nanofibers.

To ensure that the chemical immobilization of COOH-PEG-biotin was successful, we performed the same streptavidin immobilization procedure without the incorporation of both EDC and Sulfo-NHS. Such a reaction will not chemically immobilize COOH-PEG-biotin on the nanofibers, and we should therefore not be able to visualize any binding of the streptavidin. As shown in Figure 3-27B, the nanofibers exhibit minimal fluorescence signal, confirming our finding.

As the nanofibers have an increased surface area-to-volume ratio, the amount of chemically immobilized streptavidin on the nanofiber arrays should be much higher than that on thin film of the same composition. To test this hypothesis, the fluorescence intensity obtained on the nanofibers and thin film were measured after the immobilization. The intensity measured on the nanofibers was approximately 15 times that measured on the thin film, confirming our hypothesis (Figure 3-27C).

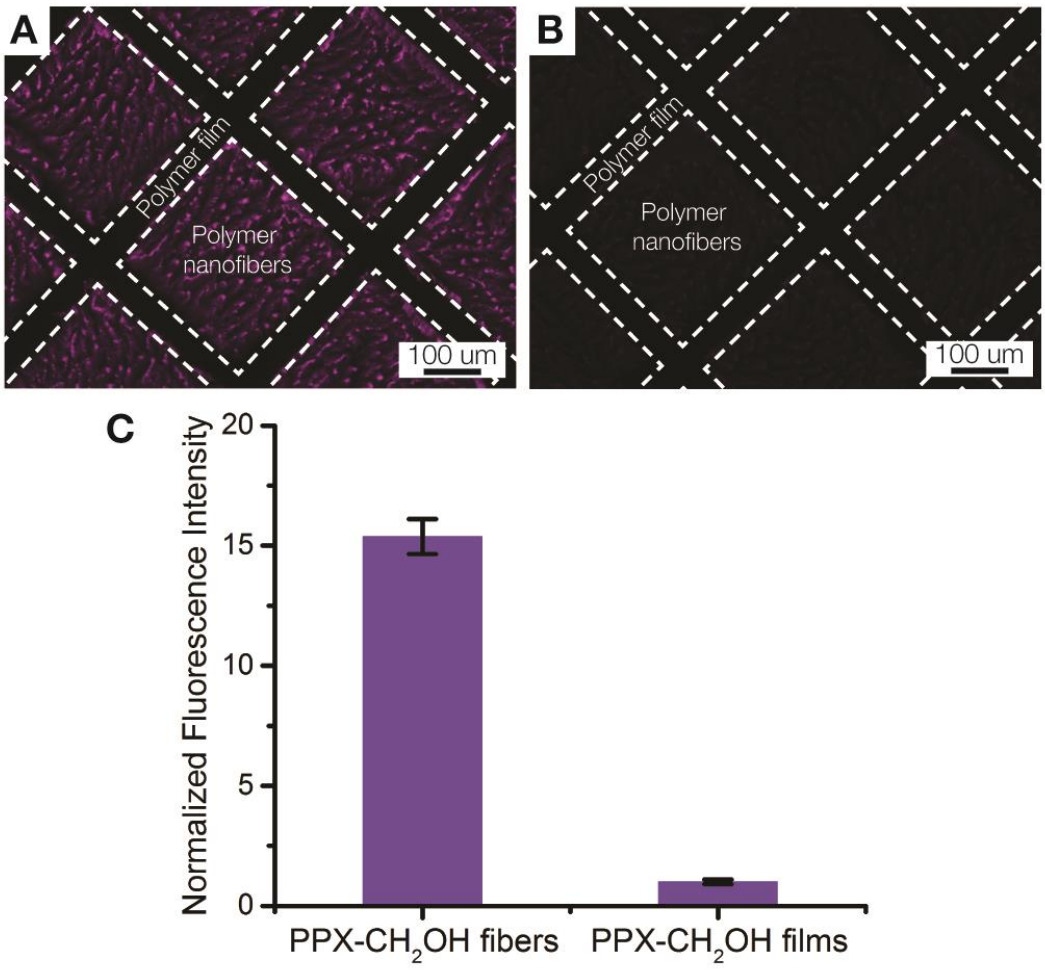

Figure 3-27: (A) Fluorescence micrograph of a patterned polymer 2a nanofiber arrays after undergoing the 2-step immobilization strategy shown in Figure 3-26. (B) Fluorescence micrograph of a patterned polymer 2a nanofiber arrays after undergoing the same 2-step immobilization strategy but without the inclusion of EDC/Sulfo-NHS. (C) Normalized fluorescence intensity measured on polymer **2a** nanofibers and polymer **2a** thin film after the 2-step immobilization. Normalized fluorescence intensity is measured as the mean grey value of region 1-4 divided by the mean grey value measured in region 4.

The CVD polymerization of functionalized [2.2]paracyclophanes not only provides access to a broad arsenal of functional groups [11], but also allows for co-presentation of multiple chemical groups on the same surface, which subsequently enables concurrent

immobilization of different biomolecules [18]. Figure 3-28 shows a synthetic route used to synthesize multifunctional nanofibers followed by co-immobilization of two distinct ligands using bio-orthogonal immobilization strategies. After CVD co-polymerization [18] of **1a** and **1b** into a patterned substrate which presented 285 micron squares of a 18 micron thick film of E7 and LC removal, nanofiber assemblies were found resembling the original LC patterns.

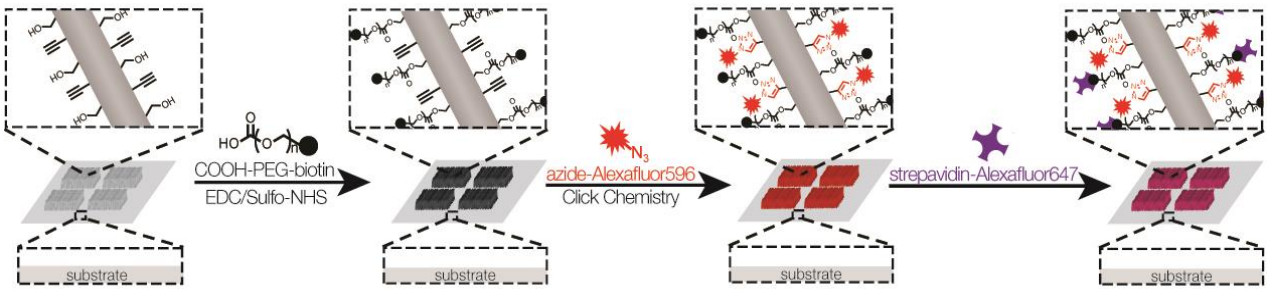

Figure 3-28: Graphical illustration of the immobilization of COOH-PEG-biotin via EDC chemistry, azide-Alexafluor596 via copper-catalyzed click chemistry, and the subsequent immobilization of streptavidin-Alexafluor647 on a patterned surface of polymer 2c nanofibers containing hydroxy and ethynyl groups.

Chemical analysis of the nanofibers confirmed the presence of free hydroxy and ethynyl groups on the nanofibers (Figure 3-13B). Next, the nanofiber assemblies were reacted with an activated biotin ester, that readily binds to hydroxyl groups [118], as well as azide-functionalized Alexa Flour® 596, which exhibited high selectivity towards the ethynyl groups (Figure 3-29A). Finally, Alexa Flour® 647-conjugated streptavidin derivative was used to visualize the presence of biotin groups on the surface of the nanofibers (Figure 3-29B). Co-

immobilization and homogenous distribution of both molecules are revealed in the overlay of images shown in Figure 3-29C.

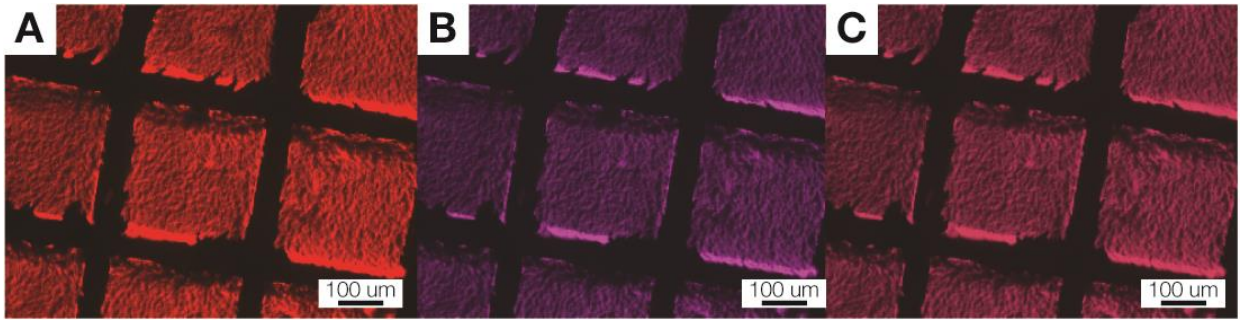

Figure 3-29: Fluorescence Image confirming immobilization of azide-Alexafluor596 (A) and strepavidin-Alexafluor647 (B) on polymer 2c nanofibers containing hydroxy and ethynyl groups. (C) Overlay image of (A) and (B).

To confirm that COOH-PEG-biotin and azide-Alexafluor596 were chemically immobilized on the polymer **2c** nanofibers, we performed the same immobilization on polymer **2a** and **2b** nanofibers that contain only hydroxyl and ethynyl groups, respectively. When polymer **2a** nanofibers that lack ethynyl groups underwent copper-catalyzed click chemistry, minimal azide-Alexafluor 596 were bound to the surface, indicating the unsuccessful immobilization of azide-Alexafluor 596. Similarly, when polymer **2b** nanofibers that lack hydroxy groups underwent EDC reaction followed by incubation in streptavidin-Alexafluor647, minimal streptavidin-Alexafluor647were bound to the surface, indicating the unsuccessful immobilization of streptavidin-Alexafluor647 (Figure 3-30).

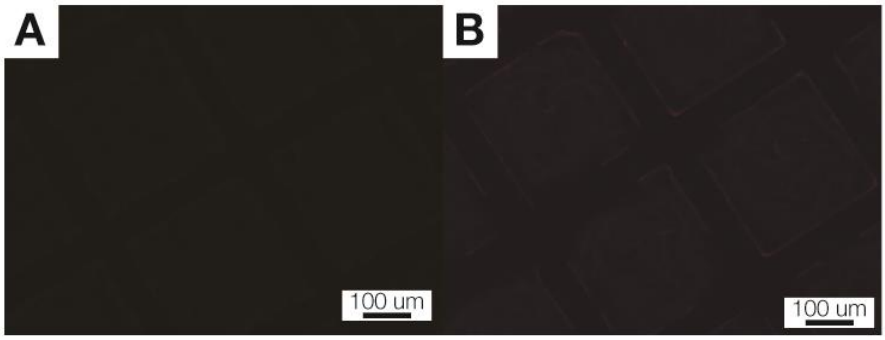

Figure 3-30: (A) Fluorescence Image confirming minimal binding of azide-Alexafluor596 on polymer 2a nanofibers containing only hydroxy groups. (B) Fluorescence Image confirming minimal binding of COOH-PEG-biotin/streptavidin-Alexafluor647 on polymer 2b nanofibers containing only ethynyl groups. These observation demonstrates that the binding of fluorescence molecules in Figure 3-29 is due to chemical immobilization instead of physical adsorption.

3.4. Conclusions

In conclusion, we believe that our work opens a new platform for designing functional polymer nanostructures with programmable geometry, alignment and chemistry. In particular, we have demonstrated that templated nanofiber assemblies are stable material' structures that can effectively modulate the circular polarization of light. Our simple and potentially scalable approach to chiral films of controlled thicknesses should lend itself to systematic studies of chiral material properties that may guide further progress in the development of optical and optoelectronic functionalities. The ability to create functional and programmable nanostructures on a broad range of materials and complex geometries will be attractive to a

variety of applications, ranging from biomedical sensors, to filtrations, to catalytic reaction supports.

CHAPTER 4 Directed Assembly of Twisted Nanofibers via CVD Polymerization of Chiral-Substituted [2.2] Paracylophanes in LC

The materials in this chapter were adapted from the following journal article:

- **Cheng, K. C. K.**, Hussal, C., Spuling, E., de France, A., Vargas, D., Abbott, N. L., Brase, N. S., Lahann, J., "Directed Assembly of Twisted Polymer Nanofibers by Chemical Vapor Deposition (CVD) in Liquid Crystals". *Manuscript* i*n preparation*.

4.1 Overview

In the previous chapter, we demonstrated the ability to create arrays of aligned polymer nanofibers when we performed CVD polymerization of [2.2] paracyclophanes in a thin film of nematic liquid crystals. During the CVD polymerization, the thermally generated di-radicals partitioned into the thin nematic liquid crystal layer and polymerized inside this layer. The LC layer acted as a template for the polymerization, and the anisotropic molecular arrangement in the LC layer guided the polymerization to form into an array of aligned polymer nanofibers. We then demonstrated that when CVD polymerization is performed on LC templates possessing

chirality (i.e. when we use cholesteric LC as the LC template for the CVD process), the helical molecular arrangement in the LC template guided the polymer to form into an assembly of helical nanofiber bundles. In this chapter, we substituted chiral centers onto [2.2] paracyclophane and explored how the incorporation of chiral substituents could influence the formation of nanofibers when it was polymerized in a thin layer of nematic LC film via CVD polymerization.

4.2 Experimental Methods

Materials

5CB, E7, TL205 and MDA-98-1602 liquid crystal (LC) / LC mixtures were purchased from EMD Millipore. 3 x 1 Glass slides were purchased from Fisher Scientific. Quartz and TEM grids were purchased from Electron Microscopy Science. All other chemicals were purchased from Sigma Aldrich.

Synthesis of chiral-substituted [2.2] paracyclophanes

The synthesis of chiral-substituted [2.2] paracyclophane **1a-f** was completed by Eduard Spruling (Braese Research Group, Karlsruhe Institute of Technology). The synthesis of chiral-

substituted [2.2] paracyclophane **1g** was completed by Christoph Hussal (Lahann Lab, Karlsruhe Institute of Technology).

Fabrication of Liquid Crystal Specimens

Glass substrates were first sonicated in isopropanol and were then rinsed with ethanol. The glass substrates were then incubated in an aqueous solution containing 0.5 wt% of HTAB for ~20 seconds, followed a thorough rinse in DI-water. TEM grids were subsequently placed on the HTAB-treated glass substrate, and a ~1 uL droplet of LC was placed on top of the grid, allowing the LC to fill the empty space within the grid. Excess LC was then removed from the grid using a capillary tube, yielding a ~18 um thick LC layer on the glass substrate supported by the TEM grids (*4*, *5*).

CVD polymerization

CVD polymerization was carried out in a custom-built CVD system, as described in the previous chapter. Briefly, a fixed amount of precursor substituted [2.2] paracyclophanes **1** was sublimed at ~100 ^{o}C under 0.1 mbar, after which the precursor vapor underwent pyrolysis at 550 ^{o}C (Scheme 4-1). Following pyrolysis, the thermally generated diradical vapors deposited into a thin film of LC placed on a cooling stage at 17 ^{o}C and the polymerization occurred inside

the LC film. The deposition rate was fixed at 0.1 - 0.3 A/s. After CVD polymerization, the specimens were rinsed repeatedly in ethanol and acetone to remove the LC film to reveal the poly-p-xylylene **2** structures anchored on the substrate.

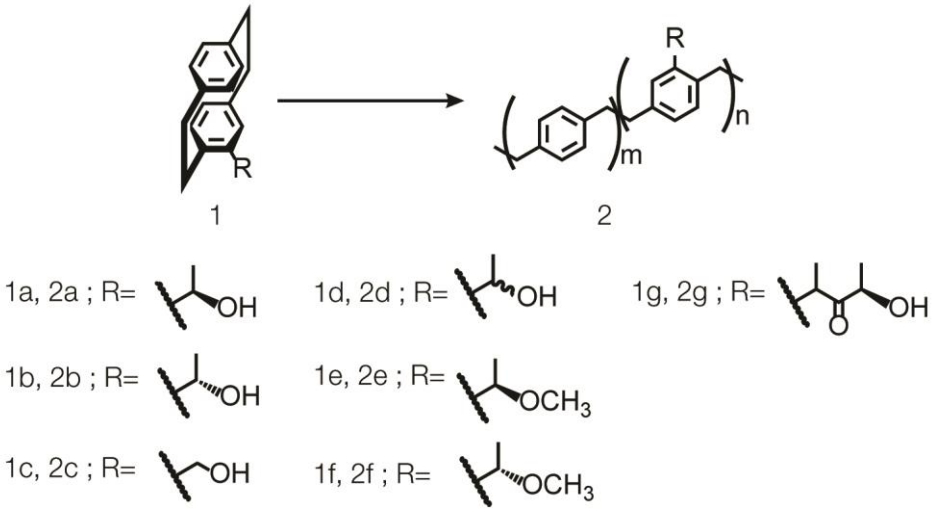

Scheme 4-1: CVD polymerization of substituted [2.2]paracyclophanes 1a-h to functional poly-p-xylylene 2a-h.

Characterization

The chemical composition of the nanofibers was characterized using FTIR and XPS (Kratos). The morphology of the nanofibers was characterized using SEM (FEI Helios). The optical properties of the nanofibers were analyzed using UV-vis absorption and circular dichroism spectroscopy. Detailed description of each characterization techniques can be found under the *Materials and Experimental* section in Chapter 3.

4.3 Results and Discussion

To explore how incorporating a chiral substituent on the [2.2]paracyclophane would influence the formation of nanofibers in the LC-templated CVD process, we synthesized a new type of [2.2]paracyclophane, **1a**, containing a S-configured ethylethan-2-ol substituent (Scheme 4-1) and subsequently performed CVD polymerization of **1a** onto a thin film of nematic LC (MDA-98-1602), as shown in Figure 4-1. Subsequent removal of LC revealed an array of twisted nanofibers anchored on the substrate surface. Each single nanofiber exhibited an exclusive clockwise (CW) twist along the fiber axis.

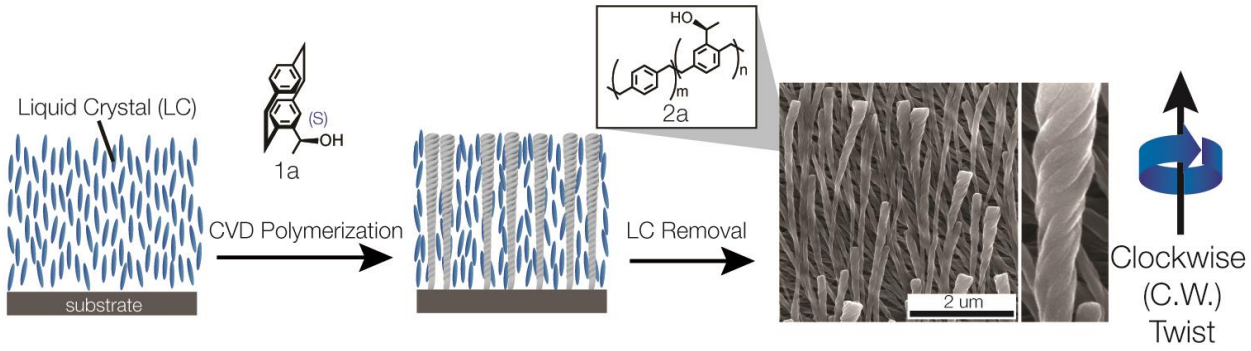

Figure 4-1: Schematic of the formation of twisted nanofibers and a representative SEM image of the twisted nanofibers decorated on the substrate surface. Substituted [2.2]paracyclophane 1a was templated in a thin film of LC (MDA-98-1602) via CVD polymerization. The LC layer was subsequently removed from the specimen to reveal the twisted nanofibers decorated on the substrate surface.

We examined the chemical composition of the resulting nanofibers via FTIR and XPS. The IR spectrum obtained from the nanofibers resembles that of the polymer thin film of the same composition. However, the signal of the characteristic bands of O-H at 3100-3600 cm^{-1} is

weaker than that on the polymer thin film. Similarly, XPS also shows less oxygen content and a weaker C-O bonds, suggesting that the thermally-generated xylylenes having chiral substituents may have lower solubility in the LC than the non-substituted xylylenes does, resulting in the formation of polymer having higher concentration of the non-substituted xylylenes and therefore a relative weaker O-H signal in FTIR and XPS.

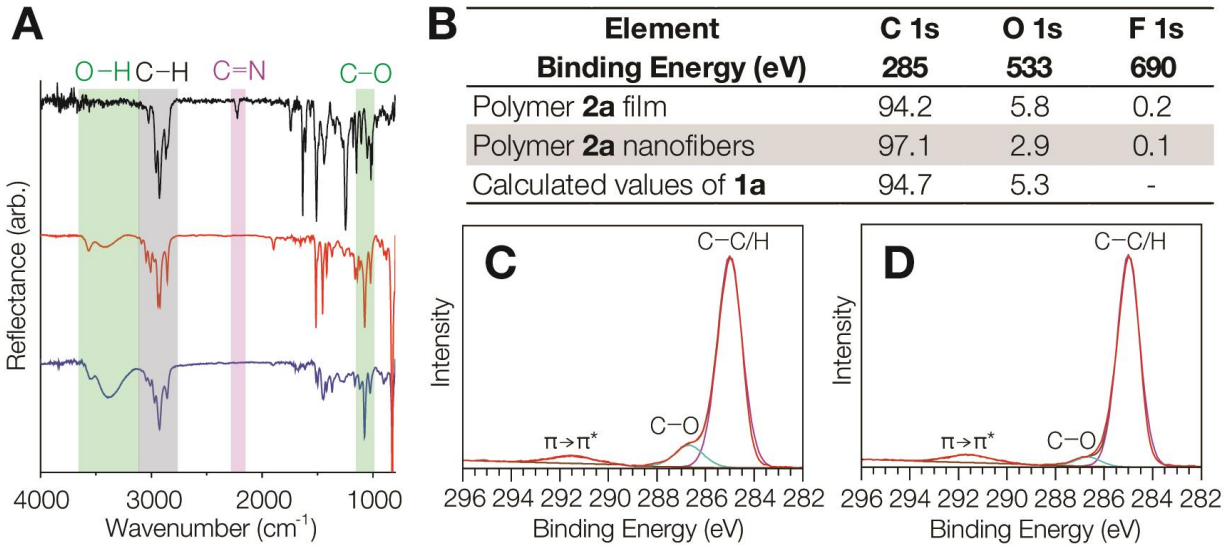

Figure 4-2: (A) FTIR spectra of (black) MDA-98-1602 LC, (red) polymer 2a nanofibers and (blue) polymer 2a thin film. (B) Elemental analysis of polymer 2a thin film and polymer 2a nanofibers by XPS and the calculated values of paracyclophane 1a as a comparison. (C-D) High-resolution C1s scan of polymer 2a (C) thin film and (D) nanofibers.

To understand how the chiral substituent on the [2.2] paracyclophane influenced the formation of the twisted nanofibers, we first compared the morphology of the nanofibers created by polymer having opposite handedness (i.e. [2.2] paracyclophane with R-configured

ethylethan-2-ol substituent). With a R-configured chiral substituent, the resulting surface anchored nanofibers (polymer **2b**) exhibited a counter-clockwise (CCW) twist along the fiber axis, opposite to that of the fibers fabricated with S-configured chiral substituent (Figure 4-3). FTIR spectrum of the R-configured **2b** nanofibers closely resembles that of the S-configured polymer **2a** nanofibers as well as the nanofibers prepared with **1c** (racemic mixture of **1a** and **1b**). To confirm that the fibers prepared from S- and R-configured chiral substituents exhibit opposite twisting direction, we analyzed the twisted nanofibers dispersed in methanol using CD spectroscopy (Figure 4-4). Both the CW- and CCW-twisted nanofibers exhibited strong circular dichroism signal in the 200-300 nm region that corresponds to the $\pi \rightarrow \pi^*$ transitions. More importantly, the sign of the CD signals of the CW-twisted nanofibers are opposite to that of the CCW-twisted nanofibers, indicating that twisted nanofibers are opposite in twist direction.

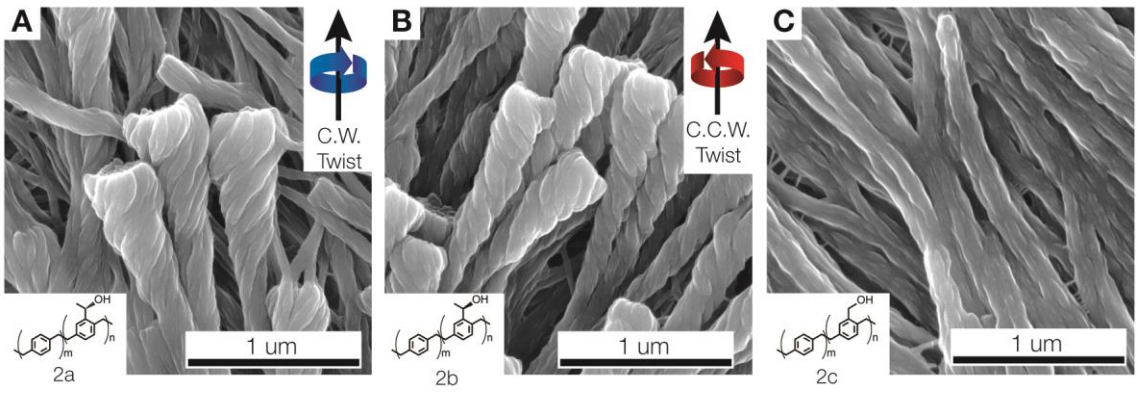

Figure 4-3: SEM images of twisted nanofibers synthesized by CVD polymerization of either (blue) S-configured 1a or (red) R-configured 1b into a thin film of LC (MDA-98-1602). LC was removed prior to imaging.

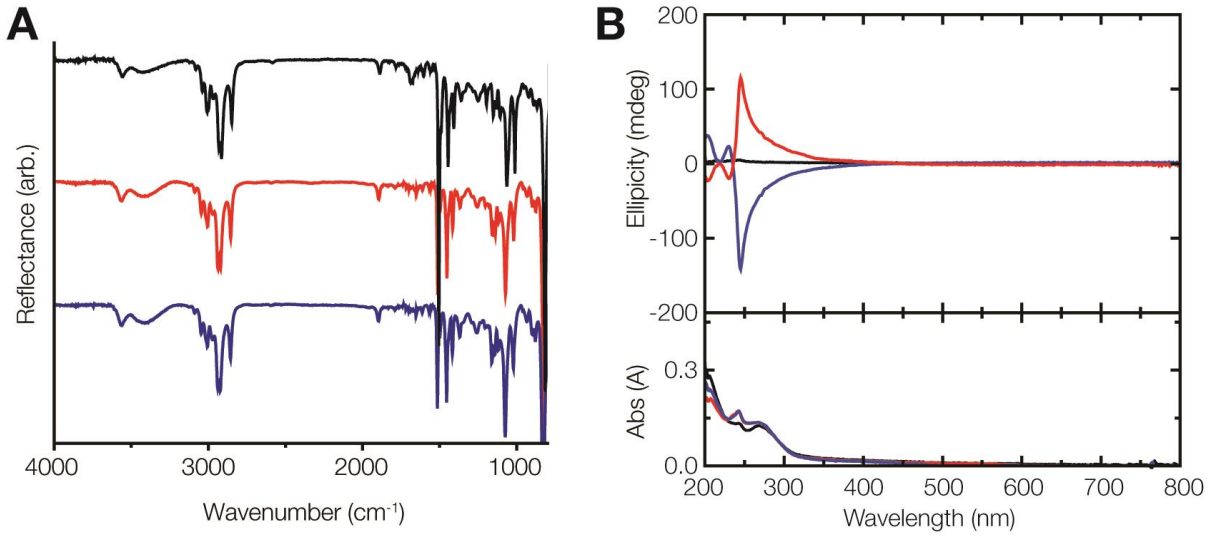

Figure 4-4**:** (A) FTIR spectra of (blue) polymer 2a nanofibers, (red) polymer 2b nanofibers and (black) polymer 2c nanofibers. (B) CD and Abs spectra of twisted nanofibers synthesized by CVD polymerization of either (blue) S-configured 1a, (red) R-configured 1b or (black) racemic mixture 1c into a thin film of LC (MDA-98-1602). LC was removed prior to imaging.

Since S-configured chiral [2.2]paracyclophane yielded exclusively CW-twisted nanofibers and R-configured chiral [2.2]paracyclophane yielded exclusively CCW-twisted nanofibers, the degree of twisting of the nanofibers could potentially be achieved by using a mixture of S- and R-configured [2.2] paracyclophane at precise ratios during the CVD process. To test this hypothesis, we prepared mixtures of S- and R-configured [2.2] paracyclophanes at different ratios and performed CVD polymerization of these mixtures of chiral [2.2] paracyclophanes onto 18 um thick films of LC (MDA-98-1602).

A common method to quantify mixtures of S- and R-configured chiral [2.2]paracyclophane is the percentage of enantiomeric excess (% E.E.) which is governed by the following equation:

$$\%\ Enantiomeric\ Excess\ (\%\ E.E.) = \frac{S_{configured} - R_{configured}}{S_{configured} + R_{configured}}$$

where,

$$S_{configured} = the\ amount\ of\ S - configured\ compound$$

$$R_{configured} = the\ amount\ of\ S - configured\ compound$$

0% E. E. corresponds to racemic mixture (equal mixture of S- and R-configured chiral [2.2] paracyclophanes), while 100% E.E. corresponds to purely S- or R-configured precursor.

We preformed CVD polymerization of chiral precursor ranging from 0% E.E. to 100% E.E. of the S-configured precursor. SEM revealed that the morphology of the resulting nanofibers prepared with different % E.E. of chiral precursor was markedly different (Figure 4-5). With 0% E.E. chiral precursor, the resulting nanofibers were mostly un-twisted. Occasionally, we observed a number of slightly twisted (both CW- and CCW-twist) nanofibers. Overall, the average twist angle was close to 0^o (0.22^o), indicating the lack of helicity on the nanofibers. The absence of CD signals also indicates that there is minimal helicity on the nanofibers prepared with 0% E.E. chiral precursor (Figure 4-6). As the % E.E. increases, the

twist angle increases, and the twist angle reached maximum at 100% E.E. (44°). The CD signals on the resulting nanofibers intensified as % E.E. of the chiral precursor used in the CVD polymerization increased, indicating an increase in helicity on the nanofibers as % E.E. increased. The change in the degree of twisting was not a result of a change in the chemical composition, as FTIR spectroscopy indicated that the resulting nanofibers prepared with different % E.E. of chiral precursors had almost the same chemical composition (Figure 4-6).

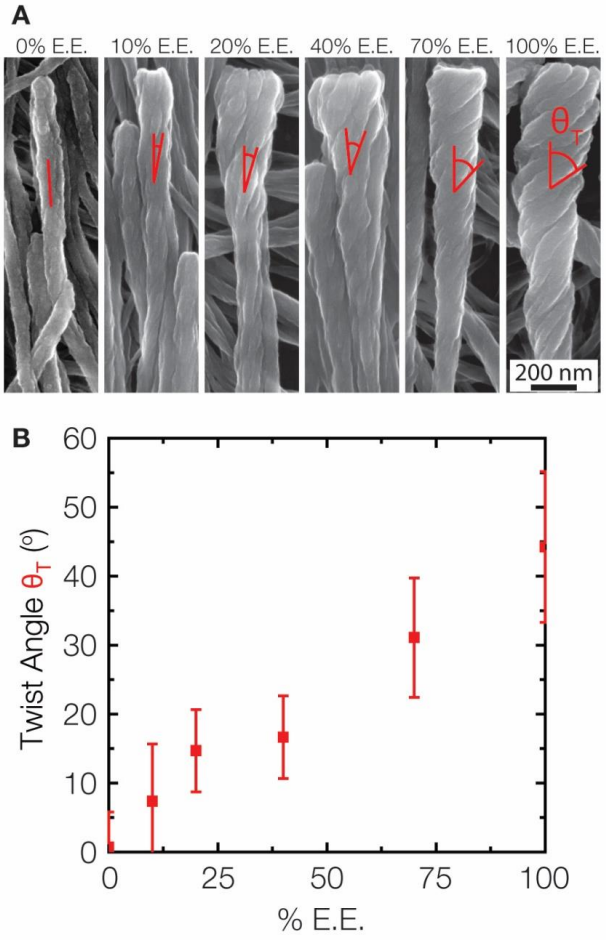

Figure 4-5: (A) Representative SEM images of nanofibers prepared by templating 1a with varying % E.E. into thin film of LC (MDA-98-1602). (B) The average twist angle measured on nanofibers prepared with varying % E.E.

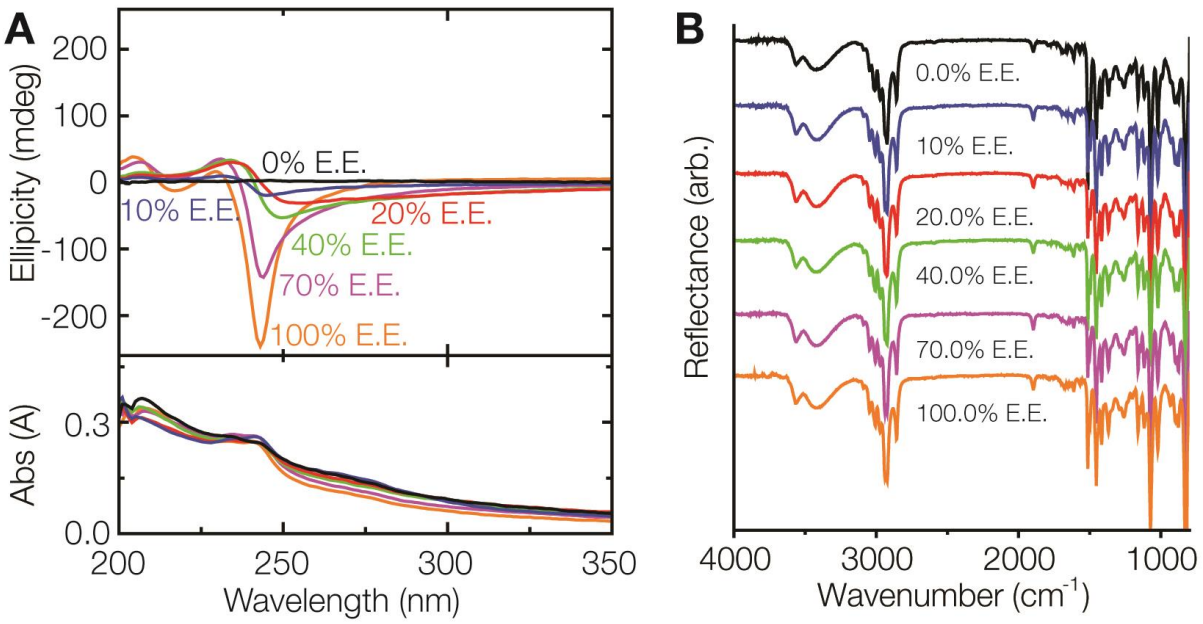

Figure 4-6: (A) CD spectra and (B) FTIR spectra of nanofibers prepared by CVD polymerization of with varying % E.E. into thin films of LC (MDA-98-1602). LC film was removed prior to CD spectroscopy.

A closer examination of the CD spectra could provide insights on how polymer chains were aligned in the nanofibers. Strong bisignate CD signals were found on both CW- and CCW twisted nanofibers at 247 nm (Figure 4-7). For C.W. twisted nanofibers (refer to the blue CD & Abs spectra in Figure 4-7), the bisignate CD signal had a positive CD band in the lower wavelength and a negative band in the higher wavelength, indicating a negative cotton effect induced by exciton coupling from π - π stacking in a CCW configuration. This negative cotton effect occured at the absorption band that corresponds to the π- π transition along the polymer chain (^1L_a transition [119]) (~244nm), suggesting that the polymer chains have a strong intermolecular interaction and would be stacking in a CCW configuration (Figure 4-7B). C.W.

twisted nanofibers showed an opposite trend in which they exhibit positive cotton effect instead, suggesting that the polymer chains would be stacking in a CW configuration.

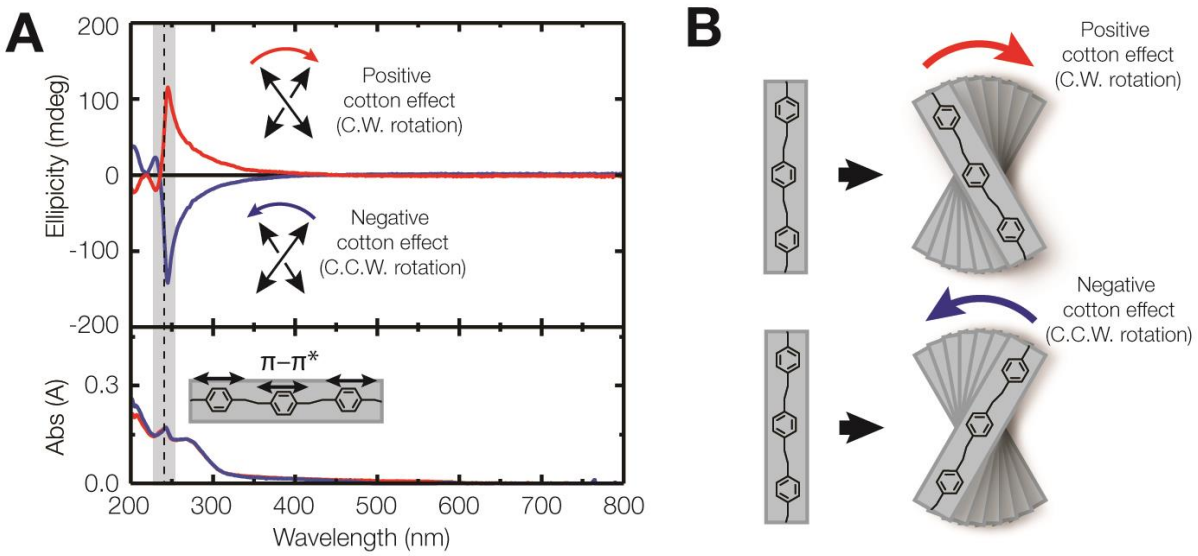

Figure 4-7: (A) CD and Abs spectra of nanofibers dispersed in methanol. Nanofibers were prepared by CVD polymerization of (blue) S-configured la and (red) R-configured 1b into a thin film of LC (MDA-98-1602). LC was removed prior to spectroscopy. (B) Schematic illustration of the proposed intermolecular interaction between polymer chains in each twisted nanofiber based on the cotton effects found in 247 nm.

Both CW- and CCW-twisted nanofibers exhibited another bisignate signal at 272 nm, but the signals were much weaker than the ones at 242 nm (Figure 4-8). CW twisted nanofibers exhibited a positive cotton effect while CCW twisted nanofibers exhibited a negative cotton effect. The cotton effects occurred at 272 nm that corresponded to the π-π transition perpendicular to the polymer chain (^1L_b transition [119]), suggesting that the polymer chain exhibited intramolecular interaction and would be rotating along the polymer chain to induce

the cotton effects (Figure 4-8C) . Polymer chains in CW-twisted nanofibers have CW rotation along the polymer chain, while CCW-twisted nanofibers have a CCW rotation. Based on the polymer configuration shown in Figure 4-7 and Figure 4-8, as well as the morphology of the nanofibers, we proposed that the polymer chains has a P-helicity and should be growing along the fiber axis, as illustrated in Figure 4-9 for CW-twisted nanofibers .

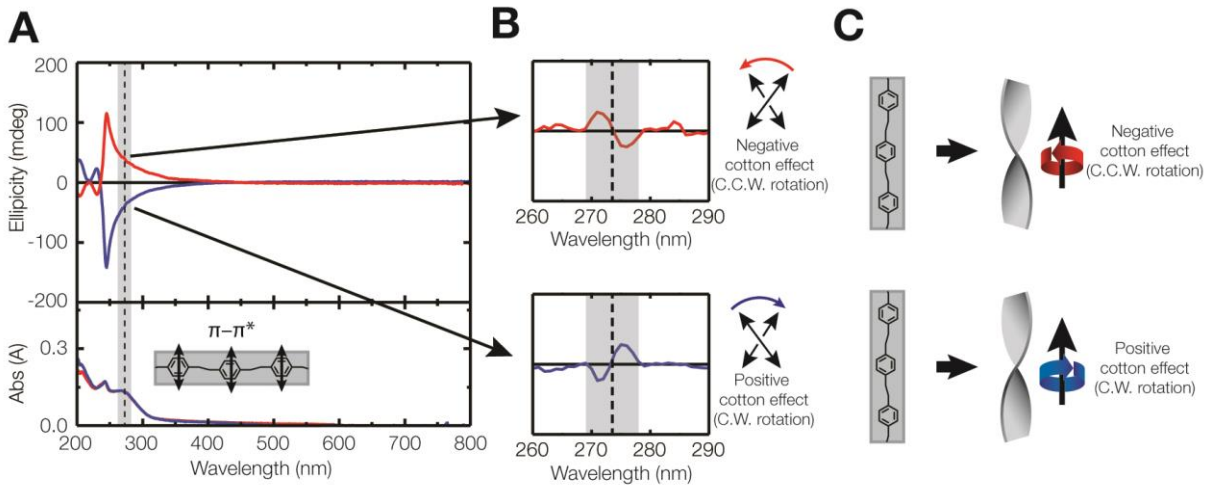

Figure 4-8: (A) CD and Abs spectra of nanofibers dispersed in methanol. Nanofibers were prepared by CVD polymerization of (blue) S-configured la and (red) R-configured 1b into a thin film of LC (MDA-98-1602). LC was removed prior to spectroscopy. (B) Zoomed-in and baseline-corrected CD spectra of (A) to reveal the bisignate signal between 269 and 278 nm. (C) Schematic illustration of the proposed intramolecular interaction on the polymer chains based on the cotton effect found in the 272 nm.

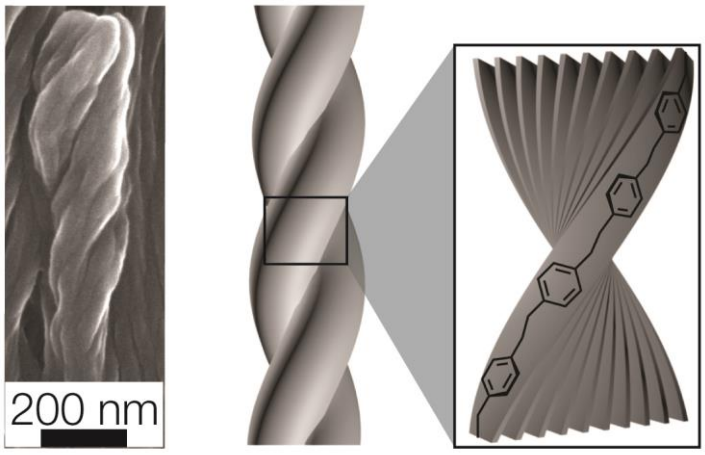

Figure 4-9: Representative SEM image of a CW-twisted nanofibers and a graphical illustration of the proposed alignment and organization of polymer chains in the nanofiber.

So far, we found that the chiral substituent on the [2.2]paracyclophane has a strong effect on the formation of twisted nanofibers. We were interested in understanding if the LC template would also have a strong influence to the formation of twisted nanofibers. To do so, we performed CVD polymerization of chiral [2.2]paracyclophane onto 4 different types of LC films (5CB, E7, TL 205 and MDA-98-1602) (Figure 4-10). The resulting nanofibers templated in all 4 LC types all exhibited CW twist, and the degree of twisting ranged between 39^{o} to 49^{o}. The chemical composition of the resulting nanofibers prepared with the 4 LC types closely resembled each other, suggesting that the LC template did not have a strong influence on the formation of twisted nanofibers (Figure 4-10E). It is worthy to note that while polymer templated in E7, TL 205 and MDA-98-1602 formed into isolated twisted nanofibers, the polymer templated in 5CB formed into interconnected nano-fibril network. This is likely

because 5CB exhibit a weak elasticity and the LCs were not able to confine each single nanofibers during the polymerization process.

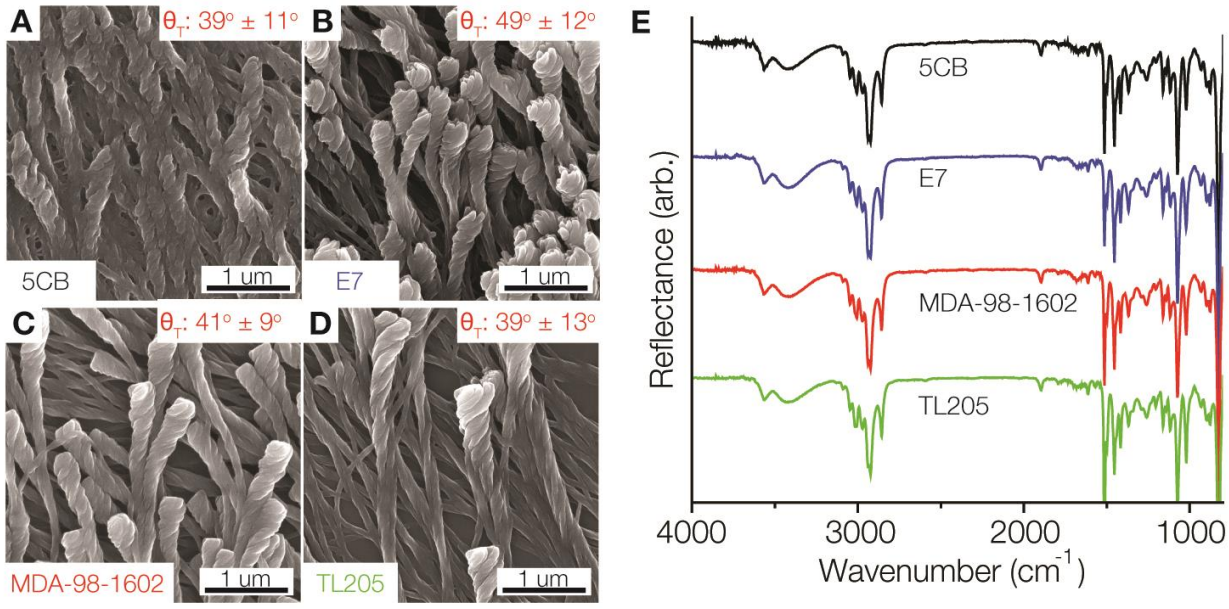

Figure 4-10: (A-D) SEM image of nanofibers prepared by CVD polymerization of 1a into 18um-thick films of (A) 5CB, (B) E7, (C) MDA-98-1602 and (D) TL205. (E) FTIR spectra of nanofibers templated in various LC types.

Mechanistic Study on the formation of twisted nanofibers

In accordance to the above observations, the chiral substituent on the [2.2]paracyclophane had the most significant role in causing the nanofibers to twist. Based on the chemical structure of the chiral substituent, ethylethan-2-ol, there are 2 potential attributes from the chiral substituent to induce the formation of twisted nanofibers: 1) hydrogen bonding and 2) steric effect.

Assessing the Effect of Hydrogen Bonding

Hydrogen bonding can play an important role to the formation of twisted nanofibers because the hydroxy moiety on the chiral substituents enabled hydrogen bonding. It is possible that the presence of hydrogen bonding restricted the stacking configuration of the polymer chains to a certain orientation and resulted in twisting on the resulting nanofibers. Hydrogen bonding is in fact a common design strategy for creating helical polymer and macromolecules via supramolecular assembly [120]–[124].

To assess the effect of hydrogen bonding, we synthesized a new type of chiral [2.2]paracyclophane that replaces the hydroxyl moiety on the chiral substituent with a methoxy moiety instead of hydroxy (**1e** & **1f**). Methoxy moiety is known to have limited hydrogen bonding, and we should therefore not have any hydrogen bonding between polymer chains. The resulting nanofibers prepared by CVD polymerization of the methoxylated chiral [2.2]paracyclophane onto a thin film of LC still exhibited a twist along the fiber axis (Figure 4-11). Specifically, S-configured **1e** yielded nanofibers with C.W. twist while R-configured **1f** yielded nanofibers with C.C.W twist, in accordance to the nanofibers prepared by the hydroxy-containing **1a** and **1b**. To ensure that the twisting of the nanofibers was not due to a change in the chemical composition, we analyzed the chemical composition of the resulting nanofibers by FTIR (Figure 4-12). The IR of the nanofibers closely resembled that of the polymer thin film of the same composition, indicating that the nanofibers are composed of the same polymer

structure as the polymer thin films and that the twisting of the nanofibers are a result of the presence of the methoxylated chiral substituents. Altogether, these results indicated that hydrogen bonding may not be the contributing factor to the formation of twisted nanofibers.

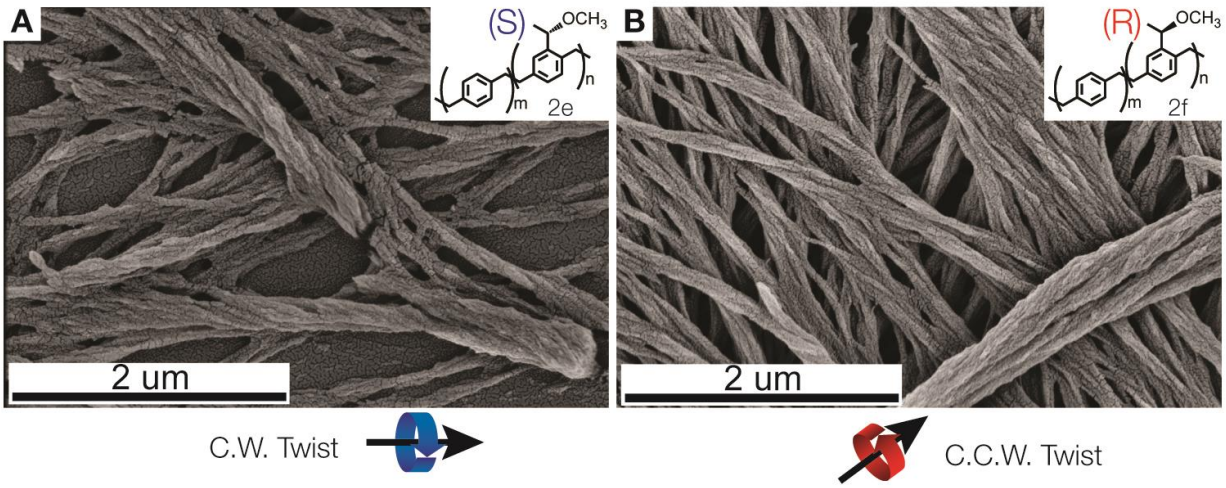

Figure 4-11: SEM images of nanofibers prepared by CVD polymerization of (A) 1e and (B) 1f into thin film of LC film (MDA-98-1602). LC was removed prior to imaging.

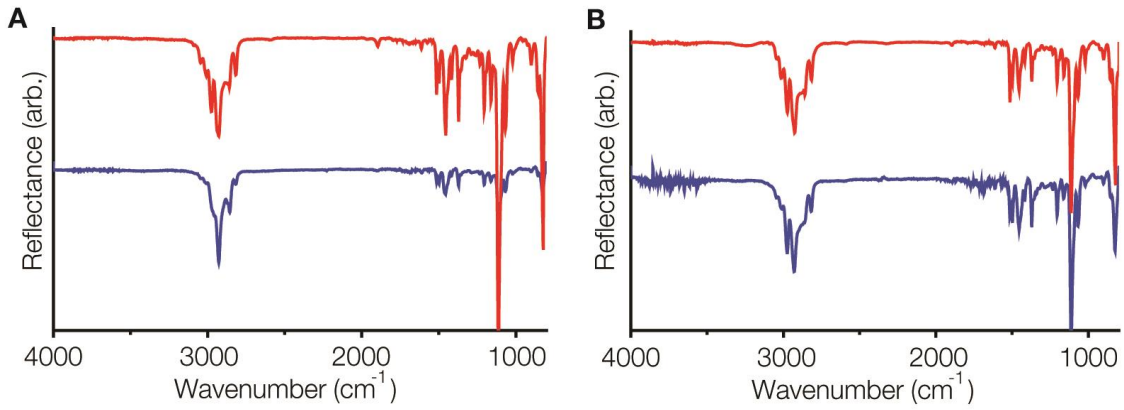

Figure 4-12: FTIR spectra of nanofibers prepared by CVD polymerization of (A) 1e and (B) 1f into thin film of LC film (MDA-98-1602). LC was removed prior to spectroscopy. Red spectra were obtained from the nanofibers while blues spectra were obtained from thin films of the same composition.

Assessing the Influence of Steric effect

In general, chiral molecules have asymmetric size and this asymmetric can induce steric packing and thus helicity in polymer [125]. Steric effect is in fact one of the key factors contributing to the twisted arrangement of mesogens in cholesteric liquid crystals [126]. By either incorporating a chiral center on the LC mesogens or introducing molecules with chiral centers into nematic liquid crystals, the asymmetric size of the chiral moiety distorts the interaction between neighboring LC mesogens. In the case of cholestogens (mesogenic compounds that contains a chiral center), the effect of steric effect depends strongly on the coupling between the mesogenic component and the chiral centers. This coupling effect depends significantly on the distance between the mesogenic component and the chiral center on the mesogen [127]. The coupling effect is strongest when the chiral center is closest to the mesogenic component, and weaken as the chiral center moves far away from the mesogenic component. Therefore, to assess whether steric effect has strong influence on the formation of twisted nanofibers, we examined how the distance between the chiral substituent and the aromatic ring influences the twisting of the nanofibers. We synthesized a new type of [2.2]paracyclophanes, **1g**, that contain a methyl (S)-2-hydroxypropanoate substituent, in which the chiral center is far away from the aromatic ring (Scheme 4-1). CVD polymerization of this chiral [2.2]paracyclophane followed by LC removal reveals surface anchored nanofibers that

do not exhibit noticeable twist along the fiber axis (Figure 4-13). The weak CD signals on the nanofibers dispersed in methanol confirms the weaker twisting on the nanofibers.

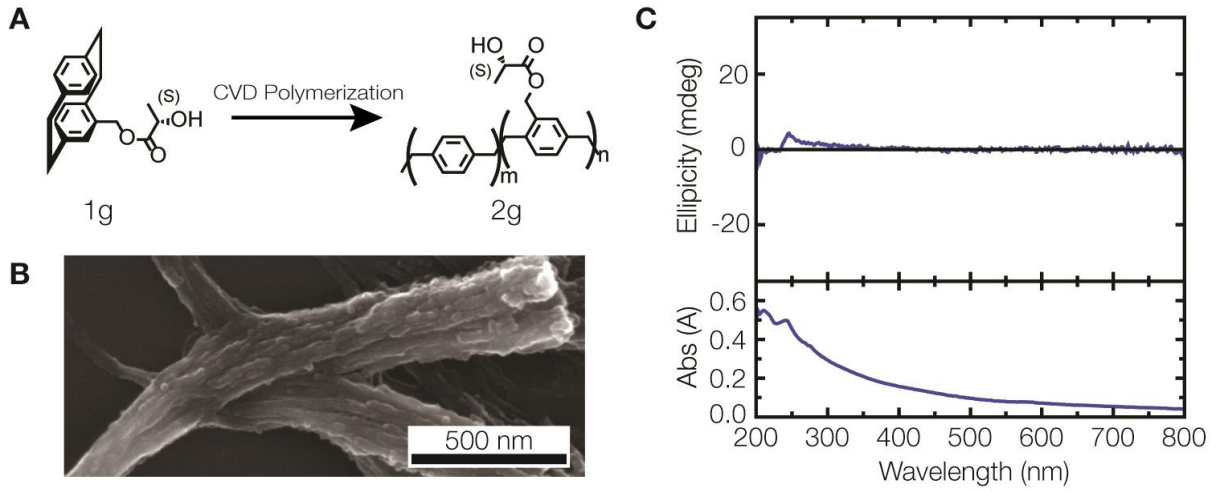

Figure 4-13: (A) Scheme of CVD of 1g into 2g. (B) A close-up SEM image of a polymer 2g nanofiber. The nanofiber was prepared by CVD polymerization of 1g in a thin film of LC (MDA-98-1602). LC was removed prior to imaging. (C) CD/Abs spectroscopy of nanofibers in (B). The nanofibers have weak CD signals, compared to that from polymer 2a nanofibers.

However, the FTIR and XPS analysis of polymer **2g** nanofibers revealed that the polymer nanofibers comprised of significantly fewer chiral side groups (Figure 4-14). Specifically, the characteristic bands of ester (1200 & 1700 cm^{-1}) and hydroxy (3100-3400 cm^{-1}) obtained on the polymer **2g** nanofibers was much weaker than that obtained on the polymer **2g** thin film and the [2.2]paracyclophane **1g**. Similarly, elemental analysis by XPS also indicated a weaker oxygen content on the nanofibers as compared to the thin film. This could be because the chiral-substituted xylylene is less soluble in the LC film than the non-substituted xylylene, and thus, the nanofibers comprise a high concentration of the non-functional xylylene.

This also suggest that the formation of weakly twisted nanofibers with polymer **2g** could be due to lack of chiral side groups instead of steric effect that we hypothesized. Therefore, this study was not sufficient to confirm our hypothesis.

A

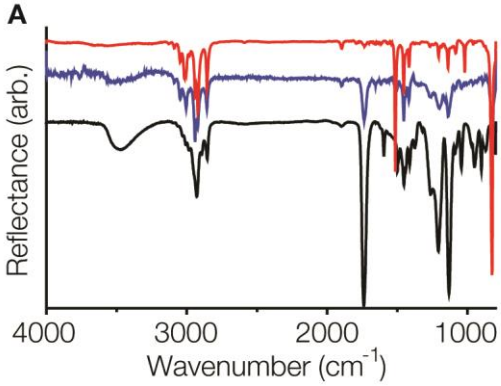

B

Element Binding Energy (eV)	C 1s 285	O 1s 533	F 1s 690
Polymer **2g** film	94.1	5.9	0
Polymer **2g** nanofibers	98.5	1.2	0.3
Calculated values of **1g**	87.0	13.0	-

Figure 4-14: (A) FTIR of (red) polymer 2g nanofibers templated in MDA-98-1602 films, (blue) polymer 2g thin film and (black) [2.2]paracyclophane 1g. (B) Elemental analysis of polymer 2g nanofibers and 2g thin film using XPS and the theoretical values calculated based on [2.2]paracyclophane 1g.

Another approach of examining the contribution of steric effect can be achieved by analyzing the formation of nanofibers with chiral centers of varying molecular sizes, as illustrated in Figure 4-15. It is hypothesized that as the molecular size of the chiral center increases, the degree of the steric effect should increase and thus the degree of twisting should increase as well. Further study using the precursors shown in Figure 4-15 is required to justify the hypothesis.

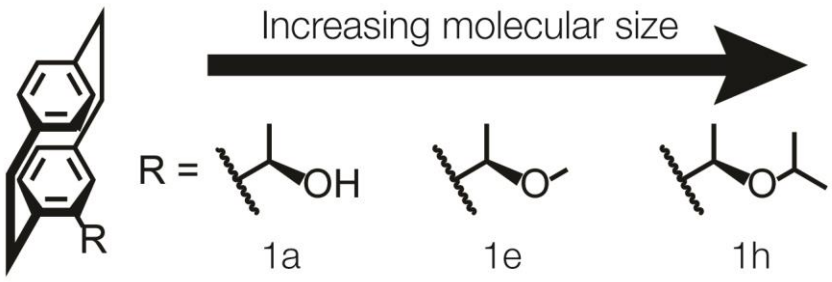

Figure 4-15: Scheme of substituted [2.2]paracyclophane 1a, 1e and 1h with chiral centers of varying sizes.

Nanofibers with hierarchical helicity

As demonstrated in the previous chapter, the shape of the resulting nanofibers can be altered during tuning the molecular arrangement inside the LC film. Herein, we explored the effect of the molecular arrangement of LC molecules on the formation of twisted nanofibers. We performed CVD polymerization of S-configured **1a** onto a thin film of cholesteric LC phase and studied the morphology of the resulting polymer nanofibers. When **1a** is polymerized in S-configured cholesteric LC phase, the resulting nanofibers exhibited CW twisting along the fiber axis, similar to the twisted nanofiber templated in nematic LCs (Figure 4-16). However, in addition to twisting along the fiber axis, the resulting nanofibers exhibited another level of helicity – the twisted nanofibers form into microscopic CW spirals, with a radius of curvature of 0.4 ± 0.1 um (Table 2-1). The formation of microscopic spirals on the twisted nanofibers was likely due to the twisted molecular arrangement inside the LC film. In other words, CVD

polymerization of chiral-substituted [2.2]paracyclophanes into cholesteric LCs resulted in the formation of nanofibers with hierarchical helicity.

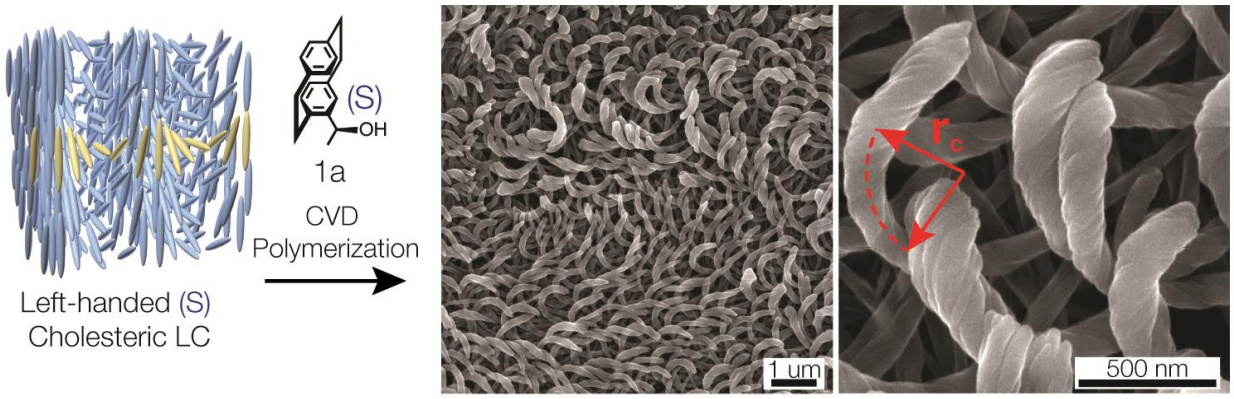

Figure 4-16: Schematic of S-configured 1a templated in R-configured cholesteric LC and SEM of the resulting polymer structure after subsequent removal of LC. The polymer forms into CW-twisted nanofibers with a microscopic CW-spiral.

Interestingly, when the S-configured [2.2]paracyclophane was polymerized into a R-configured cholesteric LC phase, the resulting nanofibers still exhibited CW twist along their fiber axis, but did not form into microscopic spirals anymore (Figure 4-17). This is likely because the S-configured chiral substituents were incompatible in the R-configured cholesteric phase. Therefore, when CW-twisted nanofibers were assembling inside the R-configured LC phase, they distorted the R-configured molecular arrangement in the LC film, resulting in the

formation of "randomly-wiggled" twisted nanofibers with a larger radius of curvature (1.3 ± 0.4 um) than that measured on the S-configured nanofibers templated in S-configured LC (

Table 4-1).

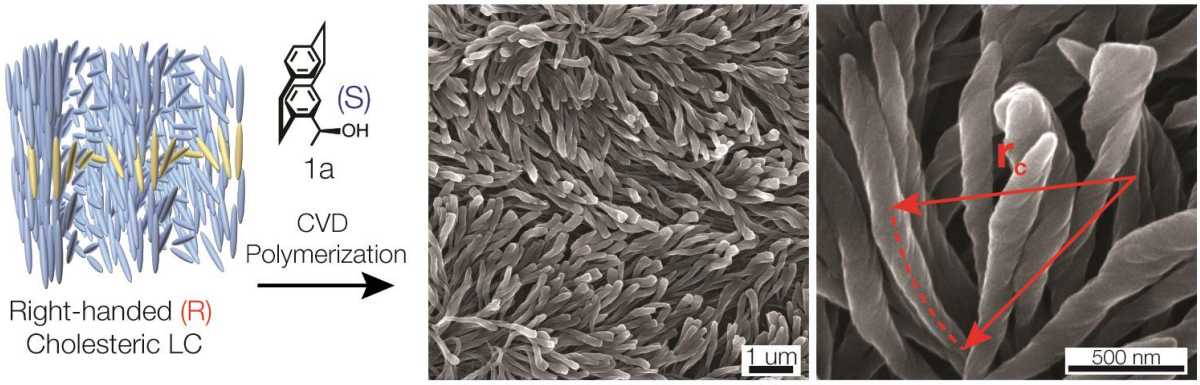

Figure 4-17: Schematic of S-configured 1a templated in R-configured cholesteric LC and SEM of the resulting polymer structure after subsequent removal of LC. The polymer forms into twisted nanofibers with a "randomly-wiggled" microscopic structure.

Table 4-1: Measurement of radius of curvature (r_c) on the nanofibers. N = 40.

Specimen	**Radius of Curvature**
S-configured nanofibers templated in S-configured LC	0.4 ± 0.1 um
S-configured nanofibers templated in R-configured LC	1.3 ± 0.4 um

4.4 Conclusion

This study demonstrated, for the first time, the ability to create polymer nanofibers with predominant twisting by CVD polymerization of chiral-substituted [2.2]paracyclophanes in nematic liquid crystals. The presence of chiral substituents on the polymer induced a rotation in the π- π stacking of the polymer chain, which in turn produced a morphologically visible twisting along the fiber axis of the nanofibers. The ability to create nanofibers with programable twist and the ability to create hierarchical twisted nanofibers create another dimension of versatility to the LC-templated CVD method. The programable twisted nanofibers can find potential use as a template for chiral catalysts and chiral metamaterials.

.

CHAPTER 5 Templated CVD Method for Synthesizing Nanofibers: Going Beyond Poly(p-xylylene)s

5.1 Overview

The LC-templated CVD process has so far been used to create poly-p-xylylene-based nanofibers. In this chapter, we show that the LC-templated CVD method could be extended to fabricating nanofibers made of other CVD-based polymer systems, such as poly(lutidine) and poly(p-phenylene vinylene).

5.2 Assembly of Poly(lutidine) nanofibers via LC-templated CVD

This sub-section is completed in collaboration with Christoph Hussal (Lahann Lab, Karlsruhe Institute of Technology). Details of the work allocation can be found in the Experimental Methods section.

5.2.1 Background

CVD polymerization based on the Gorham process has thus far been centered around poly(p-xylylene) polymer system that composes of an all carbon backbone. Such all-carbon backbone structures render the polymer surface hydrophobic and unfavorable for cell adhesion. F. Bally-Le Gall et. al. recently reported a new class of CVD-based polymer thin film coating, known as poly(2,5-lutidinelene-co-p-xylylene), or poly(lutidine) (Scheme 5-1) [128]. poly(lutidine) thin films are synthesized by CVD polymerization of [2](1,4)benzene[2](2,5)pyridinophane, or pyridinophane. The presence of nitrogen atoms on the aromatic rings of the polymer backbone render the polymer surface more positively charge, when compared to poly(p-xylylene). The more positively charged poly(lutidine) surface attracted 2.5x more HUVECs to bind onto the surface when compared to poly(p-xylylene) (Figure 5-1).

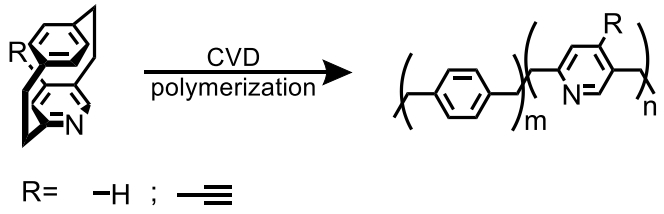

Scheme 5-1: CVD polymerization of pyridinophane and ethynyl-substituted pyridinophane into poly(2,5-lutidinelene-co-p-xylylene) (poly(lutidine)) and poly(4-ethynyl-2,5-lutidinelene-co-p-xylylene) (ethynyl-functionalized poly(lutidine)), respectively.

Furthermore, by substituting the pyridinophane precursor with a reactive moiety, such as ethynyl group, we can perform CVD polymerization of the substituted pyridinophane to create ethynyl-functionalized poly(lutidine) (poly(4-ethynyl-2,5-lutidinelene-co-p-xylylene) thin films. The incorporation of ethynyl groups on the polymer thin film enables post surface modification (via copper catalyzed click reaction) for immobilizing (bio)molecules of interest onto the polymer surface (Figure 5-2).

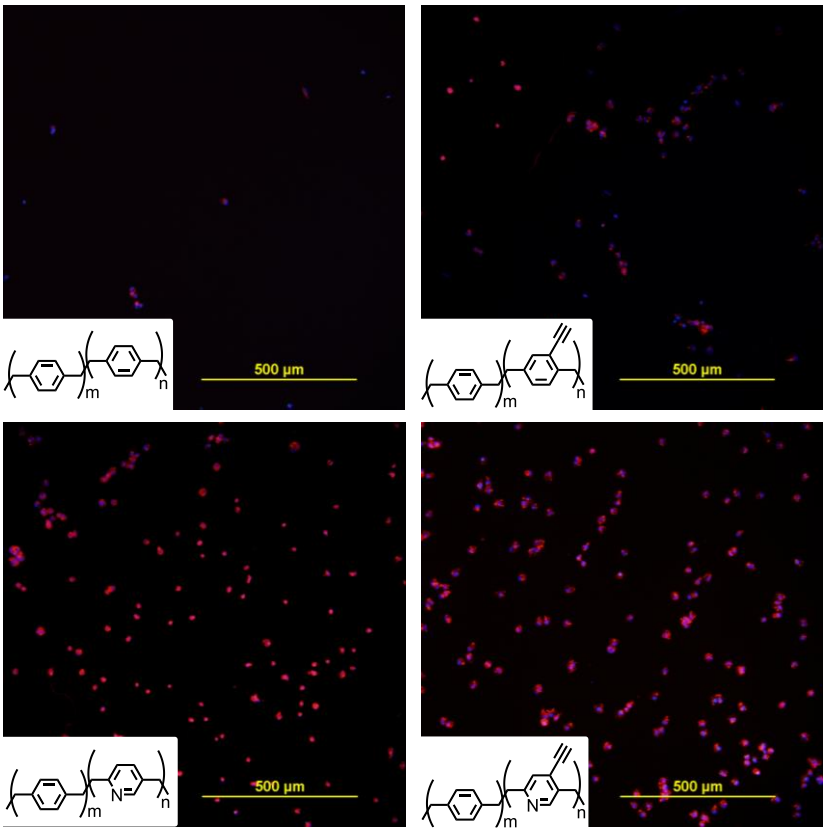

Figure 5-1: Binding of HUVEC onto various polymer coatings. (Top left: poly-p-xylylene; Top right: poly(4-ethynyl-p-xylylene-co-p-xylylene); Bottom left: poly(2,5-lutidinelene-co-p-xylylene); Bottom right: poly(4-ethynyl-2,5-lutidinelene-co-p-xylylene).

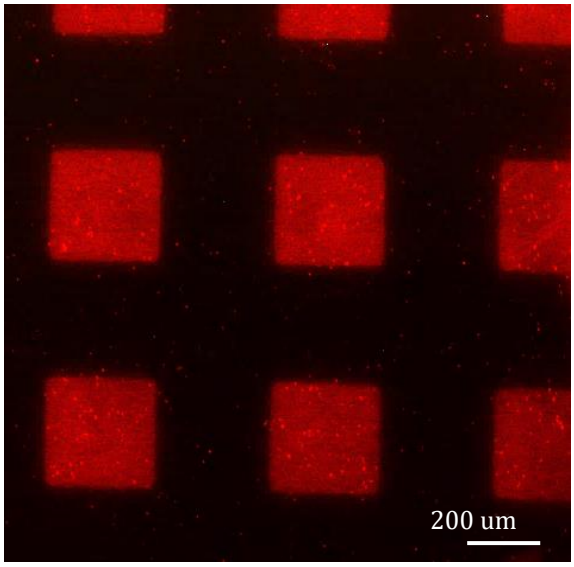

Figure 5-2: A fluorescence image of a patterned poly(lutidine)/ ethynyl-functionalized poly(lutidine) sample that had undergone copper-catalyzed click chemistry to immobilize azide-PEG-biotin and subsequent incubation in Alexafluor596-conjugated streptavidin solution. Red fluorescence signals were only found on the regions containing ethynyl-functionalized poly(lutidine), indicating that the ethynyl groups could chemically reacted with the azide-PEG-biotin linker such that the streptavidin could subsequently bind to the biotin on the linkers that had been bound to the ethynyl groups on the polymer.

5.2.2 Experimental Methods

Materials

Ethanol, acetone, iso-propanol and glass slides were purchased from Fisher Scientific. TEM grids and quartz slides were purchased from Electron Microscopy Science. The precursors were synthesized by Christoph Hussal (Lahann Lab, Karlsruhe Institute of Technology). All other chemicals were purchased from Sigma Aldrich.

LC sample preparation (Performed by Christoph Hussal)

Preparation of the LC samples are adapted from the previous chapters. Briefly, glass and quartz substrates were first sonicated in a solution of iso-propanol for several minutes to remove surface residues. Afterwards, the substrates were immersed in an aqueous solution of 0.5wt% of hexadecyltrimethylammonium bromide for ~20 seconds, and was subsequently rinsed in di-ionized water. TEM grids were then placed on the substrates, and a drop of LC was filled into the pores of the TEM grids. Excess LC was removed by extracting the excess LC using a glass capillary.

Synthesis of poly(lutidine) nanofibers via LC-templated CVD (Performed by Christoph Hussal)

CVD polymerization was performed using the same custom-built CVD system described in previous chapters. LC samples were first loaded onto a rotating stage inside the CVD deposition chamber. The rotating stage was fixed at ~17 ^{o}C. The CVD system was then brought to a reduced pressure of 0.1 mbar, after which precursor monomer, either pyridinophane or ethynyl-substituted pyridinophane, was sublimated at ~100 ^{o}C. The monomer vapor was then pyrolyzed at 550 ^{o}C to convert into di-radical vapors, and was subsequently transferred into the deposition chamber. Once entered the deposition chamber, the diradicals deposited onto the LC specimens and polymerized inside the thin layer of LC. After the CVD

process, the LC film was removed from the samples by rinsing the samples repeatedly with ethanol and acetone. The samples were then used for characterization or surface modification.

Sample Characterization (Performed by Kenneth Cheng and Christoph Hussal)

The chemical composition of the nanofibers and nanofilms was obtained by Fourier transform infrared spectroscopy (FTIR) and x-ray photoelectron spectroscopy (XPS). FTIR analysis of poly(lutidine) and ethynyl-functionalized poly(lutidine) nanofibers were completed by Christoph Hussal. FTIR spectra were obtained on a Nicolet 6700 spectrometer equipped with a grazing angle accessory (SMART SAGE). The glazing angle is set at 80^{o}. 128 measurements were obtained on each sample. XPS spectra were obtained using an Axis Ultra X-ray photoelectron spectrometer (Kratos Analyticals, UK) with mono-chromatized Al Kα X-ray source at 150 kW. All spectra were calibrated with respect to the aliphatic carbon with a binding energy of 285 eV. The morphology of the surface-decorated nanofibers was analyzed by scanning electron microscopy (SEM) (FEI Helios). A thin layer of carbon was deposited onto the specimen prior to SEM to reduce surface charging.

Surface modification (Performed by Christoph Hussal)

Patterned ethynyl-functionalized poly(lutidine) nanofiber arrays on a glass substrate were first fabricated. This is achieved by CVD polymerization of ethynyl-substituted pyridinophane onto a thin film of LC decorated on a glass substrate with TEM grids as the anchor support. Following the CVD polymerization, the LC film was removed by organic solvents and the TEM grid was peeled off from the glass substrates, leaving a 285 um x 285 um square patterns of nanofiber arrays on the glass substrate.

Following the Sample fabrication, the sample was immersed in an aqueous solution containing 10 uM azide-PEG-biotin, sodium ascorbate and copper sulfate for 1 hour, followed by repeated rinsing in DI-water. Subsequently, the sample was incubated in a buffered solution (PBS, pH 7.4) of bovine serum albumin for 10 minutes, and was then transferred into a buffered solution (PBS, pH 7.4) containing 10ug/ml Alexafluor596-conjugated streptavidin, 0.2 bovine serum albumin and 0.01 wt% Tween 20 for 1 hour. Following the incubation, the sample was washed repeatedly in PBS solution containing 0.2 bovine serum albumin and 0.01 wt% Tween 20, and was subsequently imaged using a fluorescence microscope (Nikon 80i).

5.2.3 Results and Discussion

To investigate the possibility of creating poly(lutidine) nanofibers via LC-templated CVD, we performed CVD polymerization of pyridinophane in a thin film of LC (MDA-98-1602). Subsequent removal of LC from the specimen reveals the formation of nanofibers anchored on the substrate surface (Figure 5-3).

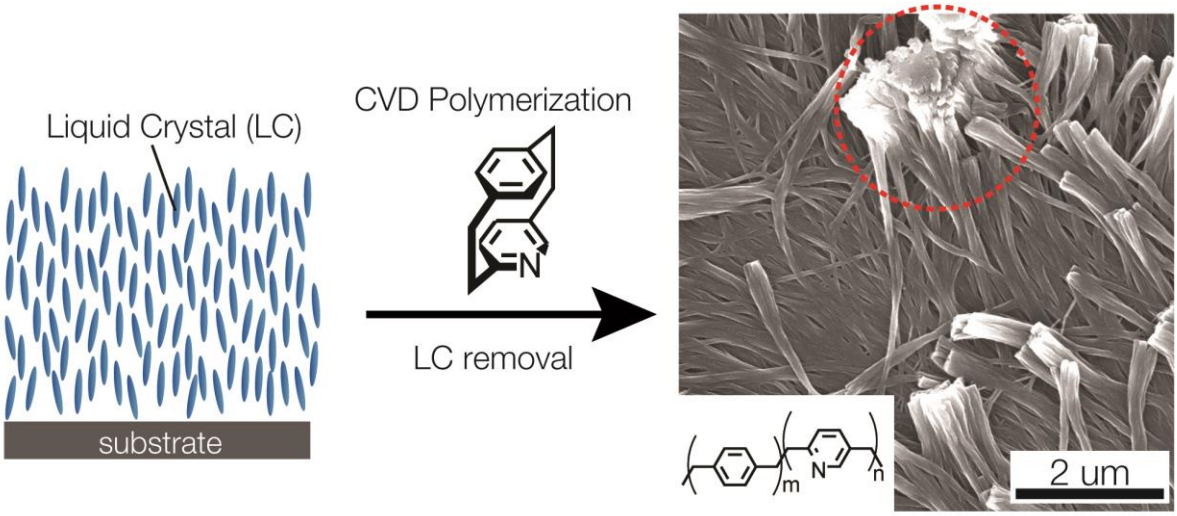

Figure 5-3: Graphical illustration showing CVD polymerization of pyridinophane onto a thin film of LC decorated on a flat substrate to create poly(lutidine) nanofibers. Red dashed circle on the SEM image indicates the aggregation of nanofibers, which is likely due to capillary force that occurs when acetone evaporates from the nanofibers during the LC removal step.

To ensure the nanofibers were composed of poly(lutidine), we conducted FTIR analysis to analyze the chemical composition of the nanofibers (Figure 5-4A). FTIR revealed the presence of characteristic bands at 2800-3100 cm^{-1}, representing the aliphatic and aromatic C-H of the lutidines and xylylenes on the polymer. We further characterized the nanofibers with XPS (Figure 5-4B). The carbon and nitrogen contents were in good agreement with the

poly(lutidine) thin film as well as with the theoretical values of the precursor, indicating that the nanofibers were composed of poly(lutidine) and that our LC-templated CVD method could be extended to creating nanofibers made with other polymer systems, such as poly(lutidine) in this case. The polymer nanofibers contained a low amount of oxygen content that was likely originated from the unreacted free radicals reacting to oxygen in air to form peroxide [129].

A

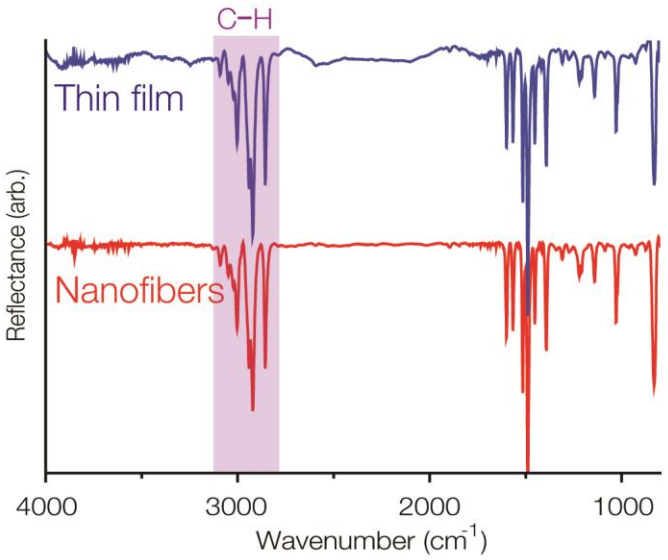

B

Elements	C 1s	N 1s	O 1s
Binding Energy (eV)	285.0	399.2± 0.2	532.8 ± 0.2
Poly(lutidine) thin film	92.5	6.9	0.7
Poly(lutidine) nanofibers	93.6	5.0	1.5
Theoretical value	93.8	6.3	0.0

Figure 5-4: (A) FTIR of poly(lutidine) (red) nanofibers and (blue) thin film. (B) Elemental analysis of poly(lutidine) nanofiber and thin film along with the calculated values from precursor, pyridinophane, as a comparison.

We then investigated the ability to create functionalized poly(lutidine)nanofibers and selected ethynyl-functionalized poly(lutidine) for our proof-of-concept study. We performed CVD polymerization of ethynyl-substituted pyridinophane onto a thin film of LC layer. Following the removal of LC film, SEM revealed the formation of nanofibers anchored onto the substrate surface (Figure 5-5). However, as shown in Figure 5-5, the nanofibers prepared here had a broaden tip, suggesting that the thermally-generated diradicals might not be soluble in the LC and tend to polymerize near the LC-vapor interface.

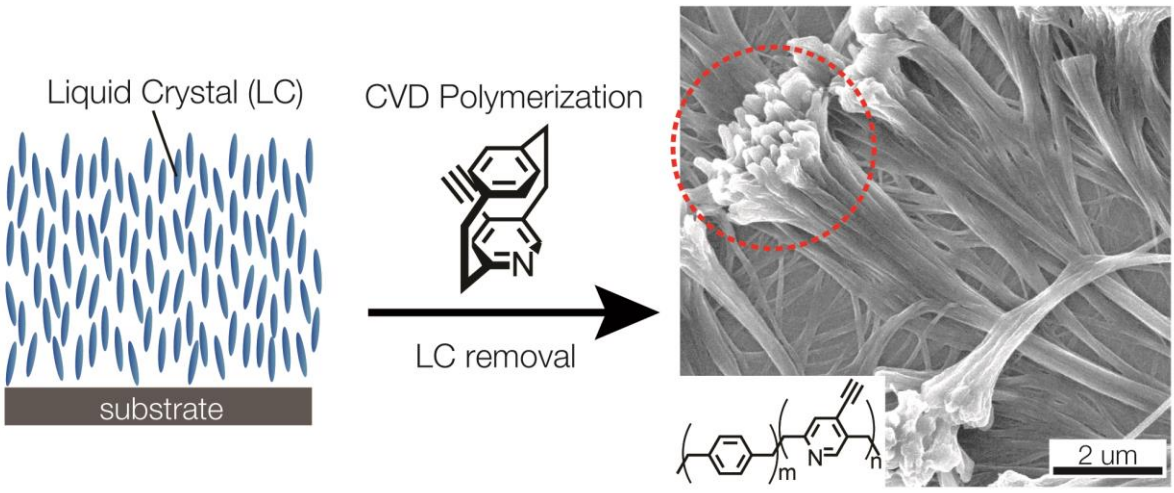

Figure 5-5: Graphical illustration showing CVD polymerization of [2](1,4)benzene[2](2,5)pyridinophane onto a thin film of LC decorated on a flat substrate to create poly(2,5-lutidinelene-co-p-xylylene) nanofibers. Red dashed circle on the SEM image indicates the broadening of nanofiber tip, which is likely due to the insolubility of the thermally-generated reactive intermediates in the LC film that resulted in the preferential polymerization close to the LC-vapor interface.

To ensure the nanofibers were composed of the ethynyl-functionalized poly(lutidine), we examined the chemical composition of the nanofibers via FTIR and XPS (Figure 5-6). The carbon and nitrogen content on the nanofibers agreed with those obtained from thin film ethynyl-functionalized poly(lutidine) as well as those obtained from theoretical calculation. The polymer nanofibers contained a low amount of oxygen content that was attributed to the free radicals on the polymer reacting with oxygen. Furthermore, the presence of characteristic bands of ethynyl at 2100 cm^{-1} (C≡C) and 3300 cm^{-1} (C≡C-H) as well as the characteristic bands of the backbone lutidine and xylylene that range from 2800 cm^{-1} to 3100 cm^{-1} confirmed the successful synthesis of ethynyl functionalized poly(lutidine) nanofibers.

A

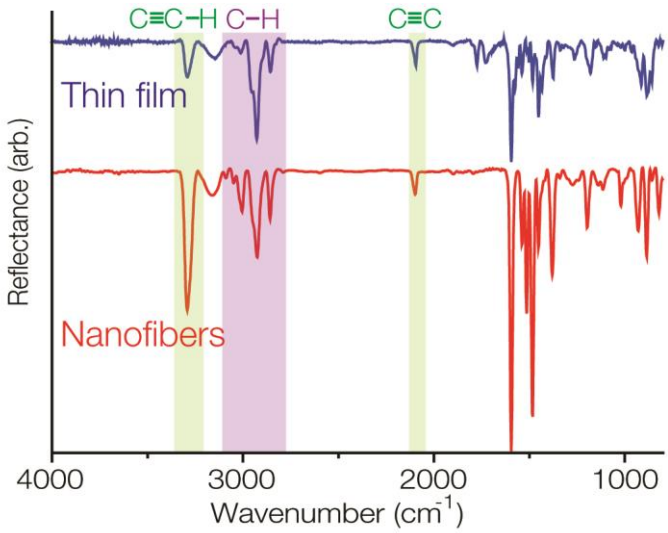

B

Elements	C 1s	N 1s	O 1s
Binding Energy (eV)	285.0	399.2± 0.2	532.8 ± 0.2
Ethynyl-functionalized Poly(lutidine) thin film	91.7	6.2	2.1
Ethynyl-functionalized Poly(lutidine) nanofibers	92.4	5.4	2.2
Theoretical value	94.4	5.6	0.0

Figure 5-6: (A) FTIR of ethynyl-functionalized poly(lutidine) (red) nanofibers and (blue) thin film. (B) Elemental analysis of ethynyl-functionalized poly(lutidine) nanofiber and thin film along with the calculated values of the corresponding precursor as a comparison.

To demonstrate the reactivity of the ethynyl functional groups on the resulting ethynyl-functionalized poly(lutidine) nanofibers, we performed a 2-step post-surface modification to selectively bind a model protein, streptavidin, to the nanofibers. The 2-step surface modification process is illustrated in Figure 5-7. Specifically, we first performed the copper-catalyzed click reaction (Huisgen 1,3-dipolar cycloaddition reaction) to bind an azide-functionalized biotin

linker to the ethynyl functionalized nanofibers. With the click reaction, the ethynyl groups reacted with the azide moiety on the linker and form into a 1,2,3-triazoles linkage, leaving the free biotin moieties on the surface of the nanofibers. We then incubated the reacted nanofibers into an aqueous solution containing streptavidin. The free biotins on the reacted nanofibers had a strong binding affinity to streptavidin that would selectively bind to streptavidin from the aqueous solution. Using a fluorescently-labelled streptavidin (streptavidin-Alexafluor596), we could easily visualize the binding of the streptavidin on the nanofibers, as shown in Figure 5-8, confirming the binding of the streptavidin on the nanofibers.

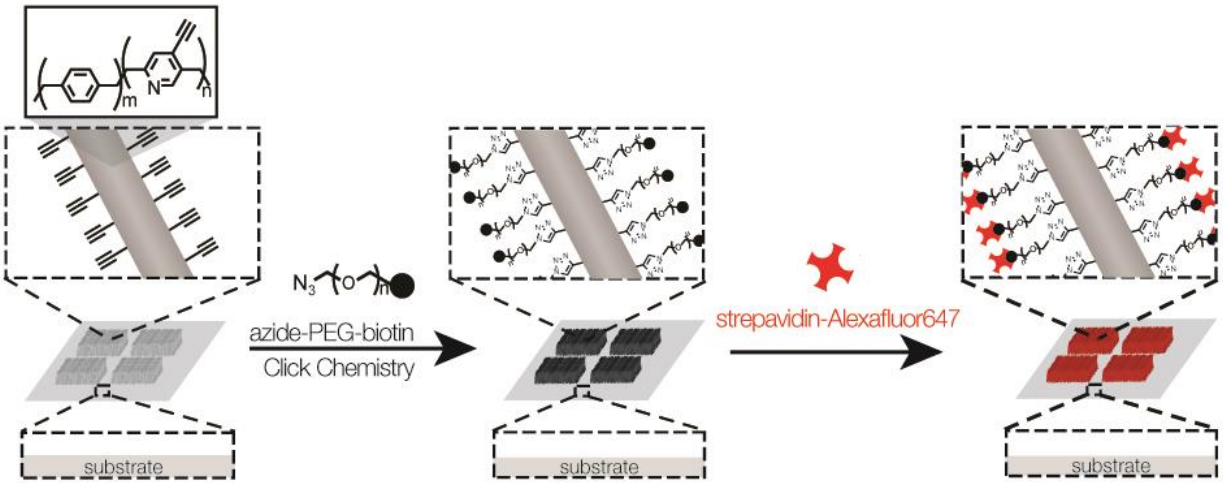

Figure 5-7: Graphical illustration showing the chemical immobilization of azide-PEG-biotin on the ethynyl-functionalized poly(lutidine) nanofibers via Huisgen 1,3-dipolar cycloaddition reaction, followed by subsequent immobilization of streptavidin-Alexafluor596 on the biotinylated nanofibers.

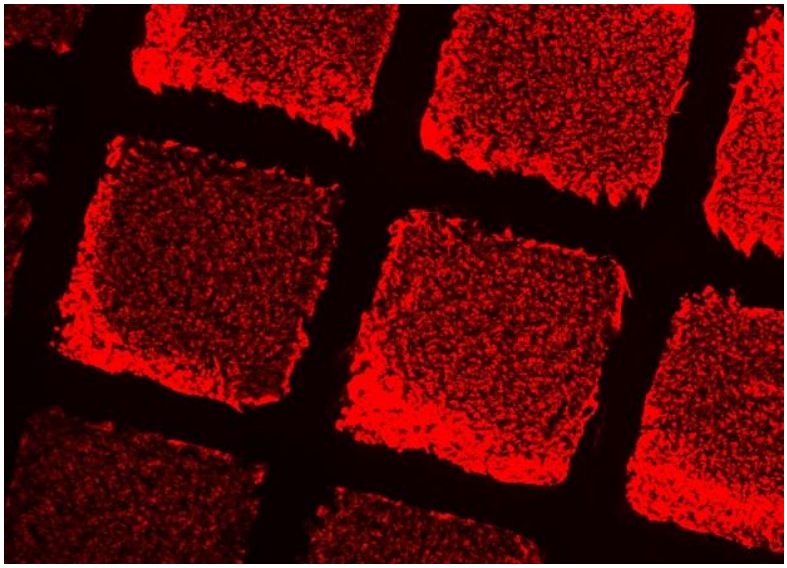

Figure 5-8: Fluorescence micrograph showing the binding of streptavidin-Alexafluor596 on the patterned ethynyl-functionalized poly(lutidine) nanofiber arrays that were biotinylated. The patterned nanofiber arrays are 285 um by 285 um in size.

5.3 Assembly of Poly(phenylene vinylene) nanofibers via LC-templated CVD

5.3.1 Background

Conjugated polymers are a class of polymers that are capable of conducting electricity[130], [131]. They generally comprise of alternating single and double bonds, which leads to the formation of sp2 orbitals that overlaps with one another and provide a "*highway for charge mobility along the backbone of the polymer chains*" [131] and provides conjugated polymers with semiconducting and metallic properties. With the semi-conducting and metallic properties, conducting polymers have garnered vast interest in a wide variety of applications,

such as organic light-emitting diodes[132], [133], organic lasers [134], field effect transistors[135], flexible electronics and biosensors [136].

Poly(phenylene vinylene) (PPV) is a types conjugated polymers that have found interests in chemical sensing as well as in electroluminescence applications, such as light-emitting diodes and lasers [132], [133], [136]–[138]. Due to the insolubility nature of PPV, PPV thin films are commonly prepared by first solvent-casting sulfonium-based polyelectrolye precursor polymer into a thin film, followed by thermal annealing to convert the precursor polymer into PPV thin film [138]. This fabrication process can yield PPV thin films with varying performance. In particular, the wrong choice of solvent and the presence of oxygen during the conversion step can result in undesirable side reaction, which can influence the polymer conjugation length and therefore the conductivity and the photoluminescent and electroluminescent efficiency of the PPV film [139], [140].

K. M. Vaeth and K. F. Jensen has previously demonstrated a 2-step CVD-based technique to create PPV thin films (Scheme 5-2) [138]. This process first creates a chlorine precursor polymer thin film from di-chloro-p-xylene via CVD polymerization, followed by a thermal annealing process at 200-300 ^{o}C under vacuum to eliminate HCl and convert the chlorine precursor polymer into PPV thin films. The PPV thin film prepared by this CVD method offer superior control over thickness of the polymer thin film, impurity incorporation and defect formation during the thin film fabrication process [138]. In this study, we explored

the possibility to extend our LC-templated CVD method to the CVD route developed by Vaeth et. al. to create PPV nanofibers.

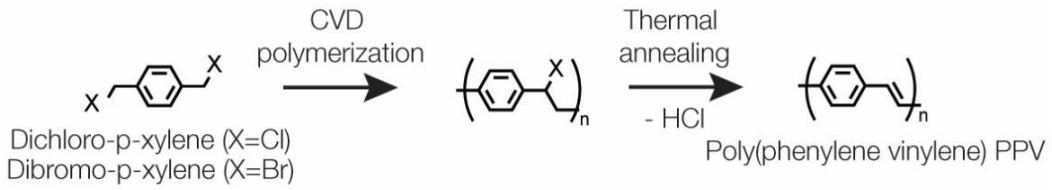

Scheme 5-2: CVD polymerization of dichloro-p-xylene or dibromo-p-xylene into either chlorinated or brominated precursor polymer thin film, and the thermal conversion of the precursor polymer into poly(phenylene vinylene) (PPV) thin films.

5.3.2 Experimental Methods

Materials

Ethanol, acetone, iso-propanol and glass slides were purchased from Fisher Scientific. TEM grids and quartz slides were purchased from Electron Microscopy Science. All other chemicals were purchased from Sigma Aldrich.

LC sample preparation

Preparation of the LC samples are adapted from the previous chapters. Briefly, glass and quartz substrates were first sonicated in a solution of iso-propanol for several minutes to

remove surface residues. Afterwards, the substrates were immersed in an aqueous solution of 0.5 wt% of hexadecyltrimethylammonium bromide for ~20 seconds, and was subsequently rinsed in di-ionized water. TEM grids were then placed on the substrates, and a drop of LC was filled into the pores of the TEM grids. Excess LC was removed by extracting the excess LC using a glass capillary.

Synthesis of poly(p-phenylene-vinylene) via 2-Step CVD process

CVD polymerization was performed using a custom-built CVD system, as described in [128]. LC samples were first loaded onto a rotating stage inside the CVD deposition chamber. The rotating stage was fixed at ~17 ^{o}C. The CVD system was then brought to a reduced pressure of 0.1 mbar, after which the precursor monomer, dichloro-para-xylene, was sublimated at ~100 ^{o}C. The monomer vapor was then pyrolyzed at 660 ^{o}C to convert into di-radical vapors, and was subsequently transferred into the deposition chamber. Once entered the deposition chamber, the diradicals deposited onto the LC specimens and polymerized inside the thin layer of LC. After the CVD process, the LC film was removed from the samples by rinsing the samples repeatedly with ethanol and acetone. Subsequently, the samples were either used directly for characterization or was loaded into the CVD system and heat treated at 300 ^{o}C under a reduced pressure of 0.1 mbar to eliminate HCl and convert chlorinated polymer nanofibers into PPV

nanofibers. To obtain PPV thin films, we perform the same process without the presence of LC (polymer was deposited directly on solid substrates that did not contain any LC film).

Sample Characterization

The chemical composition of the nanofibers and nanofilms was obtained by Fourier transform infrared spectroscopy (FTIR) and x-ray photoelectron spectroscopy (XPS). FTIR spectra were obtained on a Nicolet 6700 spectrometer equipped with a grazing angle accessory (SMART SAGE). The glazing angle is set at 80^{o}. 128 measurements were obtained on each sample. XPS spectra were obtained using an Axis Ultra X-ray photoelectron spectrometer (Kratos Analyticals, UK) with mono-chromatized Al Kα X-ray source at 150 kW. All spectra were calibrated with respect to the aliphatic carbon with a binding energy of 285 eV. UV-vis absorption spectra were obtained from a JASCO J-815 spectrometer. Photo-luminescent (PL) spectra of the nanofibers and thin films were taken by Jaehun Jung (Kim group, University of Michigan) using a photoluminescence scanner. The morphology of the surface-decorated chlorinated intermediate polymer nanofibers and PPV nanofibers were analyzed by scanning electron microscopy (SEM) (FEI Helios). A thin layer of gold or carbon was deposited onto the specimen prior to SEM to reduce surface charging.

5.3.3 Results and Discussion

To investigate the possibility of creating PPV nanofibers via our LC-templated CVD process, we first followed the CVD procedure developed by K. M. Vaeth and K. F. Jensen to polymerize dichloro-p-xylene in a thin film of nematic LC [138]. Following a subsequent LC removal step revealed an array of surface-decorated nanofibers, as shown in Figure 5-9.

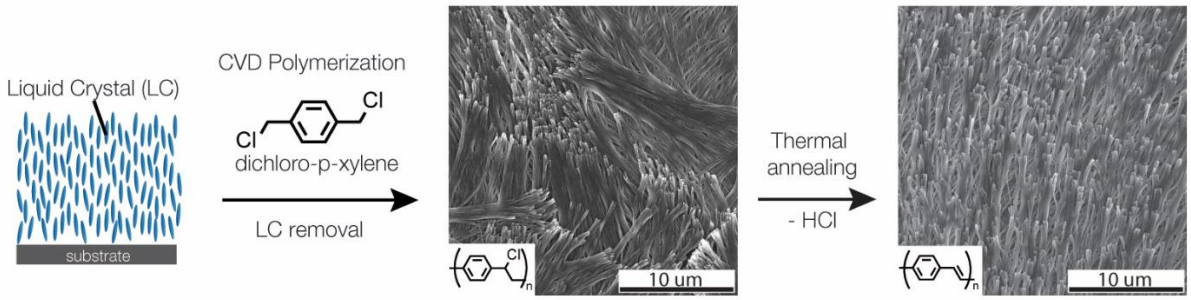

Figure 5-9: Graphical illustration showing the formation of PPV nanofibers by CVD polymerization of di-chloro-p-xylene onto a thin film of LC film decorated on a flat substrate, followed by thermal annealing to convert the chlorinated precursor polymer nanofibers

FTIR spectroscopy on the surface-decorated nanofibers revealed the presence of the characteristic bands of C-H at 2900 to 3100 cm^{-1} as well as the characteristic band of CH_2-CH-Cl at 924 cm^{-1}, that agrees with the results reported by Vaeth et. al. (Figure 5-11) [138]. Similarly, XPS shows that the elemental content on the nanofibers resembles that of the thin film and the theoretical values, suggesting the successful preparation of chlorinated nanofibers via CVD polymerization of di-chloro-p-xylene in LC (Table 2-1).

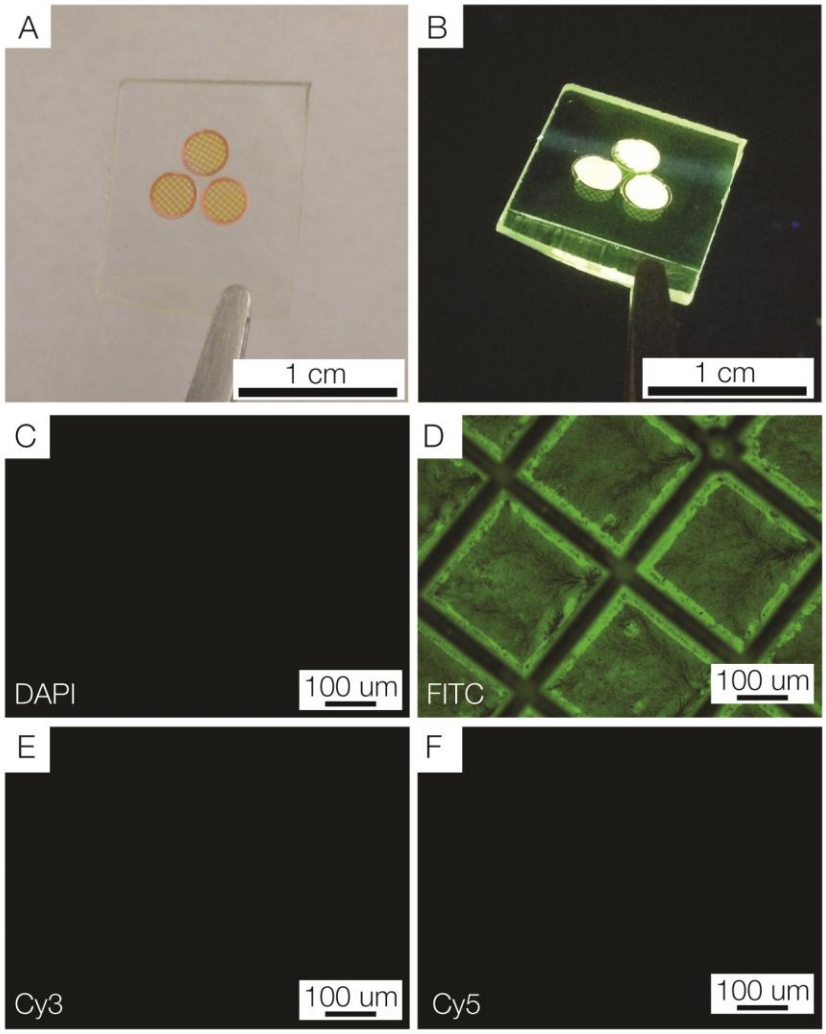

Figure 5-10: (A) Optical image of the resulting nanofibers anchored on a piece of quartz. The nanofibers are constrained within the openings of the 3 TEM grids placed on the quartz substrate. The nanofibers are yellow in color, suggesting the conversion to PPV was successful. (B) Optical image of the specimen described in (A) under UV light. The nanofibers exhibit very strong green fluorescence. Fluorescence micrograph of the nanofibers in (C) DAPI, (D) FITC, (E) Cy3 and (F) Cy5 filter.

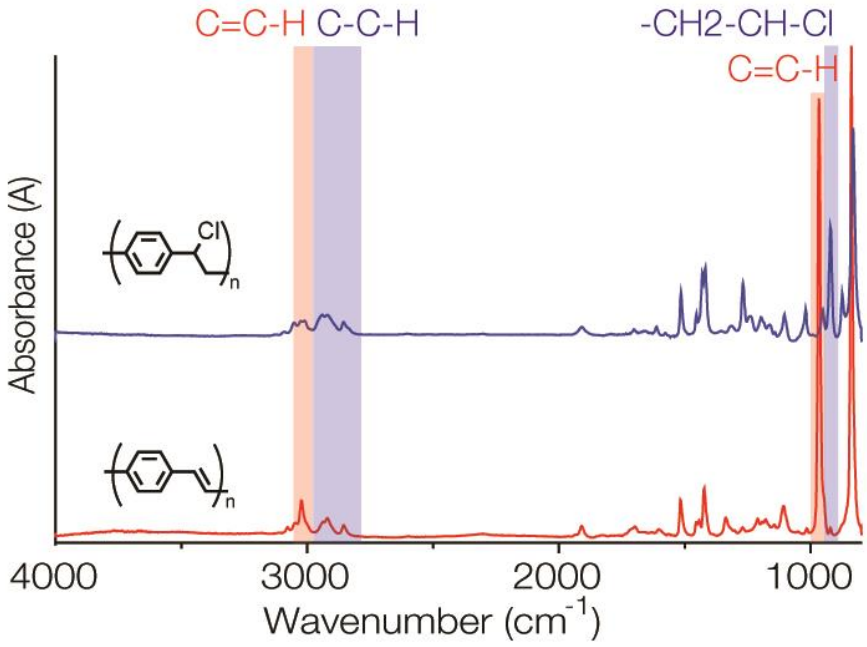

Figure 5-11: FTIR spectra of chlorinated precursor polymer nanofibers before (Blue) and after (Red) thermal annealing.

Table 5-1: The experimental chemical composition of chlorinated precursor polymer nanofibers and PPV nanofibers as determined by XPS measurements. The calculated values are included for comparison

	C 1s	O 1s	Cl 2p
Binding Energy (eV)	285 ± 0.1	533 ± 0.1	200 ± 0.1
Exp. Value of chlorinated precursor nanofibers	89.8	0.5	9.7
Calc. Value of chlorinated precursor nanofibers	88.9	-	11.1
Exp. value of PPV nanofibers	98.1	1.2	0.7
Calc. value of PPV nanofibers	100	-	-

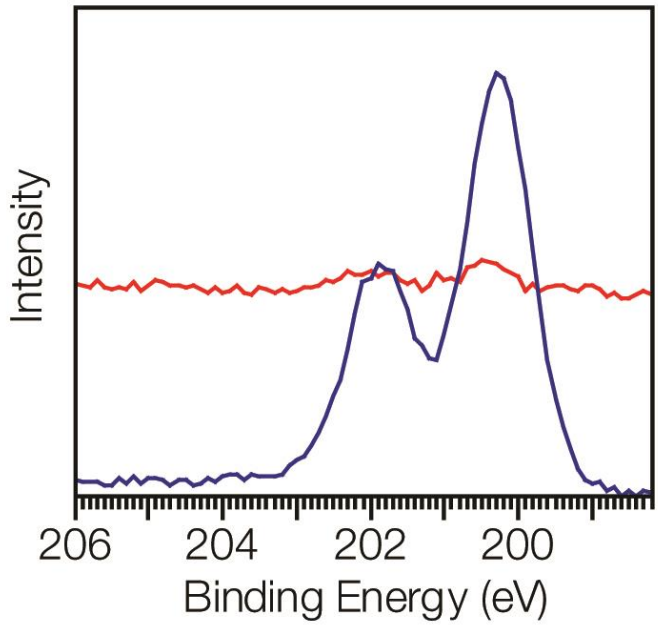

Figure 5-12: High-resolution Cl 2p spectra of chlorinated precursor polymer nanofibers before (blue) and after (red) thermal annealing.

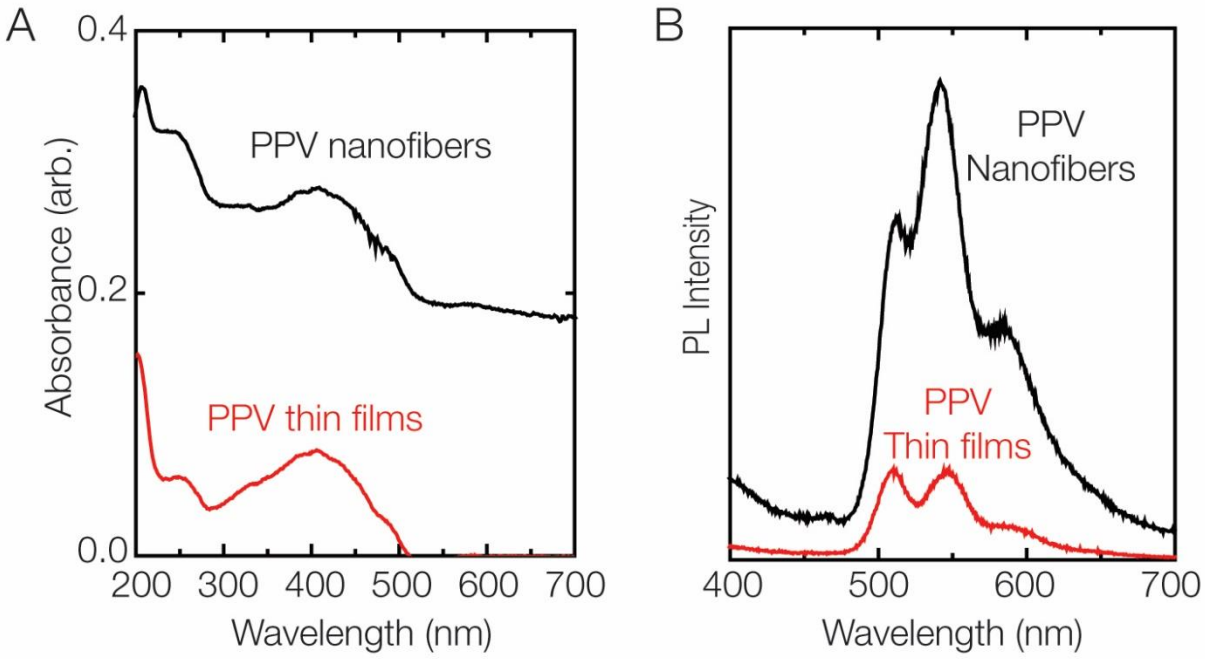

Figure 5-13: (a) UV-vis absorption spectra and (b) photoluminescence spectra of PPV nanofibers and PPV thin films.

We then examined the conversion of the chlorinated precursor polymer nanofibers to PPV nanofibers. After thermal annealing at 200 ^{o}C for 2 hours, the nanofibers retain their fiber morphology (Figure 5-9). After the conversion, the nanofibers turned yellow in color and glowed strong green fluorescence under UV light and under fluorescence microscope (Figure 5-10), suggesting the conversion to PPV nanofibers was successful. The conversion of the chlorinated precursor nanofibers to PPV nanofibers was examined using XPS (Figure 5-12). The marked reduction of chlorine content in XPS from the chlorinated precursor nanofiber to PPV nanofibers confirmed the elimination of the chlorine. The minimal presence of chlorine atoms on the PPV nanofibers suggested that the conversion was indeed not 100%. FTIR also revealed that the characteristic band of CH_2-CH-Cl at 924 cm^{-1} has drastically reduced, and that the characteristic bands of sp^2 C-H at 965cm^{-1}, 3100 cm^{-1} increased, suggesting that the chlorinated precursor polymer nanofibers were successfully converted into PPV (Figure 5-11). The presence of aliphatic sp^3 C-H, however, indicated that the presence of unconjugated polymer, suggesting that the conversion was not 100%.

To further confirm the presence of conjugated PPV, we characterized the PPV nanofibers with UV-Vis absorption spectroscopy and photoluminescence spectroscopy (Figure 5-13). UV vis absorption spectroscopy revealed the characteristic absorption bands of conjugated PPV at 400 nm, which was in accordance to the values published by others [132], [137]. The presence of strong absorption at 200 to 250 nm, however, indicated the presence of

unconjugated polymer, suggesting the incomplete conversion of the chlorinated polymer to PPV. Nevertheless, the PL spectrum of the PPV nanofibers closely resembled those reported by others, confirming that PPV nanofibers were successfully prepared.

5.4 Conclusion

This chapter demonstrates the successful synthesis of poly(lutidine) and poly(phenylene vinylene) nanofibers via LC-templated CVD. The ability to create functionalized poly(lutidine) nanofibers enables one to develop nanostructured cell culture substrates and to investigate the effect of shape and arrangement of the poly(lutidine) nanofibers on cells. On the other hand, though the electroluminescence property has yet to be examined, PPV nanofibers can find potential application in flexible electronics. Functionalization of PPV nanofibers can also enable the development of bio-sensors. Overall, with the ability to extend the use of the LC-templated CVD method to poly(lutidine) and PPV, we envisioned that the LC-templated CVD method can be applicable to prepared nanofibers with other CVD-based polymer systems.

CHAPTER 6 Conclusion and Future Directions

6.1 Conclusion

The work described in this dissertation serves as an extension to previous work on CVD polymerization [6], [11], [32]. Specifically, this dissertation further addressed the use of reactive poly(p-xylylene) coatings prepared by CVD polymerization as a surface modification strategy to surface modify and conjugate biomolecules on a broad range of materials. Adenoviral vectors can selectively bound to CVD-polymer-coated tissue scaffolds and be used for delivering safe and efficient viral-based gene therapy. In addition, this dissertation also demonstrated the ability to extend the use of CVD polymerization from a 2-D fabrication technique to a 3-D fabrication method. Chapter 3 addresses the formation of surface-anchored polymer nanofibers with programmable dimension, shape and surface chemical properties via CVD onto surfaces coated with a thin layer of LC. Chapter 3 also addressed the ability to apply LC-templated CVD-based polymer nanofiber arrays onto 3-D complex geometries and to tune the surface functionalities of the nanofibers. Chapter 4 and 5 demonstrated the ability to induce

twisting to the nanofibers and extended this nanofiber synthesis route to other CVD-based polymer systems, such as poly(lutidine) and poly(phenylene vinylene).

6.2 Future Directions

6.2.1 Developing biodegradable reactive polymer coatings for gene therapy

Reactive poly(p-xylylene) coatings prepared by CVD polymerization can be utilized to surface modify and conjugate biomolecules on a broad range of materials, as demonstrated by others and in Chapter 2 of this dissertation[11]. However, poly(p-xylylene) backbone cannot be hydrolytically cleaved, making the polymer coating non-degradable and impractical for some of the biomedical applications that require the tissue scaffolds to be biodegradable. To overcome this challenge, the Lahann Lab has recently demonstrated, for the first time, the ability to create backbone-degradable CVD-based poly(p-xylylene) coatings via CVD co-polymerization[141]. A future outlook would be to examine the use of CVD-based degradable polymer coating in in-vitro and in-vivo studies and to apply CVD-based degradable polymer coatings to different biomedical applications, such as gene therapy, as described in Chapter 2.

6.2.2 Future directions for LC-templated CVD

LC-templated CVD in different LC types

So far, the work shown in this dissertation focuses on the use of nematic and cholesteric LC phases as the template. There is in fact a plethora of LC phases that can be examined as the template in the future, as shown in Figure 6-1 and Figure 6-2. These different types of LCs exhibit distinct molecular orderings, which can potentially enable us to create nanofibers with different geometries and/or polymer with complex nanostructures. We attempted to perform LC-templated CVD using 8CB, a type of smectic A LC phase (Figure 6-3), as the template and observed the formation of nanofibers. The nanofibers, however, exhibits a broadened tip, suggesting the insolubility of the xylylenes in 8CB and therefore the polymerization occurred preferentially near the vapor-LC interface, forming nanofibers with broadened heads.

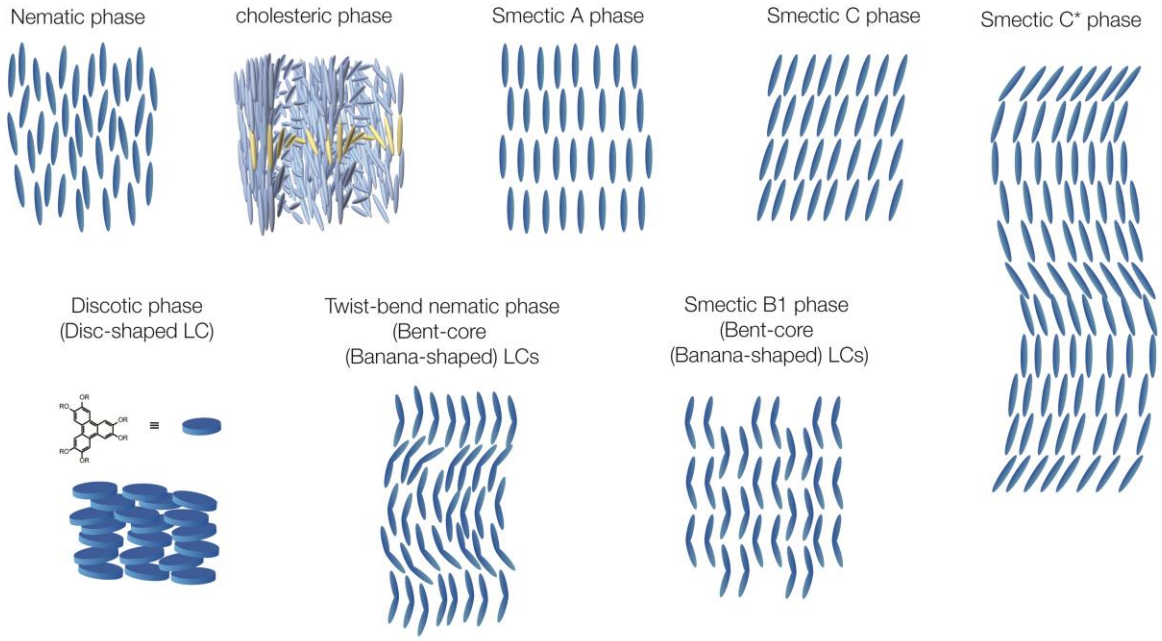

Figure 6-1: Graphical illustration of different LC phases that can be potentially used as the templated for LC-templated CVD process to create polymer nanostructures with different geometries. This dissertation focuses extensively on using nematic and cholesteric phases as the template.

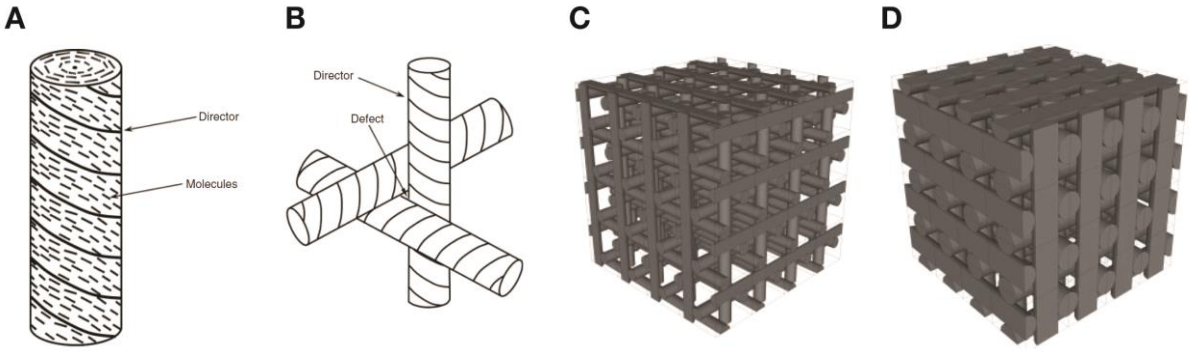

Figure 6-2: Graphical illustration of blue phase LC phase. (A) Within the blue phase LC phase, mesogens arrange themselves into a double-twist cylinder. These double-twist cylinders have preferred local arrangement shown in (B). Three dimensional structure of (C) blue phase I and (D) blue phase II. [126] Using blue phase LC as the template, the polymer chains may potentially form along the double-twist cylinder and assemble into 3-dimensional polymer lattices.

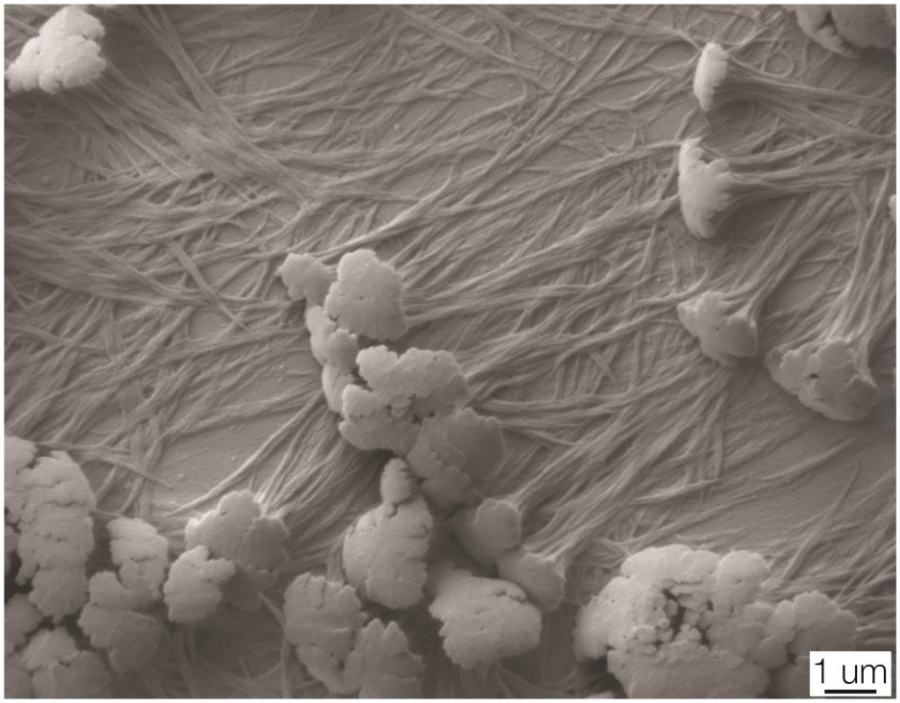

Figure 6-3: Representative SEM image of nanofibers prepared by CVD polymerization of 4-hydroxymethyl-[2.2]paracyclophane (1a in Chapter 3) onto a thin film of 8CB, a type of smectic A phase). Nanofibers are formed using 8CB as the template. The nanofibers contain broadened tips, suggesting that the thermally-generated diradicals are not likely to partition through the 8CB layer and therefore preferentially polymerize near the LC-vapor interface.

Studying the effect of substituent of [2.2]paracyclophane on LC-templated CVD

As shown in Chapter 3, certain substituted [2.2]paracyclophanes were insoluble or incompatible in certain LCs (i.e. 4-hydroxymethyl-[2.2]-paracyclophane is not as soluble in TL205 as it is in E7 or 5CB), and the insolubility of the precursor in LC could lead to a change in the morphology of the resulting nanofibers (e.g. broadened fiber tip). Similarly, in Chapter 4, precursors with chiral substituents were not as soluble in LC as those with achiral substituents.

As the chiral substituent become bulkier, the effect of insolubility seems to be more prominent. Nevertheless, a more systematic investigation is required to study the relationship between the precursor and the LC to better understand the formation of nanofibers during the LC-templated CVD process.

LC-templated CVD co-polymerization

The Lahann Lab has recently demonstrated the ability to create degradable polymer coatings via CVD co-polymerization of [2.2]paracyclophanes and cyclic ketene acetals, molecules that polymerize under the same radical polymerization mechanism as CVD polymerization of [2.2]paracyclophane [141]. This copolymerization strategy can be incorporated into the LC-templated CVD method to create degradable polymer nanofiber arrays. We can also extend this strategy to other types of molecules that also follows the radical polymerization mechanism to create polymer nanofibers with other functionalities, such as monomers with photoactive and electroactive properties to create actuating CVD-based polymer nanofibers.

LC-templated CVD in the presence of external stimuli such as electric/magnetic field

The molecular arrangement of LC can be aligned by external stimulus, such as by electric field or by magnetic field [142], [143]. With sufficient electric or magnetic field, LC

molecules rearrange themselves to align along the electric/magnetic field. Performing LC-templated CVD on a thin film of LC film in the presence of electric/magnetic field enables one to control the alignment of the resulting nanofibers. These well-aligned nanofibers may exhibit interesting anisotropic optical, thermal and electrical properties. In addition, the ability to create poly(lutidine) nanofibers with controllable fiber alignment enables one to examine the effect of the fiber alignment on the binding of cells onto poly(lutidine) nanofibers.

Potential applications for polymer nanofibers prepared by LC-templated CVD

Chemical and biological sensors

The ability to control the surface reactive sites on the nanofibers, the high surface area-to-volume ratio and the versatility of the preparation process make the LC-templated nanofibers attractive for chemical and biological sensing applications. Unpublished data shows that certain substituted poly(p-xylylene)s show selective binding to explosive chemical, trinitrotoluene (TNT). Although the exact mechanism towards the binding of TNT is still unclear, substituted poly(p-xylylene)s can be used as the materials for pre-concentrator component in mass-spectroscopy-based sensing platforms.

Researchers have shown that they can take advantage of the electroluminescence and photoluminescence properties of PPV for bio-sensing applications. However, it may be necessary to incorporate functional side groups on the PPV polymer in order to create efficient

bio-sensors [144]. A future opportunity would be to examine the formation of substituted PPV nanofibers and its potential use in bio-sensing applications.

Affinity filtration systems

The ability to create nanofibers in the form of membranes (Figure 3-24) that span the empty spaces within mesh structures and at the orifice of glass capillaries could be attractive for filtration systems. The extra benefit of having tunable surface reactive sites on the nanofibers enables one to selectively capture and filter biomolecules of interest from a given solution.

Probing the interaction between biomolecules and functional polymer nanostructures

Cells behaves differently on a flat surface and on a structured surface. With the ability to create cell-attracting poly(lutidine) nanofibers and the ability to control the shape of the nanofibers, one can examine the effect of the nanofiber shape on the interaction between cells and poly(lutidine) as well as cell migration due to the poly(lutidine) nanofiber alignment.

Development of metamaterials with unique optical properties

LC-templated nanofibers having tunable helicity can be used as scaffolds/templates for creating metamaterials having interesting optical properties. As a demonstration, a thin layer of

gold was sputtered onto a surface decorated with twisted nanofiber. As the thickness of the gold film increased, the CD signal at became stronger and more prominent., suggesting that the helical feature of the twisted nanofibers is imprinted on the gold film, thus inducing CD signal at 600-900 nm as gold was sputtered onto the twisted nanofibers. As the thickness of the gold film increased, the CD signal became stronger and more prominent. This imprinting phenomenon was not observed on nanofibers that did not exhibit twisting.

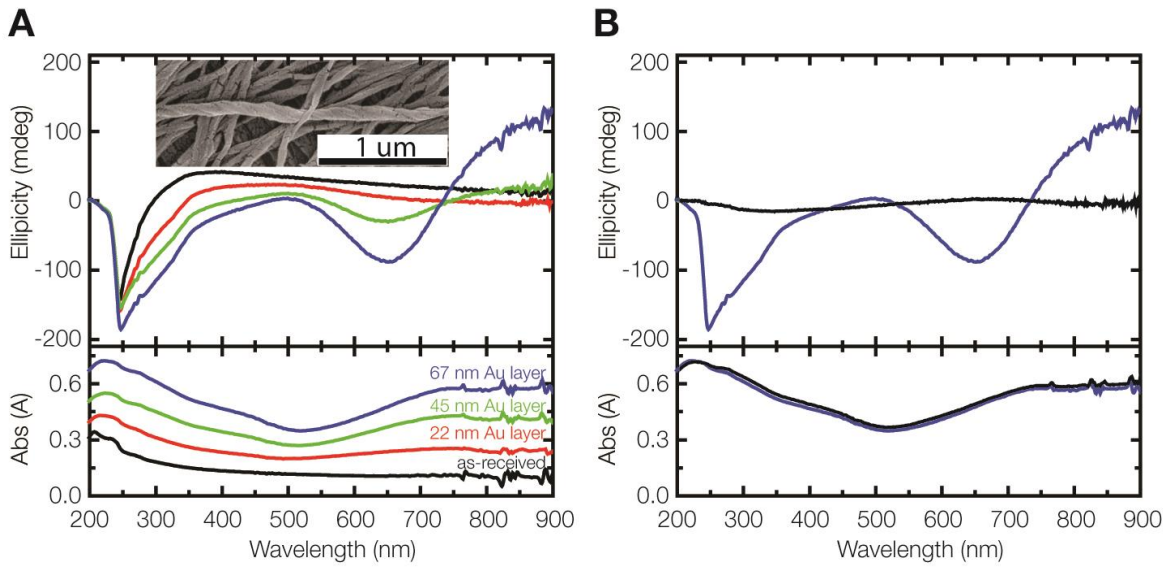

Figure 6-4: (A) CD and Abs spectra of a surface decorated with CW-twisted nanofibers with different thicknesses of gold (Au) layer sputtered on. Black: As-received nanofibers (no Au layer); red: nanofibers with 22 nm Au layer; green: nanofibers with 45 nm Au layer; Blue: nanofibers with 67 nm Au layer.) (B) CD and Abs of gold a surface decorated with (blue) CS-twsited nanofibers and (black) non-twisted nanofibers. Both specimens were sputtered with 67nm thick Au layer. Gold film sputtered on non-twisted nanofibers did not exhibit any CD signals above 500 nm.

References

[1] D. G. Castner and B. D. Ratner, “Biomedical surface science: Foundations to frontiers,” *Surf. Sci.*, vol. 500, no. 1–3, pp. 28–60, 2002.

[2] S. Cosnier, “Biomolecule immobilization on electrode surfaces by entrapment or attachment to electrochemically polymerized films. A review,” *Biosens. Bioelectron.*, vol. 14, no. 5, pp. 443–456, 1999.

[3] K. S. Siow, L. Britcher, S. Kumar, and H. J. Griesser, “Plasma Methods for the Generation of Chemically Reactive Surfaces for Biomolecule Immobilization and Cell Colonization - A Review,” *Plasma Process. Polym.*, vol. 3, no. 6–7, pp. 392–418, Aug. 2006.

[4] H. Shin, S. Jo, and A. G. Mikos, “Biomimetic materials for tissue engineering,” *Biomaterials*, vol. 24, no. 24, pp. 4353–4364, 2003.

[5] A. Ulman, “Formation and Structure of Self-Assembled Monolayers,” *Chem. Rev.*, vol. 96, pp. 1533–1554, 1996.

[6] J. Lahann, “Vapor based polymer coatings for potential biomedical applications,” *Polym. Int.*, vol. 1370, no. February, pp. 1361–1370, 2006.

[7] S. Tawfick, X. Deng, A. J. Hart, and J. Lahann, “Nanocomposite microstructures with tunable mechanical and chemical properties,” *Phys. Chem. Chem. Phys.*, vol. 12, no. 17, pp. 4446–4451, 2010.

[8] T. D. Y. Kozai *et al.*, “Ultrasmall implantable composite microelectrodes with bioactive surfaces for chronic neural interfaces.,” *Nat. Mater.*, vol. 11, no. 12, pp. 1065–73, 2012.

[9] A. Greiner, S. Mang, O. Schäfer, and P. Simon, “Poly(p-xylylene)s: Synthesis, polymer analogous reactions, and perspectives on structure-property relationships,” *Acta Polym.*, vol. 48, no. 1–2, pp. 1–15, 1997.

[10] Haoqing Hou, Zeng Jun, Arndt Reuning, Andreas Schaper, and Joachim H. Wendorff, and A. Greiner*, “Poly(p-xylylene) Nanotubes by Coating and Removal of Ultrathin Polymer Template Fibers,” 2002.

[11] X. Deng and J. Lahann, “Orthogonal surface functionalization through bioactive vapor-based polymer coatings,” *Journal of Applied Polymer Science*, vol. 131, no. 14. 2014.

[12] J. Lahann, I. S. Choi, J. Lee, K. F. Jensen, and R. Langer, “A new method toward

microengineered surfaces based on reactive coating," *Angew. Chemie - Int. Ed.*, vol. 40, no. 17, pp. 3166–3169, 2001.

[13] J. Lahann, D. Klee, W. Pluester, and H. Hoecker, "Bioactive immobilization of r-hirudin on CVD-coated metallic implant devices," *Biomaterials*, vol. 22, no. 8, pp. 817–826, 2001.

[14] F. Bally *et al.*, "Co-immobilization of biomolecules on ultrathin reactive chemical vapor deposition coatings using multiple click chemistry strategies," *ACS Appl. Mater. Interfaces*, vol. 5, no. 19, pp. 9262–9268, 2013.

[15] X. Jiang, H. Y. Chen, G. Galvan, M. Yoshida, and J. Lahann, "Vapor-based initiator coatings for atom transfer radical polymerization," *Adv. Funct. Mater.*, vol. 18, no. 1, pp. 27–35, 2008.

[16] X. Deng, T. W. Eyster, Y. Elkasabi, and J. Lahann, "Bio-orthogonal polymer coatings for co-presentation of biomolecules," *Macromol. Rapid Commun.*, vol. 33, no. 8, pp. 640–645, 2012.

[17] A. A. Yu, T. A. Savas, G. S. Taylor, A. Guiseppe-Elie, H. I. Smith, and F. Stellacci, "Supramolecular nanostamping: Using DNA as movable type," *Nano Lett.*, vol. 5, no. 6, pp. 1061–1064, 2005.

[18] Y. Elkasabi, H. Y. Chen, and J. Lahann, "Multipotent polymer coatings based on chemical vapor deposition copolymerization," *Adv. Mater.*, vol. 18, no. 12, p. 1521–+, 2006.

[19] S. Y. Han and Y. A. Kim, "Recent development of peptide coupling reagents in organic synthesis," *Tetrahedron*, vol. 60, no. 11, pp. 2447–2467, 2004.

[20] H.-Y. Chen *et al.*, "Vapor-based tri-functional coatings.," *Chem. Commun. (Camb).*, vol. 49, no. 40, pp. 4531–3, 2013.

[21] A. J. Ridley *et al.*, "Cell migration: integrating signals from front to back.," *Science*, vol. 302, no. 5651, pp. 1704–9, 2003.

[22] L. Liu, B. D. Ratner, E. H. Sage, and S. Jiang, "Endothelial cell migration on surface-density gradients of fibronectin, VEGF, or both proteins," *Langmuir*, vol. 23, no. 22, pp. 11168–11173, 2007.

[23] S. Jayaraman and A. C. Hillier, "Construction and reactivity mapping of a platinum catalyst gradient using the scanning electrochemical microscope," *Langmuir*, vol. 17, no. 25, pp. 7857–7864, 2001.

[24] N. L. Jeon, S. K. W. Dertinger, D. T. Chiu, I. S. Choi, A. D. Stroock, and G. M. Whitesides, "Generation of solution and surface gradients using microfluidic systems," *Langmuir*, vol. 16, no. 22, pp. 8311–8316, 2000.

[25] J. A. Burdick, A. Khademhosseini, and R. Langer, "Fabrication of gradient hydrogels using a microfluidics/photopolymerization process," *Langmuir*, vol. 20, no. 13, pp. 5153–5156, 2004.

[26] N. Ballav, A. Shaporenko, A. Terfort, and M. Zharnikov, “A flexible approach to the fabrication of chemical gradients,” *Adv. Mater.*, vol. 19, no. 7, pp. 998–1000, 2007.
[27] Y. Elkasabi and J. Lahann, “Vapor-based polymer gradients,” *Macromol. Rapid Commun.*, vol. 30, no. 1, pp. 57–63, 2009.
[28] Y. M. Elkasabi, J. Lahann, and P. H. Krebsbach, “Cellular transduction gradients via vapor-deposited polymer coatings,” *Biomaterials*, vol. 32, no. 7, pp. 1809–1815, 2011.
[29] † Etienne Menard *et al.*, “Micro- and Nanopatterning Techniques for Organic Electronic and Optoelectronic Systems,” 2007.
[30] D. Falconnet, G. Csucs, H. Michelle Grandin, and M. Textor, “Surface engineering approaches to micropattern surfaces for cell-based assays,” *Biomaterials*, vol. 27, no. 16. pp. 3044–3063, 2006.
[31] Z. Nie and E. Kumacheva, “Patterning surfaces with functional polymers.,” *Nat. Mater.*, vol. 7, no. 4, pp. 277–290, 2008.
[32] H. Y. Chen and J. Lahann, “Designable biointerfaces using vapor-based reactive polymers,” *Langmuir*, vol. 27, no. 1. pp. 34–48, 2011.
[33] H. Y. Chen, M. Hirtz, X. Deng, T. Laue, H. Fuchs, and J. Lahann, “Substrate-independent dip-pen nanolithography based on reactive coatings,” *J. Am. Chem. Soc.*, vol. 132, no. 51, pp. 18023–18025, 2010.
[34] A. Homsy *et al.*, “Solid on liquid deposition, a review of technological solutions,” *Microelectron. Eng.*, vol. 141, pp. 267–279, 2015.
[35] Binh-Khiem Nguyen, Eiji Iwase, Kiyoshi Matsumoto, and Isao Shimoyama, “Electrically driven varifocal micro lens fabricated by depositing parylene directly on liquid,” in *2007 IEEE 20th International Conference on Micro Electro Mechanical Systems (MEMS)*, 2007, pp. 305–308.
[36] N. Binh-Khiem, K. Matsumoto, and I. Shimoyama, “Porous Parylene and effects of liquid on Parylene films deposited on liquid,” in *2011 IEEE 24th International Conference on Micro Electro Mechanical Systems*, 2011, pp. 111–114.
[37] N. Binh-Khiem, K. Matsumoto, and I. Shimoyama, “Tensile film stress of parylene deposited on liquid,” *Langmuir*, vol. 26, no. 24, pp. 18771–18775, 2010.
[38] N. Binh-Khiem, K. Matsumoto, and I. Shimoyama, “Polymer thin film deposited on liquid for varifocal encapsulated liquid lenses,” *Appl. Phys. Lett.*, vol. 93, no. 12, 2008.
[39] T. Kan, H. Aoki, N. Binh-Khiem, K. Matsumoto, and I. Shimoyama, “Ratiometric optical temperature sensor using two fluorescent dyes dissolved in an ionic liquid encapsulated by parylene film,” *Sensors (Switzerland)*, vol. 13, no. 4, pp. 4138–4145, 2013.
[40] A. Takei, Y. Yoshihata, and I. Shimoyama, “Microprism using capillary alignment,” *J. Micromechanics Microengineering*, vol. 21, no. 8, p. 85009, 2011.
[41] R. J. Frank-Finney, P. D. Haller, and M. Gupta, “Ultrathin free-standing polymer films

deposited onto patterned ionic liquids and silicone oil," *Macromolecules*, vol. 45, no. 1, pp. 165–170, 2012.

[42] P. D. Haller, R. J. Frank-Finney, and M. Gupta, "Vapor-phase free radical polymerization in the presence of an ionic liquid," *Macromolecules*, vol. 44, no. 8, pp. 2653–2659, 2011.

[43] R. Langer and D. A. Tirrell, "Designing materials for biology and medicine," *Nature*, vol. 428, no. 6982, pp. 487–492, 2004.

[44] C. J. Wilson, R. E. Clegg, D. I. Leavesley, and M. J. Pearcy, "Mediation of Biomaterial–Cell Interactions by Adsorbed Proteins: A Review," *Tissue Eng.*, vol. 11, no. 1–2, pp. 1–18, 2005.

[45] J. Lahann, "Reactive polymer coatings for biomimetic surface engineering," *Chem. Eng. Commun.*, vol. 193, no. 11, pp. 1457–1468, 2006.

[46] G. Ozaydin-Ince, A. M. Coclite, and K. K. Gleason, "CVD of polymeric thin films: Applications in sensors, biotechnology, microelectronics/organic electronics, microfluidics, MEMS, composites and membranes," *Reports Prog. Phys.*, vol. 75, no. 1, 2012.

[47] M. E. Alf *et al.*, "Chemical vapor deposition of conformal, functional, and responsive polymer films," *Adv. Mater.*, vol. 22, no. 18, pp. 1993–2027, 2010.

[48] Q. Wu and K. K. Gleason, "Plasma-enhanced chemical vapor deposition of low-k dielectric films using methylsilane, dimethylsilane, and trimethylsilane precursors," *J. Vac. Sci. Technol. A Vacuum, Surfaces Film.*, vol. 21, no. 2, pp. 388–393, 2003.

[49] W. E. Tenhaeff and K. K. Gleason, "Initiated and oxidative chemical vapor deposition of polymeric thin films: ICVD and oCVD," *Adv. Funct. Mater.*, vol. 18, no. 7, pp. 979–992, 2008.

[50] W. F. Gorham, "A New, General Synthetic Method for the Preparation of Linear Poly-p-xylylenes," *J. Polym. Sci. Part A-1 Polym. Chem.*, vol. 4, no. 12, pp. 3027–3039, 1966.

[51] J. Doostzadeh, L. N. Clark, S. Bezenek, W. Pierson, P. R. Sood, and K. Sudhir, "Recent progress in percutaneous coronary intervention: evolution of the drug-eluting stents, focus on the XIENCE V drug-eluting stent," *Coron. Artery Dis.*, vol. 21, no. 1, pp. 46–56, 2010.

[52] J. Lahann, D. Klee, and H. Höcker, "Chemical vapour deposition polymerization of substituted [2.2]paracyclophanes," *Macromol. Rapid Commun.*, vol. 19, no. 9, pp. 441–444, 1998.

[53] H. Hopf, "[2.2]Paracyclophanes in polymer chemistry and materials science," *Angew. Chemie - Int. Ed.*, vol. 47, no. 51, pp. 9808–9812, 2008.

[54] J. Lahann, H. Höcker, and R. Langer, "Synthesis of Amino[2.2]paracyclophanes - Beneficial Monomers for Bioactive Coating of Medical Implant Materials," *Angew.*

Chemie - Int. Ed., vol. 40, no. 4, pp. 726–728, 2001.

[55] J. Lahann *et al.*, "Reactive polymer coatings: A platform for patterning proteins and mammalian cells onto a broad range of materials," *Langmuir*, vol. 18, no. 9, pp. 3632–3638, 2002.

[56] Y. Elkasabi *et al.*, "Partially fluorinated poly-p-xylylenes synthesized by CVD polymerization," *Chem. Vap. Depos.*, vol. 15, no. 4–6, pp. 142–149, 2009.

[57] H. Nandivada, H. Y. Chen, and J. Lahann, "Vapor-based synthesis of poly[(4-formyl-p-xylylene)-co-(p-xylylene)] and its use for biomimetic surface modifications," *Macromol. Rapid Commun.*, vol. 26, no. 22, pp. 1794–1799, 2005.

[58] H. Nandivada, H. Y. Chen, L. Bondarenko, and J. Lahann, "Reactive polymer coatings that 'click,'" *Angew. Chemie - Int. Ed.*, vol. 45, no. 20, pp. 3360–3363, 2006.

[59] H. C. Kolb, M. G. Finn, and K. B. Sharpless, "Click Chemistry: Diverse Chemical Function from a Few Good Reactions," *Angew. Chemie - Int. Ed.*, vol. 40, no. 11, pp. 2004–2021, 2001.

[60] W. H. Binder and R. Sachsenhofer, "'Click' chemistry in polymer and materials science," *Macromol. Rapid Commun.*, vol. 28, no. 1, pp. 15–54, 2007.

[61] W. H. Binder and R. Sachsenhofer, "'Click' chemistry in polymer and material science: An Update," *Macromol. Rapid Commun.*, vol. 29, no. 12–13, pp. 952–981, 2008.

[62] H. Nandivada, X. Jiang, and J. Lahann, "Click chemistry: Versatility and control in the hands of materials scientists," *Adv. Mater.*, vol. 19, no. 17, pp. 2197–2208, 2007.

[63] J. Lahann, *Click Chemistry for Biotechnology and Materials Science*. 2009.

[64] V. V Rostovtsev, L. G. Green, V. V Fokin, and K. B. Sharpless, "A stepwise huisgen cycloaddition process: Copper(I)-catalyzed regioselective 'ligation' of azides and terminal alkynes," *Angew. Chemie - Int. Ed.*, vol. 41, no. 14, pp. 2596–2599, 2002.

[65] N. K. Devaraj *et al.*, "Chemoselective covalent coupling of oligonucleotide probes to self-assembled monolayers," *J. Am. Chem. Soc.*, vol. 127, no. 24, pp. 8600–8601, 2005.

[66] J. K. Lee, Y. S. Chi, and I. S. Choi, "Reactivity of acetylenyl-terminated self-assembled monolayers on gold: Triazole formation," *Langmuir*, vol. 20, no. 10, pp. 3844–3847, 2004.

[67] Y. Zhang *et al.*, "Carbohydrate-protein interactions by 'clicked' carbohydrate self-assembled monolayers," *Anal. Chem.*, vol. 78, no. 6, pp. 2001–2008, 2006.

[68] J. M. Spruell *et al.*, "Heterogeneous catalysis through microcontact printing," *Angew. Chemie - Int. Ed.*, vol. 47, no. 51, pp. 9927–9932, 2008.

[69] C. Wendeln and B. J. Ravoo, "Surface patterning by microcontact chemistry," *Langmuir*, vol. 28, no. 13, pp. 5527–5538, 2012.

[70] X. Deng, C. Friedmann, and J. Lahann, "Bio-orthogonal 'double-click' chemistry based on multifunctional coatings," *Angew. Chemie - Int. Ed.*, vol. 50, no. 29, pp.

6522–6526, 2011.
[71] O. Michel and B. J. Ravoo, “Carbohydrate microarrays by microcontact ‘click’ chemistry,” *Langmuir*, vol. 24, no. 21, pp. 12116–12118, 2008.
[72] X. Deng and J. Lahann, “A generic strategy for co-presentation of Heparin-binding growth factors based on CVD polymerization,” *Macromol. Rapid Commun.*, vol. 33, no. 17, pp. 1459–1465, 2012.
[73] H. Y. Chen and J. Lahann, “Vapor-assisted micropatterning in replica structures: A solventless approach towards topologically and chemically designable surfaces,” *Adv. Mater.*, vol. 19, no. 22, pp. 3801–3808, 2007.
[74] L. Bondarenko, I. Dix, H. Hinrichs, and H. Hopf, “Cyclophanes. Part LII: Ethynyl[2.2]paracyclophanes - New building blocks for molecular scaffolding,” *Synthesis (Stuttg).*, no. 16, pp. 2751–2759, 2004.
[75] S. P. Pilipchuk *et al.*, “Tissue engineering for bone regeneration and osseointegration in the oral cavity,” *Dent Mater*, vol. 31, no. 4, pp. 317–338, 2015.
[76] C. H. Park *et al.*, “Biomimetic hybrid scaffolds for engineering human tooth-ligament interfaces,” *Biomaterials*, vol. 31, no. 23, pp. 5945–5952, 2010.
[77] E. Saito, E. E. Liao, W. W. Hu, P. H. Krebsbach, and S. J. Hollister, “Effects of designed PLLA and 50:50 PLGA scaffold architectures on bone formation in vivo,” *J Tissue Eng Regen Med*, vol. 7, no. 2, pp. 99–111, 2013.
[78] J. J. Patel, J. E. Modes, C. L. Flanagan, P. H. Krebsbach, S. P. Edwards, and S. J. Hollister, “Dual Delivery of EPO and BMP2 from a Novel Modular Poly-varepsilon-Caprolactone Construct to Increase the Bone Formation in Prefabricated Bone Flaps,” *Tissue Eng Part C Methods*, 2015.
[79] Y. Zhang *et al.*, “The effects of Runx2 immobilization on poly (epsilon-caprolactone) on osteoblast differentiation of bone marrow stromal cells in vitro,” *Biomaterials*, vol. 31, no. 12, pp. 3231–3236, 2010.
[80] W. W. Hu *et al.*, “The use of reactive polymer coatings to facilitate gene delivery from poly (epsilon-caprolactone) scaffolds,” *Biomaterials*, vol. 30, no. 29, pp. 5785–5792, 2009.
[81] P. C. Chang *et al.*, “PDGF-B gene therapy accelerates bone engineering and oral implant osseointegration,” *Gene Ther*, vol. 17, no. 1, pp. 95–104, 2010.
[82] M. J. Hawker, A. Pegalajar-Jurado, and E. R. Fisher, “Conformal encapsulation of three-dimensional, bioresorbable polymeric scaffolds using plasma-enhanced chemical vapor deposition,” *Langmuir*, vol. 30, no. 41, pp. 12328–12336, 2014.
[83] H. Y. Chen and J. Lahann, “Fabrication of discontinuous surface patterns within microfluidic channels using photodefinable vapor-based polymer coatings,” *Anal Chem*, vol. 77, no. 21, pp. 6909–6914, 2005.
[84] G. Avila, K. Misch, P. Galindo-Moreno, and H. L. Wang, “Implant surface treatment

using biomimetic agents," *Implant Dent*, vol. 18, no. 1, pp. 17–26, 2009.
[85] A. Ross *et al.*, "Selective and Reversible Binding of Thiol-Functionalized Biomolecules on Polymers Prepared via Chemical Vapor Deposition Polymerization," *Langmuir*, vol. 31, no. 18, pp. 5123–5129, 2015.
[86] M. A. Kennedy and R. J. Parks, "Adenovirus virion stability and the viral genome: size matters," *Mol Ther*, vol. 17, no. 10, pp. 1664–1666, 2009.
[87] J. Hao *et al.*, "Multigrowth Factor Delivery via Immobilization of Gene Therapy Vectors," *Adv. Mater.*, vol. 28, no. 16, pp. 3145–3151, 2016.
[88] A. J. Hudspeth, "Integrating the active process of hair cells with cochlear function," *Nat Rev Neurosci*, vol. 15, no. 9, pp. 600–614, 2014.
[89] E. Kandel and J. Schwartz, *Principles of Neural Science, Fifth Edition*. McGraw-Hill Education, 2013.
[90] H. E. M. Liwanag, A. Berta, D. P. Costa, S. M. Budge, and T. M. Williams, "Morphological and thermal properties of mammalian insulation: the evolutionary transition to blubber in pinnipeds," *Biol. J. Linn. Soc.*, vol. 107, no. 4, pp. 774–787, 2012.
[91] N. Hirokawa, "Kinesin and dynein superfamily proteins and the mechanism of organelle transport," *Science (80-.).*, vol. 279, no. 5350, pp. 519–526, 1998.
[92] W. Barthlott and C. Neinhuis, "Purity of the sacred lotus, or escape from contamination in biological surfaces," *Planta*, vol. 202, no. 1, pp. 1–8, 1997.
[93] K. Autumn *et al.*, "Adhesive force of a single gecko foot-hair," *Nature*, vol. 405, no. 6787, pp. 681–685, 2000.
[94] S. Tawfick *et al.*, "Engineering of Micro- and Nanostructured Surfaces with Anisotropic Geometries and Properties," *Adv. Mater.*, vol. 24, no. 13, pp. 1628–1674, 2012.
[95] B. Pokroy, S. H. Kang, L. Mahadevan, and J. Aizenberg, "Self-Organization of a Mesoscale Bristle into Ordered, Hierarchical Helical Assemblies," *Science (80-.).*, vol. 323, no. 5911, pp. 237–240, 2009.
[96] J. Paek and J. Kim, "Microsphere-assisted fabrication of high aspect-ratio elastomeric micropillars and waveguides," *Nat. Commun.*, vol. 5, 2014.
[97] M. F. L. De Volder, S. H. Tawfick, R. H. Baughman, and A. J. Hart, "Carbon Nanotubes: Present and Future Commercial Applications," *Science (80-.).*, vol. 339, no. 6119, pp. 535–539, 2013.
[98] T. Aida, E. W. Meijer, and S. I. Stupp, "Functional Supramolecular Polymers," *Science (80-.).*, vol. 335, no. 6070, pp. 813–817, 2012.
[99] B. M. Rosen, C. J. Wilson, D. A. Wilson, M. Peterca, M. R. Imam, and V. Percec, "Dendron-Mediated Self-Assembly, Disassembly, and Self-Organization of Complex Systems," *Chem. Rev.*, vol. 109, no. 11, pp. 6275–6540, 2009.

[100] K. Akagi, “Helical Polyacetylene: Asymmetric Polymerization in a Chiral Liquid-Crystal Field,” *Chem. Rev.*, vol. 109, no. 11, pp. 5354–5401, 2009.
[101] I. Dierking, “Polymer network-stabilized liquid crystals,” *Adv. Mater.*, vol. 12, no. 3, p. 167–+, 2000.
[102] Y. K. Fung, D. K. Yang, S. Ying, L. C. Chien, S. Zumer, and J. W. Doane, “Polymer Networks Formed in Liquid-Crystals,” *Liq. Cryst.*, vol. 19, no. 6, pp. 797–801, 1995.
[103] T. Svedberg, “Chemical reactions in anisotropic fluids.,” *Kolloid-Zeitschrift*, vol. 18, no. 2, pp. 54–56, 1916.
[104] A. Matsumoto, S. Nagahama, and T. Odani, “Molecular design and polymer structure control based on polymer crystal engineering. Topochemical polymerization of 1,3-diene mono- and dicarboxylic acid derivatives bearing a naphthylmethylammonium group as the countercation,” *J. Am. Chem. Soc.*, vol. 122, no. 38, pp. 9109–9119, 2000.
[105] R. G. Weiss, “Liquid-Crystalline Solvents as Mechanistics Probes .30. Thermotropic Liquid-Crystals as Reaction Media for Mechanistic Investigations,” *Tetrahedron*, vol. 44, no. 12, pp. 3413–3475, 1988.
[106] X. G. Wang, D. S. Miller, E. Bukusoglu, J. J. de Pablo, and N. L. Abbott, “Topological defects in liquid crystals as templates for molecular self-assembly,” *Nat. Mater.*, vol. 15, no. 1, p. 106–+, 2016.
[107] X. G. Wang, Y. K. Kim, E. Bukusoglu, B. Zhang, D. S. Miller, and N. L. Abbott, “Experimental Insights into the Nanostructure of the Cores of Topological Defects in Liquid Crystals,” *Phys. Rev. Lett.*, vol. 116, no. 14, 2016.
[108] X. G. Wang *et al.*, “Synthesis of Optically Complex, Porous, and Anisometric Polymeric Microparticles by Templating from Liquid Crystalline Droplets,” *Adv. Funct. Mater.*, vol. 26, no. 40, pp. 7343–7351, 2016.
[109] F. Mondiot, X. G. Wang, J. J. de Pablo, and N. L. Abbott, “Liquid Crystal-Based Emulsions for Synthesis of Spherical and Non-Spherical Particles with Chemical Patches,” *J. Am. Chem. Soc.*, vol. 135, no. 27, pp. 9972–9975, 2013.
[110] J. Lahann and R. Langer, “Surface-initiated ring-opening polymerization of epsilon-caprolactone from a patterned poly(hydroxymethyl-p-xylylene),” *Macromol. Rapid Commun.*, vol. 22, no. 12, pp. 968–971, 2001.
[111] M. A. B. Pantoja and N. L. Abbott, “Surface-Controlled Orientational Transitions in Elastically Strained Films of Liquid Crystal That Are Triggered by Vapors of Toluene,” *ACS Appl. Mater. Interfaces*, vol. 8, no. 20, pp. 13114–13122, 2016.
[112] J. M. Brake, A. D. Mezera, and N. L. Abbott, “Effect of surfactant structure on the orientation of liquid crystals at aqueous-liquid crystal interfaces,” *Langmuir*, vol. 19, no. 16, pp. 6436–6442, 2003.
[113] J. M. Brake, M. K. Daschner, Y. Y. Luk, and N. L. Abbott, “Biomolecular interactions at phospholipid-decorated surfaces of liquid crystals,” *Science (80-.).*, vol. 302, no.

5653, pp. 2094–2097, 2003.
[114] I. M. Ward, *Structure and Properties of Oriented Polymers*. Springer Netherlands, 1997.
[115] D. Demus, *Handbook of liquid crystals*, no. v. 2, pt. 2. Wiley-VCH, 1998.
[116] R. Kuroda and T. Honma, "CD spectra of solid-state samples," *Chirality*, vol. 12, no. 4, pp. 269–277, 2000.
[117] M. F. Maestre, C. Bustamante, T. L. Hayes, J. A. Subirana, and I. Tinoco, "Differential Scattering of Circularly Polarized-Light by the Helical Sperm Head from the Octopus Eledone-Cirrhosa," *Nature*, vol. 298, no. 5876, pp. 773–774, 1982.
[118] G. T. Hermanson, "Bioconjugate Techniques, 3rd Edition," in *Bioconjugate Techniques, 3rd Edition*, Elsevier, 2013, pp. 259–273.
[119] C. Rosini, R. Ruzziconi, S. Superchi, F. Fringuelli, and O. Piermatti, "Circular dichroism spectra (350-185 nm) of a new series of 4- substituted [2.2]paracyclophanes: A quantitative analysis within the devoe polarizability model," *Tetrahedron Asymmetry*, vol. 9, no. 1, pp. 55–62, 1998.
[120] Maarten M. J. Smulders, * and Albertus P. H. J. Schenning, and E. W. Meijer*, "Insight into the Mechanisms of Cooperative Self-Assembly: The 'Sergeants-and-Soldiers' Principle of Chiral and Achiral C3-Symmetrical Discotic Triamides," 2007.
[121] L. Brunsveld, J. A. J. M. Vekemans, J. H. K. K. Hirschberg, R. P. Sijbesma, and E. W. Meijer, "Hierarchical formation of helical supramolecular polymers via stacking of hydrogen-bonded pairs in water.," *Proc. Natl. Acad. Sci. U. S. A.*, vol. 99, no. 8, pp. 4977–82, Apr. 2002.
[122] E. W. Meijer, J. H. K. K. Hirschberg, L. Brunsveld, A. Ramzi, J. A. J. M. Vekemans, and R. P. Sijbesma, "Helical self-assembled polymers from cooperative stacking of hydrogen-bondedpairs," *Nature*, vol. 407, no. 6801, pp. 167–170, Sep. 2000.
[123] P. A. Korevaar *et al.*, "Pathway complexity in supramolecular polymerization," *Nature*, vol. 481, no. 7382, pp. 492–496, Jan. 2012.
[124] K. Hanabusa, M. Yamada, M. Kimura, and H. Shirai, "Prominent Gelation and Chiral Aggregation of Alkylamides Derived fromtrans-1,2-Diaminocyclohexane," *Angew. Chemie Int. Ed. English*, vol. 35, no. 17, pp. 1949–1951, Sep. 1996.
[125] Y. Okamoto, K. Suzuki, K. Ohta, K. Hatada, and H. Yuki, "Optically active poly(triphenylmethyl methacrylate) with one-handed helical conformation," *J. Am. Chem. Soc.*, vol. 101, no. 16, pp. 4763–4765, Aug. 1979.
[126] J. W. Goodby, D. Demus, J. Goodby, G. W. Gray, H.-W. Spiess, and V. Vill, "Symmetry and Chirality in Liquid Crystals," *Handb. Liq. Cryst. Set*, pp. 115–132, 1998.
[127] G. W. Gray and D. G. McDonnell, "The Relationship Between Helical Twist Sense, Absolute Configuration and Molecular Structure for Non-Sterol Cholesteric Liquid

Crystals," *Mol. Cryst. Liq. Cryst.*, vol. 34, no. 9, pp. 211–217, Sep. 1976.
[128] F. Bally-Le Gall *et al.*, "Polylutidines: Multifunctional surfaces via vapour-based polymerization of substituted pyridinophanes," *Rev.*
[129] L. A. Errede and M. Szwarc, "Chemistry of p-xylylene, its analogues, and polymers," *Q. Rev. Chem. Soc.*, vol. 12, no. 4, p. 301, 1958.
[130] A. G. MacDiarmid, "'Synthetic Metals': A Novel Role for Organic Polymers (Nobel Lecture)," *Angew. Chemie Int. Ed.*, vol. 40, no. 14, pp. 2581–2590, Jul. 2001.
[131] A. J. Heeger, "Semiconducting and Metallic Polymers: The Fourth Generation of Polymeric Materials (Nobel Lecture)," *Angew. Chemie Int. Ed.*, vol. 40, no. 14, pp. 2591–2611, Jul. 2001.
[132] J. H. Burroughes *et al.*, "Light-emitting diodes based on conjugated polymers," *Nature*, vol. 347, pp. 539–541, 1990.
[133] K. M. Vaeth and K. F. Jensen, "Chemical vapor deposition of poly (p -phenylene vinylene) based light emitting diodes with low turn-on voltages," *Appl. Phys. Lett.*, vol. 71, no. October, pp. 2091–2093, 1997.
[134] A. J. C. Kuehne and M. C. Gather, "Organic Lasers: Recent Developments on Materials, Device Geometries, and Fabrication Techniques," *Chem. Rev.*, vol. 116, no. 21, pp. 12823–12864, Nov. 2016.
[135] C. M. Hangarter, M. Bangar, A. Mulchandani, and N. V. Myung, "Conducting polymer nanowires for chemiresistive and FET-based bio/chemical sensors," *J. Mater. Chem.*, vol. 20, no. 16, p. 3131, 2010.
[136] D. Tyler McQuade, A. E. Pullen, and T. M. Swager, "Conjugated polymer-based chemical sensors," *Chem. Rev.*, vol. 100, no. 7, pp. 2537–2574, 2000.
[137] R. H. Friend *et al.*, "Electroluminescence in conjugated polymers," *Nature*, vol. 397, no. 6715, pp. 121–128, 1999.
[138] K. M. Vaeth and K. F. Jensen, "Chemical vapor deposition of thin polymer films used in polymer-based light emitting diodes," *Adv. Mater.*, vol. 9, no. 6, pp. 490–493, Jun. 1997.
[139] I. Murase, T. Ohnishi, Toshihiro Noguchi, M. Hirooka, and M. Shigezo, "Highly Conducting Poly(P-Phenylene Vinylene) Prepared From Sulfonium Salt," *Mol. Cryst. Liq. Cryst.*, vol. 118, pp. 333–336, 1985.
[140] F. Papadimitrakopoulos, K. Konstadinidis, T. M. Miller, R. Opila, E. A. Chandross, and M. E. Galvin, "The Role of Carbonyl Groups in the Photoluminescence of Poly(p-phenylenevinylene)," *Chem. Mater.*, vol. 6, no. 9, pp. 1563–1568, Sep. 1994.
[141] F. Xie *et al.*, "Backbone-Degradable Polymers Prepared by Chemical Vapor Deposition," *Angew. Chemie Int. Ed.*, vol. 56, no. 1, pp. 203–207, Jan. 2017.
[142] P. Oswald and P. Pieranski, *Nematic and cholesteric liquid crystals : concepts and physical properties illustrated by experiments*. Taylor & Francis/CRC Press, 2005.

[143] M. Wang, L. He, S. Zorba, and Y. Yin, “Magnetically Actuated Liquid Crystals,” *Nano Lett.*, vol. 14, no. 7, pp. 3966–3971, Jul. 2014.

[144] L. Chen, D. W. McBranch, H. L. Wang, R. Helgeson, F. Wudl, and D. G. Whitten, “Highly sensitive biological and chemical sensors based on reversible fluorescence quenching in a conjugated polymer.,” *Proc. Natl. Acad. Sci. U. S. A.*, vol. 96, no. 22, pp. 12287–92, Oct. 1999.